UNIVERSITÄTSKLINIKUM HAMBURG-EPPENDORF

III. Department of Medicine - Nephrology

Prof. Dr. med. Tobias B. Huber

Tissue-specific adaptation and function of innate lymphoid cells

Dissertation

To obtain the doctoral degree Dr. rer. biol. hum.
from the Medical Faculty of University of Hamburg.

Submitted by:

Nikhat Shaikh
from Mumbai, India

Hamburg 2023

I

Angenommen von der
Medizinischen Fakultät der Universität Hamburg am: 02.05.2024

Veröffentlicht mit Genehmigung der
Medizinischen Fakultät der Universität Hamburg.

Prüfungsausschuss, der Vorsitzende: Prof. Dr. Jan-Eric Turner

Prüfungsausschuss, zweiter Gutachter: Prof. Dr. Hans-Willi Mittrücker

Prüfungsausschuss, dritter Gutachter: Prof. Dr. David Vöhringer

Dobby has no master,

Dobby is a free elf!

- J. K. Rowling,

Table of Contents

1. Summary

Immune cell phenotype and function is strongly shaped by the tissue microenvironment. Adaptation of immune cells to tissue-specific microenvironment is, therefore, an essential process in homeostasis and inflammation. Innate lymphoid cells (ILCs) exhibit tissue-specific heterogeneity and function and are known to be key players as early responders in tissue inflammation and injury. However, the factors influencing ILC phenotype and function remain to be elucidated. Therefore, we aimed to the study the role of ILCs in the context of tissue adaptation and function under homeostasis and disease conditions. In the first study, we focused on the phenotypic adaptation of type 2 ILCs (ILC2s) in different organs and the factors influencing this process. We show that the murine effector ILC2s derived from various organs are capable in repopulating the niche of ILC2s at other anatomical locations where they undergo phenotypic adaptation specific to the tissue microenvironment. Using single-cell RNA sequencing of ILC2 populations, we observed an upregulation in the retinoic acid (RA) signalling in ILC2s adapting to the small-intestinal microenvironment. We also observed RA signalling-mediated reprogramming of ILC2s to the intestinal phenotype *in vitro* and *in vivo*. In the absence of RA signalling, ILC2s failed to acquire the intestinal phenotype and exhibited impaired worm expulsion during *Strongyloides ratti* infection, indicating the functional importance of tissue-specific imprinting of ILC2s. In conclusion, our study highlights an important attribute of effector ILC2s in retaining flexibility to adapt to changing tissue-specific microenvironment, enabling them to exert tissue-specific functions such as controlling intestinal helminth infections. In the second study, we aimed to characterise natural cytotoxicity receptor (NCR) and T-bet expressing ILC populations in murine kidney and study their functional role in crescentic glomerulonephritis. Detailed profiling of NCR$^+$ T-bet$^+$ ILCs in murine kidney revealed conventional natural killer (cNK) cells and type 1 ILCs (ILC1s) as two major subsets. In a mouse model of crescentic glomerulonephritis, induction of renal inflammation did not have a substantial influence on the abundance and phenotype of NK cells or ILC1s. We utilized widely used depletion antibodies for total NCR$^+$ ILCs (anti-NK1.1 antibody) and for cNK cells (anti-asialoGM1 serum) to perform the functional analyses in this model. However, these strategies proved to be unreliable tools as they were associated with significant off-target depletion of kidney natural killer T cells (NKT; anti-NK1.1) and CD8$^+$ T cells (anti-asialoGM1). Furthermore, we

observed that neither the depletion of cNK and ILC1s in NKT cell-deficient mice and CD8$^+$ T cell-deficient mice nor the specific genetic deletion of cNK cells in *Ncr1$^{Cre/wt}$* × *Eomes$^{fl/fl}$* mice altered the progression of disease in experimental glomerulonephritis. In summary, we show that cNK cells and ILC1s do not play a vital role in initiation and progression of glomerulonephritis and suggest caution while using standard antibody depletion methods to study the functional role of NCR$^+$ T-bet$^+$ ILCs in mouse models.

2. Zusammenfassung

Das Mikromilieu innerhalb eines Gewebes übt starken Einfluss auf den Phänotyp und die Funktion von Immunzellen aus. Die Anpassung der Immunzellen an die gewebespezifische Umgebung ist daher ein wesentlicher Prozess in Homöostase und Entzündung. Innate Lymphoid Cells (ILCs) weisen eine gewebespezifische Heterogenität sowie Funktion auf und sind als frühe „Responder" bei Gewebeentzündungen und -verletzungen bekannt. Welche Faktoren dabei den Phänotyp und die Funktion der ILCs beeinflussen ist bis dato allerdings noch nicht abschließend geklärt. Das Ziel der vorgelegten Arbeiten war es daher die Rolle der ILCs in Bezug auf ihre gewebespezifische Anpassung und Funktion unter homöostatischen und inflammatorischen Bedingungen zu untersuchen. In der ersten Studie konzentrierten wir uns auf die phänotypische Anpassung von Typ 2 ILCs (ILC2s) in verschiedenen Organen und die Faktoren, die diesen Prozess beeinflussen. Wir konnten zeigen, dass murine Effektor-ILC2s aus verschiedenen Organen, in der Lage sind, die Nische der ILC2s in anderen Geweben zu besiedeln, indem sie eine gewebespezifische, phänotypische Anpassung durchlaufen. Mithilfe von Einzelzell-RNA-Sequenzierung von ILC2-Populationen konnten wir eine Hochregulierung des Vitamin A-Signalwegs während der Adaptation von ILC2s an die Mikroumgebung des Dünndarms beobachten. Darüber hinaus konnten wir *in vitro* und *in vivo* zeigen, dass sich ILC2s Vitamin A-vermittelt in Richtung des intestinalen Phänotyps umprogrammieren. Die Blockade des Vitamin A-Signalwegs verhinderte weiterhin die intestinale Adaptation der ILC2s und beeinträchtigte die protektive Immunantwort gegen eine Wurminfektion mit *Strongyloides ratti*, was auf die funktionelle Bedeutung der gewebespezifischen Prägung der ILC2s hinweist. Zusammenfassend unterstreicht unsere Studie, dass die Flexibilität, sich an eine veränderte gewebespezifische Mikroumgebung anzupassen eine wichtige Eigenschaft von Effektor-ILC2s ist und sie diese in die Lage versetzt gewebespezifische Funktionen wie z. B. die Kontrolle intestinaler Helmintheninfektionen auszuüben. Das Ziel der zweiten Studie war phänotypische und funktionelle Charakterisierung der NK-Zellrezeptor (NCR) und T-bet exprimierende ILC-Populationen in der Mausniere. Im Rahmen einer detaillierten Charakterisierung der NCR⁺ T-bet⁺ ILCs in der Mausniere konnten konventionelle natürliche Killerzellen (cNK) und Typ-1-ILCs (ILC1s) als zwei wichtige Subpopulationen definiert werden. Im Mausmodell der halbmondbildenden

Glomerulonephritis konnten keine wesentlichen Änderungen der Häufigkeit und des Phänotyps von cNK-Zellen oder ILC1s beobachtet werden. Zur weiteren funktionellen Charakterisierung führten wir Depletions-Experimente von NCR$^+$ ILCs (Anti-NK1.1-Antikörper) und cNK-Zellen (Anti-AsialoGM1-Serum) durch. Aufgrund signifikanter „off-target" Depletion natürlicher Killer-T-Zellen (NKT; Anti-NK1.1) und CD8$^+$ T-Zellen (Anti-AsialoGM1) in der Niere erwiesen sich diese allerdings als nicht zielführend. Weiterhin konnten wir zeigen, dass weder die Depletion von cNK und ILC1 in NKT-Zell-defizienten bzw. CD8$^+$ T-Zell-defizienten Mäusen, noch die spezifische genetische Deletion von cNK-Zellen in *Ncr1$^{Cre/wt}$* x *Eomes$^{fl/fl}$*-Mäusen die Progression der experimentellen Glomerulonephritis beeinflusste. Zusammenfassend konnten wir feststellen, dass cNK-Zellen und ILC1s keine entscheidende funktionelle Rolle im Mausmodell der halbmondbildenden Glomerulonephritis spielen. Die häufig verwendeten Standard-Antikörperdepletionsmethoden zur Untersuchung der funktionellen Rolle von NCR$^+$ T-bet$^+$ ILCs in Mausmodellen sind dabei, aufgrund signifikannter „off target" Effekte mit Vorsicht zu interpretieren.

3. Introduction

3.1 Innate lymphoid cells

The immune system employs a wide array of immune cell subtypes to overcome pathogenic challenges and suppress autoimmunity (Seehus et al., 2017). Over the last decade, innate lymphoid cells (ILCs) have been extensively studied and appreciated for their contribution to the host immunity and defence as early responders to tissue signals as well as regulators of homeostasis. ILCs form a part of the innate immune system and comprise five cell subtypes with distinct phenotypes and function consisting of natural killer (NK) cells, type 1 ILCs (ILC1s), type 2 ILCs (ILC2s), type 3 ILCs (ILC3s), and lymphoid tissue inducer (LTi) cells (Gury-BenAri et al., 2016; Meininger et al., 2020; Vivier et al., 2018). ILCs are mainly tissue resident under homeostatic conditions, except for circulating NK cells, and are found in lymphoid (bone marrow and secondary lymphoid organs) and non-lymphoid tissues. They are particularly enriched at mucosal sites and barrier surfaces such as the intestine, lung, and skin (Gasteiger et al., 2015). ILCs rapidly produce both proinflammatory and regulatory cytokines in response to local tissue injury, infection, inflammation, and perturbations caused by commensal microbiota (Riggan et al., 2019). Their ability to promptly respond to tissue inflammation and stress reinforces their critical role in the regulation of tissue homeostasis and repair during infection or injury. Furthermore, based on the tissue microenvironment, ILCs are known to adapt their phenotype and function to mount an appropriate response to pathogens (Castellanos and Longman, 2019; Eberl et al., 2015).

3.1.1 Development of innate lymphoid cells

Increasing evidence suggests that ILCs are generated in waves of development from fetal to adult life in a process referred to as layered ontogeny (Oherle et al., 2020; Schneider et al., 2019). ILCs seed the tissues in early life and adopt tissue-specific signatures and functions depending on the signals received from their microenvironment. Several studies have shown that ILCs expand locally, acquire effector repertoire, and establish tissue-specific transcriptomic profiles that are maintained through life (Gury-BenAri et al., 2016; Ricardo-Gonzalez et al., 2018).

In general, ILC differentiation, in initial stages, takes place in the fetal liver, and after birth, in the bone marrow, spleen, and peripheral tissues (Figure 1) (Constantinides et al., 2014; Ghaedi and Takei, 2021). In adult mice, ILCs originate from the common lymphoid precursor (CLP) in the bone marrow. CLPs, lacking myeloid potential, develop into committed T cell, B cell, and ILC progenitors. From this stage, innate and adaptive lymphocyte development diverges and an early stage of committed innate precursors are formed known as early ILC precursor (EILP). EILPs retain the potential for both ILCs and NK cells but lack the expression of CD127, unlike their upstream precursors and downstream progeny. EILPS are defined by the expression of nuclear factor IL-3 induced (NFIL3), thymocyte selection-associated high mobility group box protein (TOX), and T cell factor 1 (TCF-1) and can differentiate into NK cell precursor (NKP) cells or common helper innate lymphoid progenitors (CHILPs) (Xu et al., 2015; Yang et al., 2015; Yu et al., 2014).
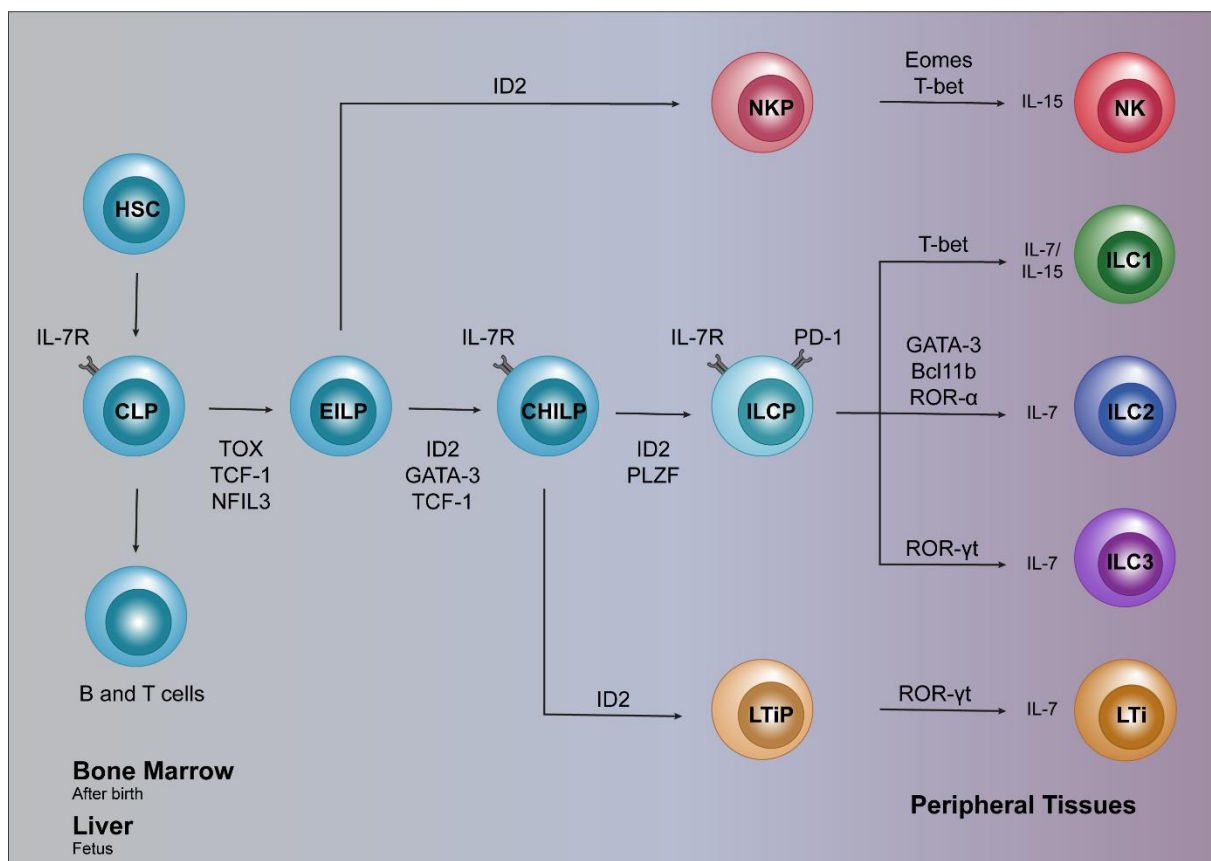
Figure 1. Developmental path of ILCs. Common lymphoid progenitors (CLPs) undergo ID2-mediated suppression of alternative lymphoid cell fates of B and T cells and ultimately become innate lymphoid cell (ILC) precursors (ILCPs), NK cell precursor (NKP), or lymphoid tissue inducer precursor (LTiPs). NKPs and LTiPs give rise to NK cell and LTi cells, respectively. ILCPs give rise to ILC1s, ILC2s, and ILC3s. At different stages of the developmental fate of ILCPs, various transcription factors such as TOX, NFIL3, GATA-3, and TCF-1 define the cell fate. CHILP, common helper innate lymphoid progenitor; EILP, early ILC precursor; HSC, hematopoietic stem cell.

It has been suggested that IL-15 signalling is essential for NK cell development from NKPs. NKPs give rise to immature NK cells through the expression of transcription factors (TFs) NFIL3 and ETS-1 (Barton et al., 1998; Male et al., 2014). The expression of NKG2D also marks the developmental stage of immature NKs (Abel et al., 2018; Huntington et al., 2007). Furthermore, IL-15 induces the expression of TFs such as NFIL3, Eomesodermin (Eomes), ETS-1, TOX, and T-box transcription factor TBX21 (T-bet) that are required for the development of mature NK cells from immature NKs (Ghaedi and Takei, 2021; Wang and Malarkannan, 2020). On the other hand, CHILPs are defined by the expression inhibitor of DNA binding 2 (ID2), Gata-binding protein (GATA-3), and TCF-1 (Constantinides et al., 2014; Klose et al., 2014; Serafini et al., 2014; Yagi et al., 2014). ID2 expression is important and assures CHILPs commitment to ILC lineage development rather than B and T cell fates (Moro et al., 2010; Satoh-Takayama et al., 2010). CHILPs show variable levels of promyelocytic zinc finger (PLZF), and depending on the PLZF expression, they can further give rise to PLZF-dependent ILC precursors or PLZF-independent LTi precursors (Constantinides et al., 2014). The expression of these different TFs at every stage is essential for ILC fate commitment and development as gene-deficient mice for one of these TFs lead to developmental defects in most ILCs (Boos et al., 2007; Harly et al., 2019; Seehus et al., 2015; Yagi et al., 2014).

The concomitant induction of TFs that polarize helper ILCs lead to the development of ILC1s, ILC2s, and ILC3s. As such, the development of ILC1s is strongly dependent on T-bet (Klose et al., 2014) and that of ILC3s is dependent on RAR-related orphan receptor γt (RORγt) (Satoh-Takayama et al., 2010; Sawa et al., 2011). The development of ILC2s, on the other hand, depends on TFs GATA-3, RORα, Bcl11b, and Gfi1 (Hoyler et al., 2012; Spooner et al., 2013; Walker et al., 2015; Wong et al., 2012). In addition to the key TFs, ILC2s and ILC3s are also dependent on IL-7 for their development and maintenance, whereas both IL-7 and IL-15 are needed for ILC1s. While several factors are involved in the development of ILCs, ILCs exert their effector functions in the peripheral tissues in a tissue-specific manner by incorporating the microenvironmental cues. This characteristic of ILCs make them an attractive target for studying tissue-specific immunity during inflammatory and pathological conditions.

3.1.2 Characteristics and functions of innate lymphoid cells

NK cells are known as the first members of the ILC family followed by LTi cells (Kiessling et al., 1975; Mebius, 1997). This discovery allowed for a more comprehensive look into the developmental trajectories and potential function of these newly discovered ILC members that showed absence of specific antigen receptors while exhibiting similar functionalities to certain T cells. NK cells are dependent on TFs T-bet and Eomes, without which NK cells cannot differentiate (Branzk et al., 2018; Gordon et al., 2012), have cytotoxic functions, and produce interferon-γ (IFN-γ), granzymes, and perforin. NK cells are regarded as innate counterparts of CD8$^+$ cytotoxic T (T$_C$) cells and play an important role in fighting against intracellular pathogens and tumours through perforin-dependent cytotoxicity and IFN-γ production (Biron et al., 1989; Straub et al., 2018). LTi cells, in contrast, require RORγt for their development and play an important role during the fetal period in the secondary lymphoid organ formation (Eberl et al., 2004; Onder et al., 2017; Yoshida et al., 1999).

Concomitantly, ILC1s, ILC2s, and ILC3s are referred as "helper-like" ILCs. ILCs are further compartmentalised based on their TF and distinct cytokine production profiles, with helper-like ILCs mirroring CD4$^+$ T helper (T$_H$) cell subsets (Figure 2) (Spits and Di Santo, 2011; Vivier et al., 2018). In this regard, ILC1s, ILC2s, and ILC3s mirror T$_H$1, T$_H$2, and T$_H$17 cells, respectively. ILC1s are dependent on T-bet, are generally less cytotoxic than NK cells, respond to IL-12 and IL-18, and produce type 1 cytokines such as IFN-γ and tumour necrosis factor (TNF). They mediate responses to intracellular pathogens such as viruses (Klose et al., 2014; Vivier et al., 2018; Weizman OE, 2017). ILC2s require GATA-3, respond to IL-33, IL-25, and TSLP, and produce type 2 cytokines such as IL-5 and IL-13 in addition to amphiregulin (Areg), IL-4, and IL-9. ILC2s respond to extracellular parasites and allergens (Gerbe et al., 2016; Howitt et al., 2016). ILC3s are dependent on RORγt, respond to IL-23 or IL-1β, and produce type 3 cytokines such as IL-17A, IL-17F, IL-22, granulocyte-macrophage colony-stimulating factor, and TNF. They mount responses against extracellular microbes such as bacteria and fungi (Goto et al., 2014; Hernandez et al., 2015). Thus, based on their functionality, helper-like ILCs are regarded as the innate counterparts of T$_H$ cells. Unlike their T$_H$ cell counterparts, ILCs lack rearranged antigen receptors, such as T

and B cells, and specific cell lineage markers (Puttur et al., 2019; Spits et al., 2013; Vivier et al., 2018).
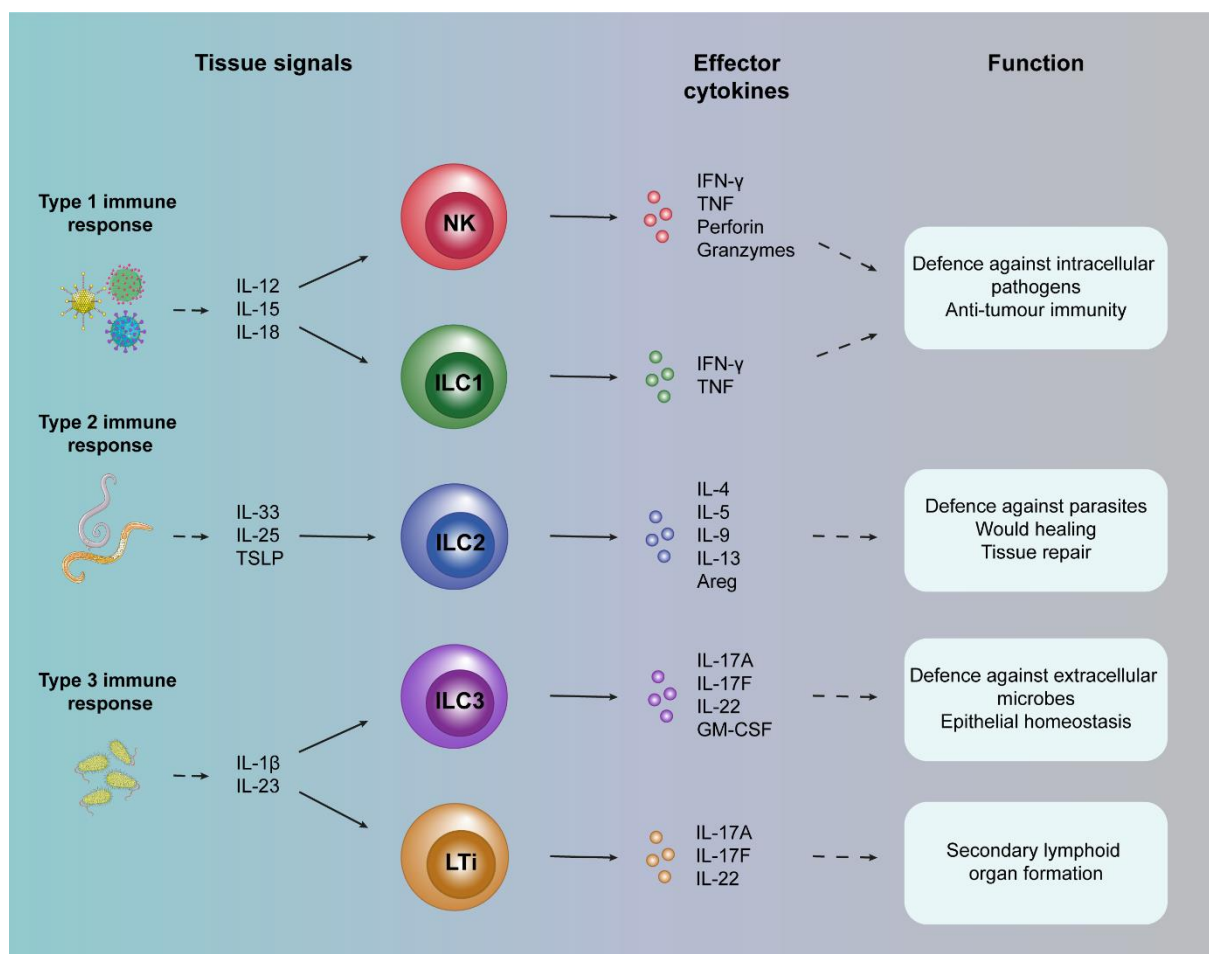
Figure 2. Activation and function of ILC subsets. Schematic representation of the different innate lymphoid cell (ILC) subsets. Each ILC subset is expanded and activated in response to distinct tissue signals derived from contact to diverse pathogens. Each ILC subset responds to specific stimuli and produces a unique set of effector cytokines to mount an appropriate functional response. NK cells and ILC1s are generally categorised as group 1 ILCs, ILC2s as group 2 ILCs, and LTi cells and ILC3s as group 3 ILCs.

3.2   Innate lymphoid cells as tissue sentinels

ILC composition majorly varies between different tissues. ILCs seed the peripheral tissues during early life and are mainly tissue-resident under homeostatic conditions. They receive and incorporate microenvironmental cues in their adaptation process to the respective tissue, leading to tissue-specific phenotype and functional activity. They exhibit heterogenous cell-surface marker expression pattern in different tissue environments and may respond to different stimuli. For example, lung ILC2s have a high expression of IL-33R and are more responsive to IL-33, whereas small intestinal and skin ILC2s exhibit high expression of IL-17RB and IL-18R and are more responsive

to IL-25 and IL-18, respectively (Ricardo-Gonzalez et al., 2018; von Moltke et al., 2016). Depending on the tissues and pathogen involved, ILCs mount tissue-specific responses. For this, ILCs establish close interactions not only with hematopoietic cells but also non-hematopoietic cells in the surrounding tissue, such as stromal cells, epithelial cells, and neurons, acting as tissue sentinels that directly respond to local tissue-derived signals to provide feedback to other tissue cells (Kim and Van Dyken, 2020; Klose and Artis, 2020). This crosstalk with surrounding tissue cells facilitates their rapid response to pathogens, thus establishing an important role that ILCs play as first line of immune defence. After tissue perturbations, ILCs initiate repair and maintain tissue integrity, thus asserting their role in homeostasis. Their roles can be further expanded to metabolism, thermal regulation, neuronal regulation, tissue remodelling, and circadian rhythms (Brestoff et al., 2015; Godinho-Silva et al., 2019; Murphy et al., 2022; Vivier et al., 2018; von Moltke et al., 2016). Concurrently, ILCs regulate both immune functions and tissue-specific processes, highlighting the importance of understanding their role and response in health and diseases.

3.2.1 Role of NK cells and ILC1s in type 1 immunity

ILCs significantly contribute to type 1, type 2, and type 3 immune responses in different tissues and disease settings. However, in our current research interest, we will focus on type 1 and type 2 responses mediated by ILCs. Type 1 immunity plays a critical role for defence against intracellular pathogens, such as viruses and some bacteria. The type 1 immune response is mainly defined by the activity of ILC1s, NK cells, and T_H1 cells that produce IFN-γ, LT-α, and TNF as effector cytokines that act on tissue cells and stimulate mononuclear phagocytes. Intracellular pathogens activate the pathogen recognition receptors on dendritic cells which thereby release IL-12 and IL-18, leading to the development of T_C cell from naïve T cells (Annunziato et al., 2015). Similarly, ILC1/NK cell-derived IFN-γ induces T_H1 and T_C1 development from naïve T cells. NK and T_C1 cells then kill the virus-infected cells, and T_H1 cells along with ILC1-derived IFN-γ trigger mononuclear phagocytes to produce matrix metallopeptidase, nitric oxide, and cytokines to allow killing and engulfment of microbial invaders (Annunziato et al., 2015).

NK cells and ILC1s form the first line of defence against viruses and some bacteria in mounting type 1 immune response. With their cytotoxic potential, NK cells can kill virus-

infected or tumour cells. Conversely, ILC1s possess weak cytotoxic potential but play a crucial role in controlling infections such as the intracellular parasite *Toxoplasma gondii* by co-producing high levels of IFN-γ and TNF or against enteric pathogen *Clostridium difficile* by mediating IFN-γ-dependent protection (Abt et al., 2015; Klose et al., 2014). During mouse cytomegalovirus infection, ILC1s have been shown to be essential for viral immunosurveillance as they were able to control the early viral load through IFN-γ production (Weizman et al., 2017). In this model, a lack of ILC1s in the liver led to increased viral load even in the presence of intact NK cell responses, depicting diverse roles for NK cells and ILC1s despite both producing IFN-γ during immune challenges. NK cells and ILC1s have also been shown to have nonredundant functions in a murine liver metastases model, wherein ILC1s were needed to control metastatic seeding and NK cells played a role in restraining tumour growth (Ducimetiere et al., 2021). In contrast to their protective role, ILC1s also have been implicated in the pathology of patients with Crohn's disease and in mouse model of colitis wherein their increased frequencies in the tissue and consequent increased production of IFN-γ potentially worsening the disease condition (Bernink et al., 2013; Fuchs et al., 2013).

While the involvement of NK cells and ILC1s has been studied in infection and tumour models in the liver and intestine, the characterisation of these cells in other tissue locations and inflammatory settings is still incomplete.

3.2.2 ILC2s as regulators of type 2 immune response

With recent advances, it has become increasingly evident that type 2 immunity plays a substantial role not only in controlling pathogenic activity and establishing host immune response but also in tissue repair and regeneration after injury. Several key immune cells of the innate and adaptive immunity contribute to establishing a robust type 2 immune response such as ILC2s, eosinophils, basophils, and T_H2 cells. In general, type 2 immune response defends the host against macro-parasites and may be an inducer of allergic diseases. It is characterised by the production of IL-13, IL-5, IL-4, and IL-9 as effector cytokines.

Type 2 responses deal with the destruction of large organisms such as helminths, and it is difficult for immune cells alone to accomplish this (Eberl, 2016). For this reason, in

response to parasitic helminths, type 2 immune response functions by restricting sites permissive for parasitic reproduction and limiting consequent tissue damage (Molofsky et al., 2015). Such a response involves induction of mucus production and collagen deposition. This response is shaped by the production of IL-25, IL-33, and TSLP via non-hematopoietic cells, leading to the activation of ILC2s and CD4^{+} T$_H$2 cells that secrete IL-4, IL-13, and IL-5 which are required for the accumulation of alternatively activated macrophages and eosinophils in the respective tissues (Figure 3) (Eberl, 2016; Walker et al., 2013). ILC2s are one of the most important immune cell populations involved in mounting an early and strong response against helminths in a weep and sweep response by increasing smooth muscle contraction, inducing IL-13-mediated mucus production by goblet cells, and inducing eosinophilia via IL-5 (Hung et al., 2013; Moro et al., 2010; Neill et al., 2010; Oliphant et al., 2014). Despite several advances in the medical field, parasitic worm infections remain a health and economic burden in developing countries (Kindermann et al., 2018). The indispensable role of ILC2s in establishing type 2 immune response for effective worm expulsion during helminth infection with *Nippostrongylus brasiliensis*, a rodent hookworm, has also been recently confirmed (Jarick et al., 2022).

Apart from their critical role in managing parasites at mucosal surfaces, the role of ILC2s has also been studied in non-barrier organs, such as kidneys, that can also be affected by different immune-related pathologies. ILC2s have been shown to be protective in Adriamycin-induced nephropathy, a murine kidney disease model for human chronic kidney disease characterised by progressive scarring of the glomeruli and fibrosis of tubulointerstitial compartment (Riedel et al., 2017). Treatment of mice with IL-33 expanded kidney-residing ILC2s led to the accumulation of eosinophils and reduction of inflammatory mononuclear phagocyte and neutrophil infiltration in kidney. ILC2s have been also studied in the context of autoimmune disorders (Duster et al., 2018; Russi et al., 2015). In a mouse model of systemic lupus erythematosus, a chronic autoimmune disorder, restoration of ILC2 numbers by IL-33 treatment has been shown to ameliorate disease progression (Duster et al., 2018).

On the other hand, ILC2s have also been implicated in allergy and asthma induction (Barlow et al., 2012; Chang et al., 2011; Halim et al., 2012; Karagiannis et al., 2020). They have been shown to contribute to the pathology of airway disease in a mouse

model of airway hyper-reactivity (AHR) induced by influenza infection through the IL-13–IL-33 axis (Chang et al., 2011). During allergic asthma, ILC2s have been shown to be potent producers of IL-13 that could directly induce AHR in the absence of CD4^{+} T cells (Barlow et al., 2012). Apart from the protective function of ILC2s, their role in the pathophysiology of diseases is equally important to be explored in detail and its underlying mechanisms need to be elucidated in order to be exploited for therapeutic potential.

3.2.3 Type 1 and type 2 immune response paradigm

Type 1 response carries the risk of initiating a cascade of pro-inflammatory response that may lead to collateral tissue damage. This damage initiates type 2 immune response that allows for repair of damaged tissue by engaging wound repair pathways following injury. These two immune responses have been shown to cross-regulate and interplay with each other in managing inflammation and infection. Based on this paradigm, the response to pathological insults can either result in resolution by regulation of the type 1 and 2 immune response or further inflammation, consequently leading to exacerbated pathological conditions. This fine tuning and cross-regulation of immune response has been recently addressed, wherein IL-33-mediated ILC2 activation that promotes tissue and metabolic homeostasis was counter-regulated by IFN-γ likely to promote inflammatory responses for host protection (Molofsky et al., 2015). Similarly, in lupus nephritis mouse model, decreased ILC2 abundance was related to disease progression, wherein the proliferation and cytokine production of ILC2s were inhibited by IFN-γ and IL-27 production via aberrantly activated T cells (Duster et al., 2018). However, the protective effects of ILC2s could be initiated with their restoration through IL-33-mediated expansion. Thus, type 1 and 2 immune response cross regulation is important for initiating and resolving inflammation for ultimately initiating tissue repair and return to homeostasis.

3.3 Tissue repair and fibrosis: the Yin and Yang of ILC2s

After tissue injury, inflammatory processes are initiated that help in promoting regeneration and repair (Figure 3). Damaged tissues release chemokines and cytokines that stimulate inflammatory cells and recruit them to the site of injury. Under normal circumstances, repair processes occur simultaneously with myofibroblast

activation, collagen deposition, and wound healing response initiation. However, persistent activation of pro-inflammatory and pro-fibrotic cell types may lead to extracellular matrix (ECM) deposition in the interstitium of tissues, and ultimately, to tissue fibrosis. Once tissue fibrosis is initiated, it leads to progressive loss of tissue elasticity and function.
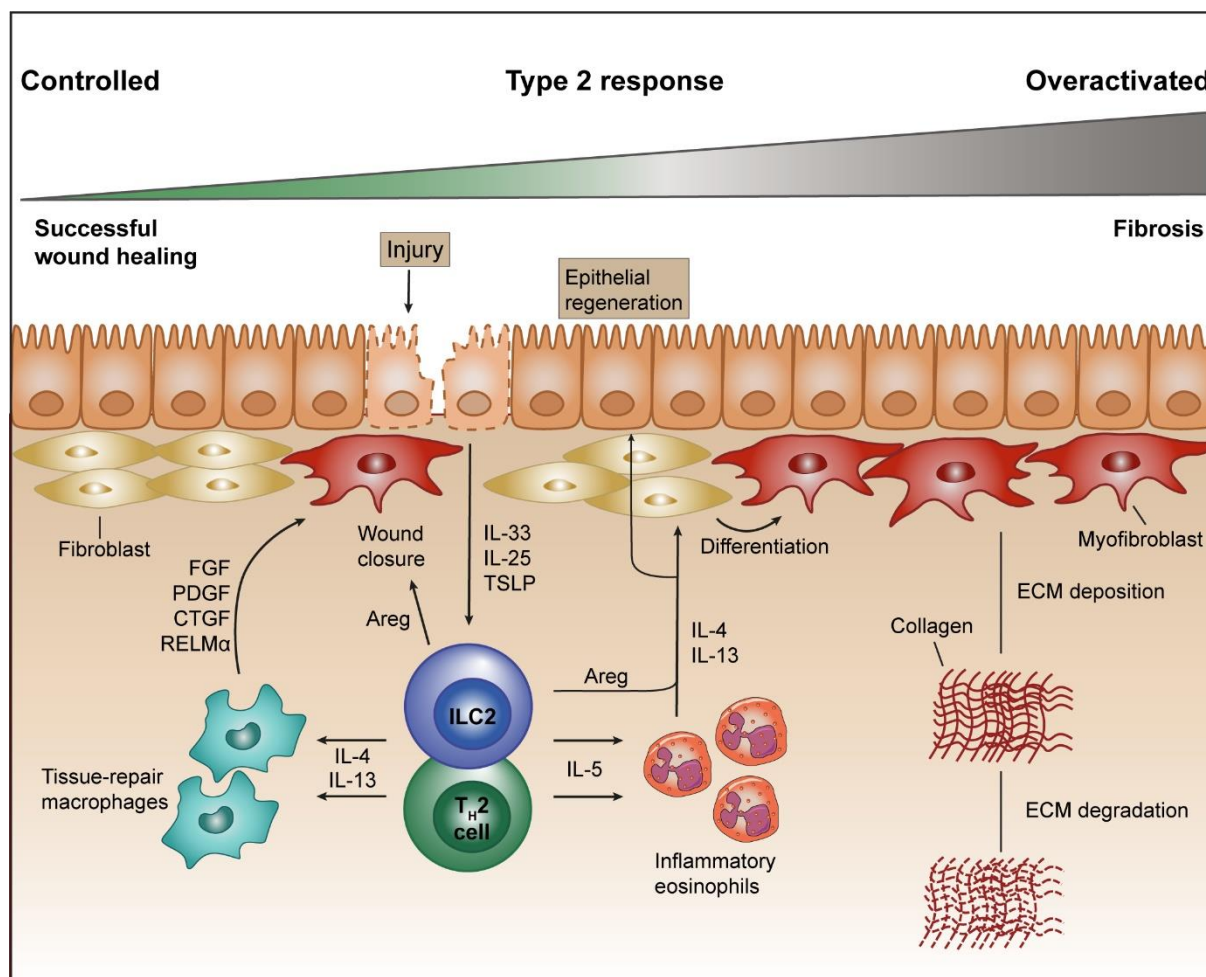
Figure 3. Role of ILC2s in tissue repair and fibrosis [adapted from (Kindermann et al., 2018)]. A controlled type 2 immune response is crucial for tissue repair and successful wound healing in response to injuries. Tissue damage leads to the release of alarmins (IL-33, IL-25, and TSLP) that activate type 2 innate lymphoid cells (ILC2s) and T helper 2 (T_H2) cells. Consequently, this leads to the secretion of type 2 effector cytokines (IL-4, IL-5, IL-13, and Areg) orchestrating the wound healing process. Tissue-repair macrophages, activated by IL-4 and IL-13, provide growth factors which can aid in wound repair and promoting fibrogenesis. Eosinophils are recruited in response to IL-5 and provide a local source of IL-4 for epithelial regeneration. In direct response to IL-4 and IL-13 signalling, epithelial cells proliferate and restore barrier function, while fibroblast secrete collagen and acquire contractile phenotype, aiding in wound closure. In contrast, excessive and uncontrolled type 2 signalling leads to chronic activation of myofibroblasts, resulting in excessive deposition of extracellular matrix (ECM). This excessive ECM deposition gradually leads to scarring and fibrosis. CTGF, connective tissue growth factor; FGF, fibroblast growth factor; PDGF, platelet-derived growth factor; RELMα, resistin-like molecule α; Areg, amphiregulin; TSLP, thymic stromal lymphopoietin.

3.3.1 ILC2s promote tissue repair and restoration

The repair and remodelling of injured tissue are complex processes that involve several factors including cytokines, growth factors, chemokines, and ECM proteins. The strategic positioning of ILCs in close proximity to barrier surfaces, in the gut, skin, and lung, not only facilitates in invoking a rapid response against invading pathogens but also limits rampant inflammation (Castellanos and Longman, 2019).

ILC2s are major contributors to tissue reparative responses. They are involved in type 2 immunity against helminths in the lung and gut, which are large multicellular pathogens that cause extensive damage to tissues as they migrate through host tissues (Allen and Maizels, 2011; Bouchery et al., 2019). ILC2s promote tissue repair following the breach of barrier in the gut and lung by parasites such as hookworms (Monticelli et al., 2011; Turner et al., 2013). Following injury, in response to IL-13 and IL-4, epithelial cells undergo proliferation and restore barrier function. In addition, IL-13 production by ILC2s stimulates the accumulation of alternatively activated macrophages in adipose and infected tissues where they promote wound healing and fibrogenesis by providing growth factors such as fibroblast growth factor, resistin-like α, and platelet-derived growth factor (Gieseck et al., 2018). IL-13 production by ILC2s has also recently shown to promote self-renewal of intestinal stem cells via IL-13Rα1 by activating β-catenin pathway (Zhu et al., 2019). During epithelial barrier damage and type 2 activation, eosinophils are recruited in response to IL-5 production by ILC2s. Eosinophils provide a local source of IL-4 and augment epithelial regeneration by triggering epithelial and parenchymal cells proliferation. On the other hand, fibroblasts also secrete collagens and adopt contractile phenotype in direct response to IL-4 and IL-13 which aid in wound closure (Gieseck et al., 2018). Furthermore, ILC2s in the gut also produce Areg, an epidermal growth factor family member, in response to IL-33 to limit intestinal inflammation and allow for ILC-dependent tissue regeneration and homeostasis (Monticelli et al., 2015). A critical role of Areg in the restoration of airway epithelial integrity in the lung after influenza infection has also been demonstrated (Monticelli et al., 2011).

Thus, type 2 cytokines secreted by ILC2s are central to initiating successful tissue repair process. In concert with macrophages, fibroblasts, and epithelial cells, ILC2s

play an important role in restoring barrier integrity, wound closure, and return to tissue homeostasis following tissue injury.

3.3.2 ILC2s in fibrotic pathologies

While ILC2s effector functions contribute to wound repair and tissue restoration, they can also contribute to exacerbation of diseases when overactivated and lead to fibrosis (Castellanos and Longman, 2019). Tissue fibrosis is a major concern as it can be progressive, have poor prognosis, and lead to irreversible changes in the tissue architecture. Excessive eosinophilia during inflammation and wound repair has the potential to become cytotoxic, increase allergic hyperactivation, and cause fibrosis. Likewise, repetitive and excessive fibroblast activation by type 2 signalling during persistent chronic damage can lead to increased ECM deposition, ultimately leading to scarring and fibrosis as the balance between production and degradation of ECM protein is lost (Kindermann et al., 2018).

In a bleomycin-induced mouse model of lung fibrosis, ILC2s have been shown to aggravate lung inflammation and fibrosis (Li et al., 2014). IL-13-producing ILC2s were also reported to be present in increased numbers in the BALF of patients with idiopathic pulmonary fibrosis, a life-threatening interstitial disease of unknown origin, compared with those of controls (Ebbo et al., 2017; Hams et al., 2014). Furthermore, another study reported that the hepatic expression of IL-33 chronically accumulated and activated ILC2s and induced severe hepatic fibrosis *in vivo* via IL-13 production, forming a pro-fibrotic cascade (McHedlidze et al., 2013). Areg has been implicated in TGF-β-induced pulmonary fibrosis and liver fibrosis by directly acting on fibroblasts, indicating that Areg production by ILC2s during tissue repair process may also contribute to fibroproliferative diseases (Perugorria et al., 2008; Zhou et al., 2012).

In conclusion, controlled type 2 response is essential for inflammation resolution, and as observed in several studies, excessive and dysregulated ILC2 response may lead to tissue fibrosis, hampering normal tissue function. Owing to this dichotomy of type 2 response by ILC2s, it is imperative to identify therapeutic targets to block aberrant signalling circuits and facilitate restoration of tissue homeostasis following injury.

3.4   ILCs in therapeutic approaches

ILCs promptly respond to infection and injury. This characteristic of ILCs could be exploited to critically enhance or hinder immune responses in early phases of vaccination, inflammatory immunopathology, and immunotherapy (Eberl et al., 2015). However, to achieve this goal, it is imperative to determine the molecular signals that control ILC diversity and commitment. The activation pathways and effector molecules used to target T cells in therapy can also be used to target ILCs at an earlier stage owing to the shared signalling and effector outcomes.

Type 1 and type 2 immune responses play an antagonistic role in several disease settings and can either exacerbate or resolve tissue inflammation, making them important therapeutic targets. Cytokines such as IL-13, IL-5, and IL-4 produced during type 2 immune response can be targeted for therapeutic purpose during tissue fibrosis and allergic inflammation. During experimental schistosomiasis and pulmonary granulomas models, blockade of IL-13 conferred significant reduction in fibrosis. However, this also led to an increase in IFN-γ production and inflammatory activity in the lung and liver. Dual blockade of IL-13 and IFN-γ not only led to reduced fibrosis but also eliminated the development of type 1 inflammation in response to IL-13 blockade alone (Ramalingam et al., 2016). Since IL-13 is associated with pathologic fibrosis, it forms an interesting and crucial therapeutic target in various organs (Hams et al., 2014; McHedlidze et al., 2013). Promising data from preclinical studies led to multiple clinical trials targeting IL-13 during asthma using humanized anti-IL-13 monoclonal antibodies, Tralokinumab and Lebrikizumab; however, these clinical trials either had limited to no success in patients with mild-to-moderate or severe asthma, with Lebrikizumab showing encouraging results (Corren et al., 2011; Piper et al., 2013). On the other hand, Mepolizumab, a monoclonal antibody targeting IL-5, has been shown to reduce the risk of asthma exacerbations and has been approved as an add-on therapy as a standard of care for patients with severe eosinophilic asthma (Chupp et al., 2017; Pavord et al., 2012; Rothenberg et al., 2008).

Therapeutic targeting of ILC2s and other important cell types that aid in type 2 immune response, while lucrative, is complicated and must be studied with caution. It is also important to consider that type 2 immune response, although involved in fibrotic diseases of various organs, forms an integral component of wound healing and tissue

repair processes and is a required response to combat extracellular parasites. Furthermore, owing to the involvement of several cytokines and cell types, dual or multi-blockade therapy must be considered and may prove to be more efficacious in disease management.

4. Hypothesis

ILCs exert tissue-specific effects in maintaining homeostasis and in driving pathology in different tissues. These tissue-specific attributes of ILCs need to be better understood. While many advances have been made regarding their roles in different types of immune response, modulating their tissue-specific features and functions for therapeutic purpose remain understudied.

The aim of the thesis was to study the role of ILCs in the context of tissue adaptation and function under homeostasis and disease conditions. Although initially known for their homogeneity, in recent years, ILC2s have been shown to differ in their phenotype and function between and within tissues. This adds a layer of complexity to understanding ILC2 development and function. Since ILCs exhibit tissue-specific phenotype and effector functions, the aim of the first project was to study the phenotypic adaptation of ILC2s in different organs and to investigate the factors that influence the adaptation process of ILC2s to the tissue microenvironment.

The role of NK cells and ILC1s in immune-mediated glomerular diseases are largely unknown. Additionally, the distinction and characterisation of NK cells and ILC1s in different anatomical locations remains ill-defined. Therefore, for the second project, the aim was to study the subset-specific expression profile of NK cells and ILC1s in murine kidney and their functional role in experimental crescentic glomerulonephritis.

5. Results

The abovementioned hypothesis and questions were thoroughly investigated, and the results have been presented in two scientific publications. The publications listed below form the basis of this cumulative dissertation and have been presented in entirety in the appendix.

Retinoic acid drives intestine-specific adaptation of effector ILC2s originating from distant sites.

Nikhat Shaikh, Alex Waterhölter, Ann-Christin Gnirck, Martina Becker, Virginia Adamiak, Lena Henneken, Malte Wunderlich, Wiebke Hartmann, Lara Linnemann, Tobias Huber, Christian Krebs, Ulf Panzer, Richard Locksley, Christoph Wilhelm, Minka Breloer, and Jan-Eric Turner (2023) *J Exp Med* 220 (12): 1-20

Conventional NK cells and type 1 innate lymphoid cells do not influence pathogenesis of experimental glomerulonephritis.

Constantin Rickassel*, Ann-Christin Gnirck*, Nikhat Shaikh, Virginia Adamiak, Alex Waterhölter, Yakup Tanriver, Katrin Neumann, Tobias B. Huber, Georg Gasteiger, Ulf Panzer, Jan-Eric Turner (2022) *J Immunol* 208 (7): 1585–1594 *contributed equally

6. Discussion

6.1 Phenotypic and functional adaptation of ILC2s

Immune cells are known to be influenced by their microenvironment in exhibiting tissue-specific phenotype and function. This dogma has been particularly well-established for the cells of myeloid lineage (Lavin et al., 2014; Roquilly et al., 2022). On the other hand, landmark studies on tissue-resident memory T cells and ILCs have brought forward the emerging concept of lymphocyte residency and adaptation in non-lymphoid tissues (Masopust and Soerens, 2019; Meininger et al., 2020). Recently, ILC2s have been reported to exhibit substantial heterogeneity across tissues, and it is believed that local niches and microenvironmental cues are responsible for this heterogeneity (Ricardo-Gonzalez et al., 2018; Spits and Mjosberg, 2022).

In the present study, using an adoptive transfer model, we show that murine effector ILC2s derived from non-lymphoid organs could successfully repopulate the niche in various peripheral tissues of alymphoid mice. These findings argue against an imprinted homing capacity of ILC2s that determines their tissue localization at developmental stage as has been previously suggested (Kim et al., 2015; Yang et al., 2016). Regardless of their tissue of origin, we observed that effector ILC2s adapted to the phenotype of the organ they came to reside in, which is a phenomenon also observed in macrophages and ILC3s adapting to the different tissue niches after transfer (Lavin et al., 2014; Nussbaum et al., 2017). To prove that the phenotypic adaptation was not due to the transfer of ILC precursors and their subsequent expansion and differentiation, we sorted for IL-33R$^+$KLRG1$^+$IL-5^{hi} ILC2s to a high purity (99.9%) and confirmed the absence of TCF-7$^+$IL-18R$^+$ ILC2 tissue progenitors in the scRNAseq analysis of transferred ILC2 populations. Indeed, formal proof of flexible adaptation of mature ILC2s could be substantiated with clonal single-cell readouts, which is rather difficult as innate cells lack rearranged antigen receptors that can be used for endogenous single-cell barcoding. In future, endogenous barcoding through somatic mitochondrial DNA mutations may be possible and allow for addressing these concerns at a clonal level (Ruckert et al., 2022). ILC2s are believed to be distributed to tissues during the perinatal window, where they maintain tissue residency. Here, they also undergo proliferation and expansion under homeostatic conditions and are replenished through tissue precursor expansion (Gasteiger et al., 2015; Huang et al.,

2018; Moro et al., 2016; Schneider et al., 2019). However, hematogenous trafficking to affected organs under chronic inflammatory conditions has been described in ILC2s (Gasteiger et al., 2015; Huang et al., 2018; Karta et al., 2018; Ricardo-Gonzalez et al., 2020; Stier et al., 2018; Zeis et al., 2020). Based on these data, the present study suggests that the interorgan trafficking of effector ILC2s, as observed in our adoptive transfer model, and their retained flexibility to adapt to tissue-specific microenvironment has relevance for studying the contribution of recruited ILC2s from different organs under inflammatory conditions.

Several recent studies indicate that ILC2s have distinct phenotypes in different tissues. However, signalling pathways that drive their tissue-specific programs remain poorly understood, and it is also unclear whether these tissue signatures can be adapted by ILC2s when they undergo interorgan trafficking. To identify potential factors that influence the flexible phenotype observed in ILC2s, we performed single-cell RNA sequencing (scRNAseq) on kidney and small intestinal lamina propria (SILP) ILC2s before adoptive transfer and on ex-kidney ILC2s isolated from the SILP at 2 and 8 weeks after adoptive transfer. Our scRNAseq data suggested that retinoic acid (RA) signalling might be one of the key drivers of kidney ILC2s toward the small intestinal phenotype (Figure 4). We then validated our scRNAseq data *in vitro* using RA on cultured kidney ILC2s. As a readout, we analysed the surface marker expression pattern of ILC2s that is specific for small intestinal adaptation. A distinct feature of successful kidney-derived ILC2 adaptation to the small intestine microenvironment, for example, is the upregulation of IL-25 receptor (IL-17RB) and downregulation of IL-33 receptor (IL-33R), a phenotype that has been previously described (Huang et al., 2018; Ricardo-Gonzalez et al., 2018; von Moltke et al., 2016). Indeed, RA addition was sufficient to upregulate the IL-17RB expression on kidney ILC2s along with changes in other surface markers indicative of intestine-specific phenotype (CD90.2^{low}KLRG1^{high}ICOS^{low}). The increased IL-17RB expression was also accompanied with increased responsiveness to subthreshold IL-25 stimulation, suggesting functional relevance of this phenotypic switch. In contrast, we did not observe any changes in the IL-33R expression in the presence of RA *in vitro*, and the sensitivity of ILC2s to IL-33 stimulation was maintained as previously described (Seehus et al., 2017). Notably, *in vivo* blocking of RA signalling after adoptive transfer of ILC2s partially inhibited their intestine-specific phenotypic adaptation. Consistent

with *in vitro* analysis, RA did not influence the expression of IL-33R *in vivo*. We further identified Notch signalling, in our scRNAseq analysis, to be a potential pathway influencing intestine-specific adaptation of ILC2s. Notch signalling has been previously implicated in ILC2 development and likely contributes in ILC2 to ILC3 plasticity (Wong et al., 2012; Zhang et al., 2017). However, on further investigation of this candidate pathway *in vitro*, we found Notch signalling to be a general inhibitor of cytokine production by IL-25- or IL-33-stimulated ILC2s, despite the upregulation of IL-17RB and downregulation of IL-33R. While combined activation of RA and Notch pathways could recapitulate the intestine-specific surface marker expression on kidney ILC2s, it failed to functionally rescue the decreased cytokine responsiveness induced by Notch signalling. Therefore, although we determined RA signalling to be an important driver of intestine-specific adaptation of ILC2s, it is evident that complete phenotypic and functional adaptation of ILC2s to the small intestinal microenvironment requires a complex combination of various signalling pathways such as RA, Notch, and others.

Tissue-specific surface receptor expression of ILC2s is known to impact their functional response in the skin and lung (Ricardo-Gonzalez et al., 2018; Zhang et al., 2022). In our study, RA-mediated intestine-specific adaptation of ILC2s was accompanied with their increased responsiveness to IL-25, leading us to hypothesize that RA in the intestinal microenvironment is essential to establish an optimal type 2 immune response against helminths in the small intestine wherein ILC2s play an important role. Consistent with this hypothesis, we observed that the inhibition of RA signalling in *Rag2*^{-/-} mice not only led to the reversal of intestinal phenotype of endogenous ILC2s, which was accompanied by reduced activation of mast cells, but also impaired their functional response for worm expulsion in acute *Strongyloides ratti* infection. We could confirm that this effect was depended on ILCs as it was not observed in ILC-deficient *Rag*^{-/-}*Il2rg*^{-/-} mice. This finding could potentially be due to the reduced production of IL-9 by ILC2s that failed to adapt to the intestinal microenvironment, which results in suboptimal activation of mast cells that are essential in eliminating *S. ratti* from the small intestine (Meiners et al., 2020; Reitz et al., 2018). We postulate that this impaired ILC2 activation could be a result of reduced responsiveness to IL-25 that is caused by a failure to upregulate the expression of IL-17RB in the absence of RA signalling. This hypothesis is corroborated by several significant studies showing that tuft cells in the small intestine constitutively produce IL-25, and a tuft cell–ILC2 feed-forward loop is

critical in mounting an effective anti-helminth immune response (Gerbe et al., 2016; Howitt et al., 2016; von Moltke et al., 2016). Certainly, to definitively prove the role of RA signalling in intestinal adaptation of ILC2s, ILC2s that are deficient in RA signalling need to be used in adoptive transfer experiments. Nonetheless, it must be considered that RA signalling pathway involves several RA receptors, and that the expression of these receptors may differ between organs (e.g., *Rara*, *Rxrb*, and *Rxrg* were expressed in SILP ILC2s), requiring multiple receptors or their downstream signalling components to be targeted in mice using complex genetic modifications. Interestingly, in a very recent study that was published after the acceptance of our manuscript, it was confirmed that intestinal ILC2s express high levels of *Rxrg* and that they depend on *Rxrg* expression as a checkpoint for ILC2 activation and response (Zang et al., 2023). In conclusion, these results show the importance of RA signalling in intestine-specific adaption and function of ILC2s.
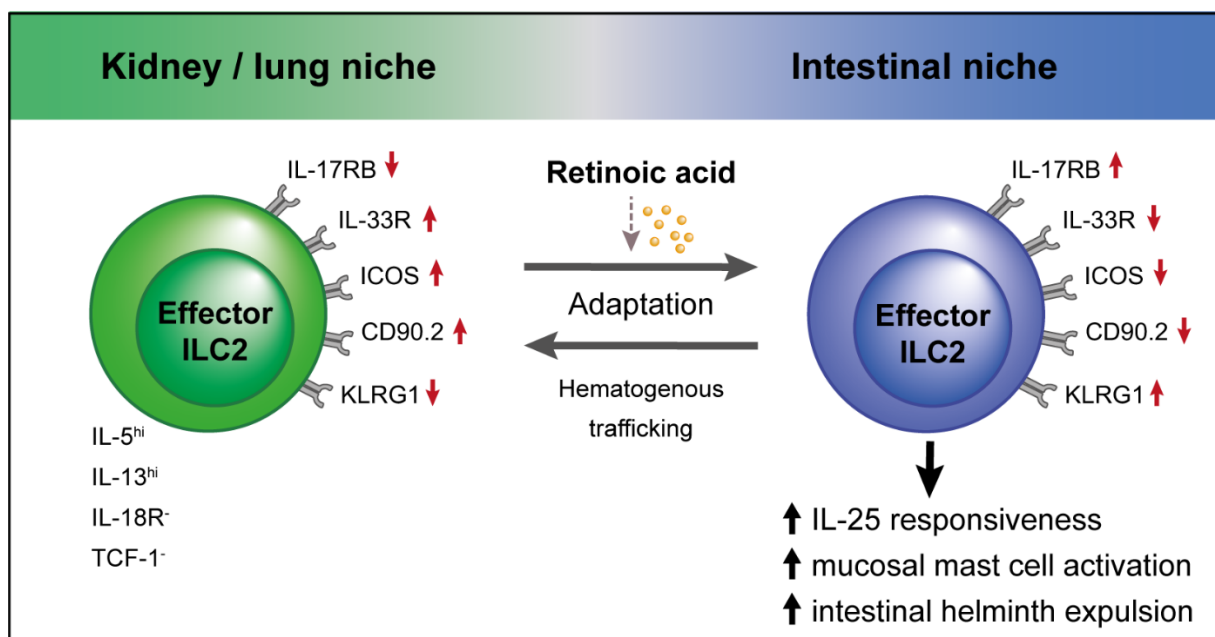
Figure 4. Graphic representation of the role of retinoic acid in ILC2 adaptation. Retinoic acid influences the phenotypic and functional adaptation of ILC2s derived from distant organs to the intestinal microenvironment.

In summary, our study highlights an important characteristic of ILC2s where they retain phenotypic flexibility, after hematogenous trafficking, to adapt to the new tissue microenvironment, which may enable them to exert tissue-specific functions. We also present a novel role of RA signalling in driving intestine-specific adaptation of ILC2s.

6.2 Role of cNK cells and ILC1s in experimental glomerulonephritis

Natural killer (NK) cells are generally defined as CD3$^-$NK1.1$^+$ and/or NKp46$^+$ lymphocytes in mice. They are further classified as circulating CD49b$^+$Eomes$^+$ T-bet$^+$ conventional NK (cNK) cells and CD49a$^+$Eomes$^-$T-bet$^+$ tissue-resident (trNK) cells (Peng et al., 2013; Sojka et al., 2014). However, in recent years, the discovery of type 1 ILCs (ILC1s) has led to the re-definition of trNK cells as ILC1s, as ILC1s share the expression of natural cytotoxicity receptors (NCRs) and transcription factor (TF) T-bet with NK cells but lack the expression of TF Eomes, exhibit less cytotoxicity, and are mainly tissue-resident (Daussy et al., 2014; Gasteiger et al., 2015; Spits et al., 2016). cNK cells and ILC1s together form the NCR$^+$ T-bet$^+$ group 1 ILCs. They populate nonlymphoid organs and play an important role in establishing type 1 immune response against viruses and tumours. Both the cell populations exhibit tissue-specific heterogeneity that also extends to their respective functions in various tissues. Numerous studies have identified the diversity, developmental pathways, and importance of group 1 ILCs in different anatomical locations; however, nonuniform nomenclature and definitions used such as cNK cells, trNK cells, and helper-like ILC1s in the research field and the relationship between them remains a matter of debate (Bjorkstrom et al., 2016; O'Sullivan, 2019; Peng and Tian, 2017; Spits et al., 2016; Weizman OE, 2017).

Recently, owing to the use of single-cell transcriptomics, key markers that can be used to define cNK cells and ILC1s across different murine tissues have been identified (Friedrich et al., 2021; McFarland et al., 2021). In these studies, it has been suggested that ILC1s should be defined by the expression of *Rorα*, *Bcl11b*, *Ahr*, and *Zfp683* (encoding for Hobit) in addition to the lack of the TF Eomes. On the other hand, cNK cells should be marked by the expression of *Eomes*, *Gzma*, and *Gzmb*. In the present study, we provide the first detailed transcriptional profiling of NCR$^+$ T-bet$^+$ ILCs in the murine kidney. Based on the recently described key markers for subset definition, we clearly identified two subsets: CD49b$^+$ cNK cells (*Eomes$^+$Gzma$^+$Gzmb$^+$*) and CD49a$^+$ ILC1s (*Eomes$^-$Rorα$^+$Bcl11b$^+$Ahr$^+$Zfp683$^+$*). This transcriptional profiling indicates that the trNK cells in the kidney should be referred as ILC1s, owing to their noticeable transcriptional similarities to ILC1s in the liver and small intestine (Friedrich et al., 2021; Peng et al., 2013; Weizman et al., 2017). The subset-specific transcriptomic signatures in our gene ontology analyses indicated that cNK cells in the kidney primarily

expressed genes involved in cytotoxic functions, whereas ILC1s expressed several genes involved in intratissue localization and regulation of other immune cells. This result corroborates with another study reporting the presence of tissue-resident CD49a^{+} ILC1s and recirculating CD49b^{+} cNK cells in the kidney (Victorino et al., 2015). Furthermore, another recent study has demonstrated an important role of TF Hobit in effector differentiation of ILC1s in various organs, including kidneys, suggesting that ILC1s in the kidney share developmental pathways, and potentially, their effector function with those in different tissues (Friedrich et al., 2021).

These data from the murine kidney are consistent with observations in the human kidney, wherein NK cells represent approximately 25% of all lymphocytes and has two distinct populations of NK cells: CD56^{dim}CD16^{+} and CD56^{bright}CD16^{-}, analogous to murine cNK cells and ILC1s, respectively (Carrega et al., 2014). Furthermore, the CD56^{bright}CD16^{-} subset expresses tissue residency marker CD69 and are perforin low, further indicating that they may resemble the ILC1 subset in murine kidney (Carrega et al., 2014; Law et al., 2017). Interestingly, in renal biopsy specimens, IFN-γ produced by this CD56^{bright}CD16^{-} subset has been shown to correlate with the degree of fibrosis, regardless of the underlying pathology. While evidence supports the involvement of NCR[+] T-bet[+] ILCs in acute and chronic kidney diseases in humans, further research on their role in other kidney disease entities, such as glomerulonephritis, is warranted.

NCR[+] ILCs have been shown to play an important role in preclinical models of renal allograft rejection and acute kidney injury (Turner et al., 2019; Zhang et al., 2015; Zhang et al., 2010); however, such studies are lacking for experimental models of glomerulonephritis. In MRL-*lpr* mouse model of systemic lupus erythematosus, NCR[+] ILCs have been shown to have a proinflammatory effect since an activated and mature phenotype of NCR[+] ILCs along with increased glomerular infiltration and IFN-γ production was observed in the kidney of affected mice (Spada et al., 2015). The role of NK cells has also been studied in a mouse model of Adriamycin nephropathy, wherein neither the depletion of cNK cells, while infiltrating the kidney, using anti-asialoGM1 (asGM1) serum or their impaired function in NOD-SCID mice altered the disease outcome (Zheng et al., 2006).

Previous studies have been mainly focused on the general role of all NCR$^+$ ILCs in kidney diseases as the strategies to target their specific subsets have been limited. However, a recent study explored the subset-specific function of cNK cells and ILC1s (i.e., trNK cells) in an ischemia-reperfusion injury model of acute kidney injury (AKI) in mice (Victorino et al., 2015). It was shown that ILC1s have a reduced expression of asGM1, relative to cNK cells. The preferential depletion of cNK cells using anti-asGM1 failed to protect kidney against injury although the complete depletion of both subsets using anti-NK1.1 antibody had shown protective effects, indicating that ILC1s, in the absence of cNK cells, promote renal tissue injury in AKI. In the present study, we adopted the same strategy and studied the subset-specific role of cNK cells and ILC1s in a widely used experimental model of crescentic glomerulonephritis (cGN) in mice. We observed disease aggravation with increased glomerular crescent formation, a sensitive marker of glomerular damage in cGN, in wild type mice in both the depletion strategies. However, on further inspection of other lymphocyte populations, we observed substantial off-target effects on kidney NKT cells and CD8$^+$ T cells when using anti-asGM1 and anti-NK1.1 antibodies, respectively. Based on these observations, we advise caution while interpreting data from studies using these depletion strategies to study the role of group 1 ILCs. Of note, in the AKI model, the involvement of group 1 ILCs could be substantiated as the protective effects of anti-NK1.1 antibody treatment was observed even in *Cd1d$^{-/-}$* mice that lack NKT cells (Victorino et al., 2015). On the other hand, depletion of total NCR$^+$ ILCs or cNK cells alone in the NKT- or CD8$^+$ T cell-deficient mice did not alter the course of disease in our experimental cGN model, suggesting that the initially observed phenotype depended on NKT cells and CD8$^+$ T cells rather than NCR$^+$ T-bet$^+$ ILCs. This data suggests that group 1 ILCs are not responsible for the alteration of the disease course in our experimental cGN model. The discrepancy observed in data between our study and that in previously published work are likely to be the outcome of considerable differences in the examined disease models. In the ischemia-reperfusion-induced AKI injury model, the ischemic necrosis of tubular epithelial cells was analysed after 24 h. The role of NK cells in this primarily non-immune-mediated has been well established, indicating that group 1 ILCs may be an important player in this context of sterile tissue injury (Turner et al., 2019). In contrast, in our study, we mainly focused on the immune-mediated glomerular damage that develops over several days resulting from the dysregulation of the adaptive immune response. In our cGN model, we observed an

increased prevalence of Th1 cells among the T-bet-expressing lymphocytes, which makes the involvement of T-bet-expressing ILC populations in disease progression less plausible.

We speculated that disease aggravation depended on NKT cells and CD8^{+} cells, respectively, due to a lack of interaction of these cell types with group 1 ILCs which would allow them to downregulate the glomerular damage, as the importance of cNK cells–CD8^{+} T cell interaction in viral infection has been previously described (Waggoner et al., 2010). However, induction of cGN in *Ncr1*[Cre/wt] *× Eomes*^{fl/fl} mice, a cNK cell-specific genetic deletion, did not alter the disease course, allowing us to discard the involvement of cNK cells. Regardless, we could not formally rule out the involvement of ILC1s in downregulating glomerular damage, but it must be emphasized that the depletion of total NCR^{+} cells, in the absence of NKT cells, also did not influence the cGN outcome, suggesting that ILC1s may not be influential in immune-mediated glomerular disease.

In summary, using RNA sequencing, we provide a detailed profile of NCR[+] T-bet[+] ILC populations in murine kidney and identify cNK cells and ILC1s as its two major subsets. Additionally, we conclude that both cNK cells and ILC1s do not play a substantial role in influencing the pathogenesis of experimental cGN. We also show that widely used antibody depletion strategies to deplete total NCR[+] ILCs and/or cNK cells have significant off-target effects and are unreliable tools to the study the function of these cells, warranting an urgent need to develop more specific models to the study the function of group 1 ILCs.

7. List of Abbreviations

AHR	airway hyper-reactivity
AKI	acute kidney injury
Areg	amphiregulin
asGM1	asialo GM1
CHILP	common helper innate lymphoid progenitor
CLP	common lymphoid precursor
cNK	conventional natural killer
CTGF	connective tissue growth factor
ECM	extracellular matrix
EILP	early ILC precursor
Eomes	Eomesodermin
FGF	fibroblast growth factor
HSC	hematopoietic stem cell
ID2	inhibitor of DNA binding 2
IFN- γ	interferon-γ
ILC1s	type 1 innate lymphoid cells
ILC2s	type 2 innate lymphoid cells
ILC3s	type 3 innate lymphoid cells
ILCs	Innate lymphoid cells
LTi	lymphoid tissue inducer
NCRs	natural cytotoxicity receptors
NFIL3	nuclear factor IL-3 induced
NK	natural killer
NKP	NK cell precursor
NKTs	natural killer T cells
PDGF	platelet-derived growth factor
PLZF	promyelocytic zinc finger
RA	retinoic acid
RELMα	resistin-like molecule α

RORγt	RAR-related orphan receptor γt
scRNAseq	single-cell RNA sequencing
SILP	small intestinal lamina propria
T-bet	T-box transcription factor TBX21
T_C	cytotoxic T
TCF-1	T cell factor 1
TF	transcription factor
T_H	T helper
TNF	tumour necrosis factor
TOX	thymocyte selection-associated high mobility group box protein
trNK	tissue-resident natural killer
TSLP	thymic stromal lymphopoietin

8. References

Abel, A.M., C. Yang, M.S. Thakar, and S. Malarkannan. 2018. Natural Killer Cells: Development, Maturation, and Clinical Utilization. *Front Immunol* 9:1869.

Abt, M.C., B.B. Lewis, S. Caballero, H. Xiong, R.A. Carter, B. Susac, L. Ling, I. Leiner, and E.G. Pamer. 2015. Innate Immune Defenses Mediated by Two ILC Subsets Are Critical for Protection against Acute Clostridium difficile Infection. *Cell Host Microbe* 18:27-37.

Allen, J.E., and R.M. Maizels. 2011. Diversity and dialogue in immunity to helminths. *Nat Rev Immunol* 11:375-388.

Annunziato, F., C. Romagnani, and S. Romagnani. 2015. The 3 major types of innate and adaptive cell-mediated effector immunity. *J Allergy Clin Immunol* 135:626-635.

Barlow, J.L., A. Bellosi, C.S. Hardman, L.F. Drynan, S.H. Wong, J.P. Cruickshank, and A.N. McKenzie. 2012. Innate IL-13-producing nuocytes arise during allergic lung inflammation and contribute to airways hyperreactivity. *J Allergy Clin Immunol* 129:191-198 e191-194.

Barton, K., N. Muthusamy, C. Fischer, C.N. Ting, T.L.L. Walunas, L.L., and J.M. Leiden. 1998. The Ets-1 transcription factor is required for the development of natural killer cells in mice. *Immunity* 9:555-563.

Bernink, J.H., C.P. Peters, M. Munneke, A.A. te Velde, S.L. Meijer, K. Weijer, H.S. Hreggvidsdottir, S.E. Heinsbroek, N. Legrand, C.J. Buskens, W.A. Bemelman, J.M. Mjosberg, and H. Spits. 2013. Human type 1 innate lymphoid cells accumulate in inflamed mucosal tissues. *Nat Immunol* 14:221-229.

Biron, C.A., K.S. Byron, and J.L. Sullivan. 1989. Severe herpesvirus infections in an adolescent without natural killer cells. *N Engl J Med* 320:1731-1735.

Bjorkstrom, N.K., H.G. Ljunggren, and J. Michaelsson. 2016. Emerging insights into natural killer cells in human peripheral tissues. *Nat Rev Immunol* 16:310-320.

Boos, M.D., Y. Yokota, G. Eberl, and B.L. Kee. 2007. Mature natural killer cell and lymphoid tissue-inducing cell development requires Id2-mediated suppression of E protein activity. *J Exp Med* 204:1119-1130.

Bouchery, T., G. Le Gros, and N. Harris. 2019. ILC2s-Trailblazers in the Host Response Against Intestinal Helminths. *Front Immunol* 10:623.

Branzk, N., K. Gronke, and A. Diefenbach. 2018. Innate lymphoid cells, mediators of tissue homeostasis, adaptation and disease tolerance. *Immunol Rev* 286:86-101.

Brestoff, J.R., B.S. Kim, S.A. Saenz, R.R. Stine, L.A. Monticelli, G.F. Sonnenberg, J.J. Thome, D.L. Farber, K. Lutfy, P. Seale, and D. Artis. 2015. Group 2 innate

lymphoid cells promote beiging of white adipose tissue and limit obesity. *Nature* 519:242-246.

Carrega, P., I. Bonaccorsi, E. Di Carlo, B. Morandi, P. Paul, V. Rizzello, G. Cipollone, G. Navarra, M.C. Mingari, L. Moretta, and G. Ferlazzo. 2014. CD56(bright)perforin(low) noncytotoxic human NK cells are abundant in both healthy and neoplastic solid tissues and recirculate to secondary lymphoid organs via afferent lymph. *J Immunol* 192:3805-3815.

Castellanos, J.G., and R.S. Longman. 2019. The balance of power: innate lymphoid cells in tissue inflammation and repair. *J Clin Invest* 129:2640-2650.

Chang, Y.J., H.Y. Kim, L.A. Albacker, N. Baumgarth, A.N. McKenzie, D.E. Smith, R.H. Dekruyff, and D.T. Umetsu. 2011. Innate lymphoid cells mediate influenza-induced airway hyper-reactivity independently of adaptive immunity. *Nat Immunol* 12:631-638.

Chupp, G.L., E.S. Bradford, F.C. Albers, D.J. Bratton, J. Wang-Jairaj, L.M. Nelsen, J.L. Trevor, A. Magnan, and A. Ten Brinke. 2017. Efficacy of mepolizumab add-on therapy on health-related quality of life and markers of asthma control in severe eosinophilic asthma (MUSCA): a randomised, double-blind, placebo-controlled, parallel-group, multicentre, phase 3b trial. *Lancet Respir Med* 5:390-400.

Constantinides, M.G., B.D. McDonald, P.A. Verhoef, and A. Bendelac. 2014. A committed precursor to innate lymphoid cells. *Nature* 508:397-401.

Corren, J., R.F. Lemanske, N.A.K. Hanania, P.E. Parsey, M.V. Parsey, J.R. Arron, J.M.S. Harris, H. Scheerens, L.C. Wu, Z. Su, S. Mosesova, M.D. Eisner, and S.P.M. Bohen, J.G Matthews. 2011. Lebrikizumab treatment in adults with asthma. *N Engl J Med* 365:1088-1098.

Daussy, C., F. Faure, K. Mayol, S. Viel, G. Gasteiger, E. Charrier, J. Bienvenu, T. Henry, E. Debien, U.A. Hasan, J. Marvel, K. Yoh, S. Takahashi, I. Prinz, S. de Bernard, L. Buffat, and T. Walzer. 2014. T-bet and Eomes instruct the development of two distinct natural killer cell lineages in the liver and in the bone marrow. *J Exp Med* 211:563-577.

Ducimetiere, L., G. Lucchiari, G. Litscher, M. Nater, L. Heeb, N.G. Nunez, L. Wyss, D. Burri, M. Vermeer, J. Gschwend, A.E. Moor, B. Becher, M. van den Broek, and S. Tugues. 2021. Conventional NK cells and tissue-resident ILC1s join forces to control liver metastasis. *Proc Natl Acad Sci U S A* 118:

Duster, M., M. Becker, A.C. Gnirck, M. Wunderlich, U. Panzer, and J.E. Turner. 2018. T cell-derived IFN-gamma downregulates protective group 2 innate lymphoid cells in murine lupus erythematosus. *Eur J Immunol* 48:1364-1375.

Ebbo, M., A. Crinier, F. Vely, and E. Vivier. 2017. Innate lymphoid cells: major players in inflammatory diseases. *Nat Rev Immunol* 17:665-678.

Eberl, G. 2016. Immunity by equilibrium. *Nat Rev Immunol* 16:524-532.

Eberl, G., M. Colonna, J.P. Di Santo, and A.N. McKenzie. 2015. Innate lymphoid cells. Innate lymphoid cells: a new paradigm in immunology. *Science* 348:aaa6566.

Eberl, G., S. Marmon, M.J. Sunshine, P.D. Rennert, Y. Choi, and D.R. Littman. 2004. An essential function for the nuclear receptor RORgamma(t) in the generation of fetal lymphoid tissue inducer cells. *Nat Immunol* 5:64-73.

Friedrich, C., R. Taggenbrock, R. Doucet-Ladeveze, G. Golda, R. Moenius, P. Arampatzi, N.A.M. Kragten, K. Kreymborg, M. Gomez de Aguero, W. Kastenmuller, A.E. Saliba, D. Grun, K. van Gisbergen, and G. Gasteiger. 2021. Effector differentiation downstream of lineage commitment in ILC1s is driven by Hobit across tissues. *Nat Immunol* 22:1256-1267.

Fuchs, A., W. Vermi, J.S. Lee, S. Lonardi, S. Gilfillan, R.D. Newberry, M. Cella, and M. Colonna. 2013. Intraepithelial type 1 innate lymphoid cells are a unique subset of IL-12- and IL-15-responsive IFN-gamma-producing cells. *Immunity* 38:769-781.

Gasteiger, G., X. Fan, S. Dikiy, S.Y. Lee, and A.Y. Rudensky. 2015. Tissue residency of innate lymphoid cells in lymphoid and nonlymphoid organs. *Science* 350:981-985.

Gerbe, F., E. Sidot, D.J. Smyth, M. Ohmoto, I. Matsumoto, V. Dardalhon, P. Cesses, L. Garnier, M. Pouzolles, B. Brulin, M. Bruschi, Y. Harcus, V.S. Zimmermann, N. Taylor, R.M. Maizels, and P. Jay. 2016. Intestinal epithelial tuft cells initiate type 2 mucosal immunity to helminth parasites. *Nature* 529:226-230.

Ghaedi, M., and F. Takei. 2021. Innate lymphoid cell development. *J ALLERGY CLIN IMMUNOL* 1549-1560.

Gieseck, R.L., 3rd, M.S. Wilson, and T.A. Wynn. 2018. Type 2 immunity in tissue repair and fibrosis. *Nat Rev Immunol* 18:62-76.

Godinho-Silva, C., F. Cardoso, and H. Veiga-Fernandes. 2019. Neuro-Immune Cell Units: A New Paradigm in Physiology. *Annu Rev Immunol* 37:19-46.

Gordon, S.M., J. Chaix, L.J. Rupp, J. Wu, S. Madera, J.C. Sun, T. Lindsten, and S.L. Reiner. 2012. The transcription factors T-bet and Eomes control key checkpoints of natural killer cell maturation. *Immunity* 36:55-67.

Goto, Y., T. Obata, J. Kunisawa, S. Sato, Ivanov, II, A. Lamichhane, N. Takeyama, M. Kamioka, M. Sakamoto, T. Matsuki, H. Setoyama, A. Imaoka, S. Uematsu, S. Akira, S.E. Domino, P. Kulig, B. Becher, J.C. Renauld, C. Sasakawa, Y. Umesaki, Y. Benno, and H. Kiyono. 2014. Innate lymphoid cells regulate intestinal epithelial cell glycosylation. *Science* 345:1254009.

Gury-BenAri, M., C.A. Thaiss, N. Serafini, D.R. Winter, A. Giladi, D. Lara-Astiaso, M. Levy, T.M. Salame, A. Weiner, E. David, H. Shapiro, M. Dori-Bachash, M. Pevsner-Fischer, E. Lorenzo-Vivas, H. Keren-Shaul, F. Paul, A. Harmelin, G. Eberl, S. Itzkovitz, A. Tanay, J.P. Di Santo, E. Elinav, and I. Amit. 2016. The Spectrum and Regulatory Landscape of Intestinal Innate Lymphoid Cells Are Shaped by the Microbiome. *Cell* 166:1231-1246 e1213.

Halim, T.Y., R.H. Krauss, A.C. Sun, and F. Takei. 2012. Lung natural helper cells are a critical source of Th2 cell-type cytokines in protease allergen-induced airway inflammation. *Immunity* 36:451-463.

Hams, E., M.E. Armstrong, J.L. Barlow, S.P. Saunders, C. Schwartz, G. Cooke, R.J. Fahy, T.B. Crotty, N. Hirani, R.J. Flynn, D. Voehringer, A.N. McKenzie, S.C. Donnelly, and P.G. Fallon. 2014. IL-25 and type 2 innate lymphoid cells induce pulmonary fibrosis. *Proc Natl Acad Sci U S A* 111:367-372.

Harly, C., D. Kenney, G. Ren, B. Lai, T. Raabe, Q. Yang, M.C. Cam, H.H. Xue, K. Zhao, and A. Bhandoola. 2019. The transcription factor TCF-1 enforces commitment to the innate lymphoid cell lineage. *Nat Immunol* 20:1150-1160.

Hernandez, P.P., T. Mahlakoiv, I. Yang, V. Schwierzeck, N. Nguyen, F. Guendel, K. Gronke, B. Ryffel, C. Hoelscher, L. Dumoutier, J.C. Renauld, S. Suerbaum, P. Staeheli, and A. Diefenbach. 2015. Interferon-lambda and interleukin 22 act synergistically for the induction of interferon-stimulated genes and control of rotavirus infection. *Nat Immunol* 16:698-707.

Howitt, M.R., S. Lavoie, M. Michaud, A.M. Blum, S.V. Tran, J.V. Weinstock, C.A. Gallini, K. Redding, R.F. Margolskee, L.C. Osborne, D. Artis, and W.S. Garrett. 2016. Tuft cells, taste-chemosensory cells, orchestrate parasite type 2 immunity in the gut. *Science* 351:1329-1333.

Hoyler, T., C.S. Klose, A. Souabni, A. Turqueti-Neves, D. Pfeifer, E.L. Rawlins, D. Voehringer, M. Busslinger, and A. Diefenbach. 2012. The transcription factor GATA-3 controls cell fate and maintenance of type 2 innate lymphoid cells. *Immunity* 37:634-648.

Huang, Y., K. Mao, X. Chen, M.A. Sun, T. Kawabe, W. Li, N. Usher, J. Zhu, J.F. Urban, Jr., W.E. Paul, and R.N. Germain. 2018. S1P-dependent interorgan trafficking of group 2 innate lymphoid cells supports host defense. *Science* 359:114-119.

Hung, L.Y., I.P. Lewkowich, L.A. Dawson, J. Downey, Y. Yang, D.E. Smith, and D.R. Herbert. 2013. IL-33 drives biphasic IL-13 production for noncanonical Type 2 immunity against hookworms. *Proc Natl Acad Sci U S A* 110:282-287.

Huntington, N.D., C.A. Vosshenrich, and J.P. Di Santo. 2007. Developmental pathways that generate natural-killer-cell diversity in mice and humans. *Nat Rev Immunol* 7:703-714.

Jarick, K.J., P.M. Topczewska, M.O. Jakob, H. Yano, M. Arifuzzaman, X. Gao, S. Boulekou, V. Stokic-Trtica, P.S. Leclere, A. Preusser, Z.A. Rompe, A. Stamm, A.M. Tsou, C. Chu, F.R. Heinrich, G.M. Guerra, P. Durek, A. Ivanov, D. Beule, S. Helfrich, C.U. Duerr, A.A. Kuhl, C. Stehle, C. Romagnani, M.F. Mashreghi, A. Diefenbach, D. Artis, and C.S.N. Klose. 2022. Non-redundant functions of group 2 innate lymphoid cells. *Nature* 611:794-800.

Karagiannis, F., S.K. Masouleh, K. Wunderling, J. Surendar, V. Schmitt, A. Kazakov, M. Michla, M. Holzel, C. Thiele, and C. Wilhelm. 2020. Lipid-Droplet Formation Drives Pathogenic Group 2 Innate Lymphoid Cells in Airway Inflammation. *Immunity* 52:620-634 e626.

Karta, M.R., P.S. Rosenthal, A. Beppu, C.Y. Vuong, M. Miller, S. Das, R.C. Kurten, T.A. Doherty, and D.H. Broide. 2018. beta2 integrins rather than beta1 integrins mediate Alternaria-induced group 2 innate lymphoid cell trafficking to the lung. *J Allergy Clin Immunol* 141:329-338 e312.

Kiessling, R., E. Klein, and H. Wigzell. 1975. "Natural" killer cells in the mouse. I. Cytotoxic cells with specificity for mouse Moloney leukemia cells. Specificity and distribution according to genotype. *Eur J Immunol* 5:112-117.

Kim, D.H., and S.J. Van Dyken. 2020. ILC2s in High Definition: Decoding the Logic of Tissue-Based Immunity. *Trends Immunol* 41:7-16.

Kim, M.H., E.J. Taparowsky, and C.H. Kim. 2015. Retinoic Acid Differentially Regulates the Migration of Innate Lymphoid Cell Subsets to the Gut. *Immunity* 43:107-119.

Kindermann, M., L. Knipfer, I. Atreya, and S. Wirtz. 2018. ILC2s in infectious diseases and organ-specific fibrosis. *Semin Immunopathol* 40:379-392.

Klose, C.S.N., and D. Artis. 2020. Innate lymphoid cells control signaling circuits to regulate tissue-specific immunity. *Cell Res* 30:475-491.

Klose, C.S.N., M. Flach, L. Mohle, L. Rogell, T. Hoyler, K. Ebert, C. Fabiunke, D. Pfeifer, V. Sexl, D. Fonseca-Pereira, R.G. Domingues, H. Veiga-Fernandes, S.J. Arnold, M. Busslinger, I.R. Dunay, Y. Tanriver, and A. Diefenbach. 2014. Differentiation of type 1 ILCs from a common progenitor to all helper-like innate lymphoid cell lineages. *Cell* 157:340-356.

Lavin, Y., D. Winter, R. Blecher-Gonen, E. David, H. Keren-Shaul, M. Merad, S. Jung, and I. Amit. 2014. Tissue-resident macrophage enhancer landscapes are shaped by the local microenvironment. *Cell* 159:1312-1326.

Law, B.M.P., R. Wilkinson, X. Wang, K. Kildey, M. Lindner, M.J. Rist, K. Beagley, H. Healy, and A.J. Kassianos. 2017. Interferon-gamma production by tubulointerstitial human CD56(bright) natural killer cells contributes to renal fibrosis and chronic kidney disease progression. *Kidney Int* 92:79-88.

Li, D., R. Guabiraba, A.G. Besnard, M. Komai-Koma, M.S. Jabir, L. Zhang, G.J. Graham, M. Kurowska-Stolarska, F.Y. Liew, C. McSharry, and D. Xu. 2014. IL-33 promotes ST2-dependent lung fibrosis by the induction of alternatively activated macrophages and innate lymphoid cells in mice. *J Allergy Clin Immunol* 134:1422-1432 e1411.

Male, V., I. Nisoli, T. Kostrzewski, D.S. Allan, J.R. Carlyle, G.M. Lord, A. Wack, and H.J. Brady. 2014. The transcription factor E4bp4/Nfil3 controls commitment to the NK lineage and directly regulates Eomes and Id2 expression. *J Exp Med* 211:635-642.

Masopust, D., and A.G. Soerens. 2019. Tissue-Resident T Cells and Other Resident Leukocytes. *Annu Rev Immunol* 37:521-546.

McFarland, A.P., A. Yalin, S.Y. Wang, V.S. Cortez, T. Landsberger, R. Sudan, V. Peng, H.L. Miller, B. Ricci, E. David, R. Faccio, I. Amit, and M. Colonna. 2021. Multi-tissue single-cell analysis deconstructs the complex programs of mouse natural killer and type 1 innate lymphoid cells in tissues and circulation. *Immunity* 54:1320-1337 e1324.

McHedlidze, T., M. Waldner, S. Zopf, J. Walker, A.L. Rankin, M. Schuchmann, D. Voehringer, A.N. McKenzie, M.F. Neurath, S. Pflanz, and S. Wirtz. 2013. Interleukin-33-dependent innate lymphoid cells mediate hepatic fibrosis. *Immunity* 39:357-371.

Mebius, R.E.R., P. Weissman, I.L. 1997. Developing lymph nodes collect CD4+CD3-LTbeta+ cells that can differentiate to APC, NK cells, and follicular cells but not T or B cells. *Immunity* 7:493-504.

Meiners, J., M. Reitz, N. Rudiger, J.E. Turner, L. Heepmann, L. Rudolf, W. Hartmann, H.J. McSorley, and M. Breloer. 2020. IL-33 facilitates rapid expulsion of the parasitic nematode Strongyloides ratti from the intestine via ILC2- and IL-9-driven mast cell activation. *PLoS Pathog* 16:e1009121.

Meininger, I., A. Carrasco, A. Rao, T. Soini, E. Kokkinou, and J. Mjosberg. 2020. Tissue-Specific Features of Innate Lymphoid Cells. *Trends Immunol* 41:902-917.

Molofsky, A.B., F. Van Gool, H.E. Liang, S.J. Van Dyken, J.C. Nussbaum, J. Lee, J.A. Bluestone, and R.M. Locksley. 2015. Interleukin-33 and Interferon-gamma Counter-Regulate Group 2 Innate Lymphoid Cell Activation during Immune Perturbation. *Immunity* 43:161-174.

Monticelli, L.A., L.C. Osborne, M. Noti, S.V. Tran, D.M. Zaiss, and D. Artis. 2015. IL-33 promotes an innate immune pathway of intestinal tissue protection dependent on amphiregulin-EGFR interactions. *Proc Natl Acad Sci U S A* 112:10762-10767.

Monticelli, L.A., G.F. Sonnenberg, M.C. Abt, T. Alenghat, C.G. Ziegler, T.A. Doering, J.M. Angelosanto, B.J. Laidlaw, C.Y. Yang, T. Sathaliyawala, M. Kubota, D. Turner, J.M. Diamond, A.W. Goldrath, D.L. Farber, R.G. Collman, E.J. Wherry, and D. Artis. 2011. Innate lymphoid cells promote lung-tissue homeostasis after infection with influenza virus. *Nat Immunol* 12:1045-1054.

Moro, K., H. Kabata, M. Tanabe, S. Koga, N. Takeno, M. Mochizuki, K. Fukunaga, K. Asano, T. Betsuyaku, and S. Koyasu. 2016. Interferon and IL-27 antagonize the function of group 2 innate lymphoid cells and type 2 innate immune responses. *Nat Immunol* 17:76-86.

Moro, K., T. Yamada, M. Tanabe, T. Takeuchi, T. Ikawa, H. Kawamoto, J. Furusawa, M. Ohtani, H. Fujii, and S. Koyasu. 2010. Innate production of T(H)2 cytokines by adipose tissue-associated c-Kit(+)Sca-1(+) lymphoid cells. *Nature* 463:540-544.

Murphy, J.M., L. Ngai, A. Mortha, and S.Q. Crome. 2022. Tissue-Dependent Adaptations and Functions of Innate Lymphoid Cells. *Front Immunol* 13:836999.

Neill, D.R., S.H. Wong, A. Bellosi, R.J. Flynn, M. Daly, T.K. Langford, C. Bucks, C.M. Kane, P.G. Fallon, R. Pannell, H.E. Jolin, and A.N. McKenzie. 2010. Nuocytes represent a new innate effector leukocyte that mediates type-2 immunity. *Nature* 464:1367-1370.

Nussbaum, K., S.H. Burkhard, I. Ohs, F. Mair, C.S.N. Klose, S.J. Arnold, A. Diefenbach, S. Tugues, and B. Becher. 2017. Tissue microenvironment dictates the fate and tumor-suppressive function of type 3 ILCs. *J Exp Med* 214:2331-2347.

O'Sullivan, T.E. 2019. Dazed and Confused: NK Cells. *Front Immunol* 10:2235.

Oherle, K., E. Acker, M. Bonfield, T. Wang, J. Gray, I. Lang, J. Bridges, I. Lewkowich, Y. Xu, S. Ahlfeld, W. Zacharias, T. Alenghat, and H. Deshmukh. 2020. Insulin-like Growth Factor 1 Supports a Pulmonary Niche that Promotes Type 3 Innate Lymphoid Cell Development in Newborn Lungs. *Immunity* 52:275-294 e279.

Oliphant, C.J., Y.Y. Hwang, J.A. Walker, M. Salimi, S.H. Wong, J.M. Brewer, A. Englezakis, J.L. Barlow, E. Hams, S.T. Scanlon, G.S. Ogg, P.G. Fallon, and A.N. McKenzie. 2014. MHCII-mediated dialog between group 2 innate lymphoid cells and CD4(+) T cells potentiates type 2 immunity and promotes parasitic helminth expulsion. *Immunity* 41:283-295.

Onder, L., U. Morbe, N. Pikor, M. Novkovic, H.W. Cheng, T. Hehlgans, K. Pfeffer, B. Becher, A. Waisman, T. Rulicke, J. Gommerman, C.G. Mueller, S. Sawa, E. Scandella, and B. Ludewig. 2017. Lymphatic Endothelial Cells Control Initiation of Lymph Node Organogenesis. *Immunity* 47:80-92 e84.

Pavord, I.D., S. Korn, P. Howarth, E.R. Bleecker, R. Buhl, O.N. Keene, H. Ortega, and P. Chanez. 2012. Mepolizumab for severe eosinophilic asthma (DREAM): a multicentre, double-blind, placebo-controlled trial. *Lancet* 380:651-659.

Peng, H., X. Jiang, Y. Chen, D.K. Sojka, H. Wei, X. Gao, R. Sun, W.M. Yokoyama, and Z. Tian. 2013. Liver-resident NK cells confer adaptive immunity in skin-contact inflammation. *J Clin Invest* 123:1444-1456.

Peng, H., and Z. Tian. 2017. Diversity of tissue-resident NK cells. *Semin Immunol* 31:3-10.

Perugorria, M.J., M.U. Latasa, A. Nicou, H. Cartagena-Lirola, J. Castillo, S. Goni, U. Vespasiani-Gentilucci, M.G. Zagami, S. Lotersztajn, J. Prieto, C. Berasain, and M.A. Avila. 2008. The epidermal growth factor receptor ligand amphiregulin participates in the development of mouse liver fibrosis. *Hepatology* 48:1251-1261.

Piper, E., C. Brightling, R. Niven, C. Oh, R. Faggioni, K. Poon, D. She, C. Kell, R.D. May, G.P. Geba, and N.A. Molfino. 2013. A phase II placebo-controlled study of tralokinumab in moderate-to-severe asthma. *Eur Respir J* 41:330-338.

Puttur, F., L. Denney, L.G. Gregory, J. Vuononvirta, R. Oliver, L.J. Entwistle, S.A. Walker, M.B. Headley, E.J. McGhee, J.E. Pease, M.F. Krummel, L.M. Carlin,

and C.M. Lloyd. 2019. Pulmonary environmental cues drive group 2 innate lymphoid cell dynamics in mice and humans. *Sci Immunol* 4:

Ramalingam, T.R., R.L. Gieseck, T.H. Acciani, M.H. K, A.W. Cheever, M.M. Mentink-Kane, K.M. Vannella, and T.A. Wynn. 2016. Enhanced protection from fibrosis and inflammation in the combined absence of IL-13 and IFN-gamma. *J Pathol* 239:344-354.

Reitz, M., W. Hartmann, N. Rudiger, Z. Orinska, M.L. Brunn, and M. Breloer. 2018. Interleukin-9 promotes early mast cell-mediated expulsion of Strongyloides ratti but is dispensable for generation of protective memory. *Sci Rep* 8:8636.

Ricardo-Gonzalez, R.R., C. Schneider, C. Liao, J. Lee, H.E. Liang, and R.M. Locksley. 2020. Tissue-specific pathways extrude activated ILC2s to disseminate type 2 immunity. *J Exp Med* 217:

Ricardo-Gonzalez, R.R., S.J. Van Dyken, C. Schneider, J. Lee, J.C. Nussbaum, H.E. Liang, D. Vaka, W.L. Eckalbar, A.B. Molofsky, D.J. Erle, and R.M. Locksley. 2018. Tissue signals imprint ILC2 identity with anticipatory function. *Nat Immunol* 19:1093-1099.

Riedel, J.H., M. Becker, K. Kopp, M. Duster, S.R. Brix, C. Meyer-Schwesinger, L.A. Kluth, A.C. Gnirck, M. Attar, S. Krohn, B. Fehse, R.A.K. Stahl, U. Panzer, and J.E. Turner. 2017. IL-33-Mediated Expansion of Type 2 Innate Lymphoid Cells Protects from Progressive Glomerulosclerosis. *J Am Soc Nephrol* 28:2068-2080.

Riggan, L., A.G. Freud, and T.E. O'Sullivan. 2019. True Detective: Unraveling Group 1 Innate Lymphocyte Heterogeneity. *Trends Immunol* 40:909-921.

Roquilly, A., J.D. Mintern, and J.A. Villadangos. 2022. Spatiotemporal Adaptations of Macrophage and Dendritic Cell Development and Function. *Annu Rev Immunol* 40:525-557.

Rothenberg, M.E.K., A.D., F.E. Roufosse, J.E. Kahn, P.F. Weller, H.U. Simon, L.B. Schwartz, L.J. Rosenwasser, J. Ring, E.F. Griffin, A.E. Haig, P.I. Frewer, J.M. Parkin, and G.J. Gleich. 2008. Mepolizumab HES Study Group. Treatment of patients with the hypereosinophilic syndrome with mepolizumab. *N Engl J Med* 358:1215-1228.

Ruckert, T., C.A. Lareau, M.F. Mashreghi, L.S. Ludwig, and C. Romagnani. 2022. Clonal expansion and epigenetic inheritance of long-lasting NK cell memory. *Nat Immunol* 23:1551-1563.

Russi, A.E., M.E. Walker-Caulfield, M.E. Ebel, and M.A. Brown. 2015. Cutting edge: c-Kit signaling differentially regulates type 2 innate lymphoid cell accumulation and susceptibility to central nervous system demyelination in male and female SJL mice. *J Immunol* 194:5609-5613.

Satoh-Takayama, N., S. Lesjean-Pottier, P. Vieira, S. Sawa, G. Eberl, C.A. Vosshenrich, and J.P. Di Santo. 2010. IL-7 and IL-15 independently program

the differentiation of intestinal CD3-NKp46+ cell subsets from Id2-dependent precursors. *J Exp Med* 207:273-280.

Sawa, S., M. Lochner, N. Satoh-Takayama, S. Dulauroy, M. Berard, M. Kleinschek, D. Cua, J.P. Di Santo, and G. Eberl. 2011. RORgammat+ innate lymphoid cells regulate intestinal homeostasis by integrating negative signals from the symbiotic microbiota. *Nat Immunol* 12:320-326.

Schneider, C., J. Lee, S. Koga, R.R. Ricardo-Gonzalez, J.C. Nussbaum, L.K. Smith, S.A. Villeda, H.E. Liang, and R.M. Locksley. 2019. Tissue-Resident Group 2 Innate Lymphoid Cells Differentiate by Layered Ontogeny and In Situ Perinatal Priming. *Immunity* 50:1425-1438 e1425.

Seehus, C.R., P. Aliahmad, B. de la Torre, I.D. Iliev, L. Spurka, V.A. Funari, and J. Kaye. 2015. The development of innate lymphoid cells requires TOX-dependent generation of a common innate lymphoid cell progenitor. *Nat Immunol* 16:599-608.

Seehus, C.R., A. Kadavallore, B. Torre, A.R. Yeckes, Y. Wang, J. Tang, and J. Kaye. 2017. Alternative activation generates IL-10 producing type 2 innate lymphoid cells. *Nat Commun* 8:1900.

Serafini, N., R.G. Klein Wolterink, N. Satoh-Takayama, W. Xu, C.A. Vosshenrich, R.W. Hendriks, and J.P. Di Santo. 2014. Gata3 drives development of RORgammat+ group 3 innate lymphoid cells. *J Exp Med* 211:199-208.

Sojka, D.K., B. Plougastel-Douglas, L. Yang, M.A. Pak-Wittel, M.N. Artyomov, Y. Ivanova, C. Zhong, J.M. Chase, P.B. Rothman, J. Yu, J.K. Riley, J. Zhu, Z. Tian, and W.M. Yokoyama. 2014. Tissue-resident natural killer (NK) cells are cell lineages distinct from thymic and conventional splenic NK cells. *Elife* 3:e01659.

Spada, R., J.M. Rojas, S. Perez-Yague, V. Mulens, P. Cannata-Ortiz, R. Bragado, and D.F. Barber. 2015. NKG2D ligand overexpression in lupus nephritis correlates with increased NK cell activity and differentiation in kidneys but not in the periphery. *J Leukoc Biol* 97:583-598.

Spits, H., D. Artis, M. Colonna, A. Diefenbach, J.P. Di Santo, G. Eberl, S. Koyasu, R.M. Locksley, A.N. McKenzie, R.E. Mebius, F. Powrie, and E. Vivier. 2013. Innate lymphoid cells--a proposal for uniform nomenclature. *Nat Rev Immunol* 13:145-149.

Spits, H., J.H. Bernink, and L. Lanier. 2016. NK cells and type 1 innate lymphoid cells: partners in host defense. *Nature Immunology* 17:758-764.

Spits, H., and J.P. Di Santo. 2011. The expanding family of innate lymphoid cells: regulators and effectors of immunity and tissue remodeling. *Nat Immunol* 12:21-27.

Spits, H., and J. Mjosberg. 2022. Heterogeneity of type 2 innate lymphoid cells. *Nat Rev Immunol*

Spooner, C.J., J. Lesch, D. Yan, A.A. Khan, A. Abbas, V. Ramirez-Carrozzi, M. Zhou, R. Soriano, J. Eastham-Anderson, L. Diehl, W.P. Lee, Z. Modrusan, R. Pappu, M. Xu, J. DeVoss, and H. Singh. 2013. Specification of type 2 innate lymphocytes by the transcriptional determinant Gfi1. *Nat Immunol* 14:1229-1236.

Stier, M.T., J. Zhang, K. Goleniewska, J.Y. Cephus, M. Rusznak, L. Wu, L. Van Kaer, B. Zhou, D.C. Newcomb, and R.S. Peebles, Jr. 2018. IL-33 promotes the egress of group 2 innate lymphoid cells from the bone marrow. *J Exp Med* 215:263-281.

Straub, T., M.A. Freudenberg, U. Schleicher, C. Bogdan, G. Gasteiger, and H. Pircher. 2018. Bacterial coinfection restrains antiviral CD8 T-cell response via LPS-induced inhibitory NK cells. *Nat Commun* 9:4117.

Turner, J.E., P.J. Morrison, C. Wilhelm, M. Wilson, H. Ahlfors, J.C. Renauld, U. Panzer, H. Helmby, and B. Stockinger. 2013. IL-9-mediated survival of type 2 innate lymphoid cells promotes damage control in helminth-induced lung inflammation. *J Exp Med* 210:2951-2965.

Turner, J.E., C. Rickassel, H. Healy, and A.J. Kassianos. 2019. Natural Killer Cells in Kidney Health and Disease. *Front Immunol* 10:587.

Victorino, F., D.K. Sojka, K.S. Brodsky, E.N. McNamee, J.C. Masterson, D. Homann, W.M. Yokoyama, H.K. Eltzschig, and E.T. Clambey. 2015. Tissue-Resident NK Cells Mediate Ischemic Kidney Injury and Are Not Depleted by Anti-Asialo-GM1 Antibody. *J Immunol* 195:4973-4985.

Vivier, E., D. Artis, M. Colonna, A. Diefenbach, J.P. Di Santo, G. Eberl, S. Koyasu, R.M. Locksley, A.N.J. McKenzie, R.E. Mebius, F. Powrie, and H. Spits. 2018. Innate Lymphoid Cells: 10 Years On. *Cell* 174:1054-1066.

von Moltke, J., M. Ji, H.E. Liang, and R.M. Locksley. 2016. Tuft-cell-derived IL-25 regulates an intestinal ILC2-epithelial response circuit. *Nature* 529:221-225.

Waggoner, S.N., R.T. Taniguchi, P.A. Mathew, V. Kumar, and R.M. Welsh. 2010. Absence of mouse 2B4 promotes NK cell-mediated killing of activated CD8+ T cells, leading to prolonged viral persistence and altered pathogenesis. *J Clin Invest* 120:1925-1938.

Walker, J.A., J.L. Barlow, and A.N. McKenzie. 2013. Innate lymphoid cells--how did we miss them? *Nat Rev Immunol* 13:75-87.

Walker, J.A., C.J. Oliphant, A. Englezakis, Y. Yu, S. Clare, H.R. Rodewald, G. Belz, P. Liu, P.G. Fallon, and A.N. McKenzie. 2015. Bcl11b is essential for group 2 innate lymphoid cell development. *J Exp Med* 212:875-882.

Wang, D., and S. Malarkannan. 2020. Transcriptional Regulation of Natural Killer Cell Development and Functions. *Cancers (Basel)* 12:

Weizman, O.E., N.M. Adams, I.S. Schuster, C. Krishna, Y. Pritykin, C. Lau, M.A. Degli-Esposti, C.S. Leslie, J.C. Sun, and T.E. O'Sullivan. 2017. ILC1 Confer Early Host Protection at Initial Sites of Viral Infection. *Cell* 171:795-808 e712.

Weizman OE, A.N., Schuster IS, Krishna C, Pritykin Y, Lau C, Degli-Esposti MA, Leslie CS, Sun JC, O'Sullivan TE. 2017. ILC1 Confer Early Host Protection at Initial Sites of Viral Infection. *Cell* 171:795-808.

Wong, S.H., J.A. Walker, H.E. Jolin, L.F. Drynan, E. Hams, A. Camelo, J.L. Barlow, D.R. Neill, V. Panova, U. Koch, F. Radtke, C.S. Hardman, Y.Y. Hwang, P.G. Fallon, and A.N. McKenzie. 2012. Transcription factor RORalpha is critical for nuocyte development. *Nat Immunol* 13:229-236.

Xu, W., R.G. Domingues, D. Fonseca-Pereira, M. Ferreira, H. Ribeiro, S. Lopez-Lastra, Y. Motomura, L. Moreira-Santos, F. Bihl, V. Braud, B. Kee, H. Brady, M.C. Coles, C. Vosshenrich, M. Kubo, J.P. Di Santo, and H. Veiga-Fernandes. 2015. NFIL3 orchestrates the emergence of common helper innate lymphoid cell precursors. *Cell Rep* 10:2043-2054.

Yagi, R., C. Zhong, D.L. Northrup, F. Yu, N. Bouladoux, S. Spencer, G. Hu, L. Barron, S. Sharma, T. Nakayama, Y. Belkaid, K. Zhao, and J. Zhu. 2014. The transcription factor GATA3 is critical for the development of all IL-7Ralpha-expressing innate lymphoid cells. *Immunity* 40:378-388.

Yang, J., S. Hu, L. Zhao, D.H. Kaplan, G.H. Perdew, and N. Xiong. 2016. Selective programming of CCR10(+) innate lymphoid cells in skin-draining lymph nodes for cutaneous homeostatic regulation. *Nat Immunol* 17:48-56.

Yang, Q., F. Li, C. Harly, S. Xing, L. Ye, X. Xia, H. Wang, X. Wang, S. Yu, X. Zhou, M. Cam, H.H. Xue, and A. Bhandoola. 2015. TCF-1 upregulation identifies early innate lymphoid progenitors in the bone marrow. *Nat Immunol* 16:1044-1050.

Yoshida, H., K. Honda, R. Shinkura, S. Adachi, S. Nishikawa, K. Maki, K. Ikuta, and S.I. Nishikawa. 1999. IL-7 receptor alpha+ CD3(-) cells in the embryonic intestine induces the organizing center of Peyer's patches. *Int Immunol* 11:643-655.

Yu, X., Y. Wang, M. Deng, Y. Li, K.A. Ruhn, C.C. Zhang, and L.V. Hooper. 2014. The basic leucine zipper transcription factor NFIL3 directs the development of a common innate lymphoid cell precursor. *Elife* 3:

Zang, Y., S. Liu, Z. Rao, Y. Wang, B. Zhang, H. Li, Y. Cao, J. Zhou, Z. Shen, S. Duan, D. He, and H. Xu. 2023. Retinoid X receptor gamma dictates the activation threshold of group 2 innate lymphoid cells and limits type 2 inflammation in the small intestine. *Immunity* 56:2542-2554.

Zeis, P., M. Lian, X. Fan, J.S. Herman, D.C. Hernandez, R. Gentek, S. Elias, C. Symowski, K. Knopper, N. Peltokangas, C. Friedrich, R. Doucet-Ladeveze, A.M. Kabat, R.M. Locksley, D. Voehringer, M. Bajenoff, A.Y. Rudensky, C. Romagnani, D. Grun, and G. Gasteiger. 2020. In Situ Maturation and Tissue Adaptation of Type 2 Innate Lymphoid Cell Progenitors. *Immunity* 53:775-792 e779.

Zhang, J., J. Qiu, W. Zhou, J. Cao, X. Hu, W. Mi, B. Su, B. He, J. Qiu, and L. Shen. 2022. Neuropilin-1 mediates lung tissue-specific control of ILC2 function in type 2 immunity. *Nat Immunol* 23:237-250.

Zhang, K., X. Xu, M.A. Pasha, C.W. Siebel, A. Costello, A. Haczku, K. MacNamara, T. Liang, J. Zhu, A. Bhandoola, I. Maillard, and Q. Yang. 2017. Cutting Edge: Notch Signaling Promotes the Plasticity of Group-2 Innate Lymphoid Cells. *J Immunol* 198:1798-1803.

Zhang, Z.X., X. Huang, J. Jiang, A. Lau, Z. Yin, W. Liu, A. Haig, and A.M. Jevnikar. 2015. Natural Killer Cells Mediate Long-term Kidney Allograft Injury. *Transplantation* 99:916-924.

Zhang, Z.X., K. Shek, S. Wang, X. Huang, A. Lau, Z. Yin, H. Sun, W. Liu, B. Garcia, S. Rittling, and A.M. Jevnikar. 2010. Osteopontin expressed in tubular epithelial cells regulates NK cell-mediated kidney ischemia reperfusion injury. *J Immunol* 185:967-973.

Zheng, G., L. Zheng, Y. Wang, H. Wu, L. Kairaitis, C. Zhang, Y.C. Tay, Y. Wang, S.I. Alexander, and D.C. Harris. 2006. NK cells do not mediate renal injury in murine adriamycin nephropathy. *Kidney Int* 69:1159-1165.

Zhou, Y., J.Y. Lee, C.M. Lee, W.K. Cho, M.J. Kang, J.L. Koff, P.O. Yoon, J. Chae, H.O. Park, J.A. Elias, and C.G. Lee. 2012. Amphiregulin, an epidermal growth factor receptor ligand, plays an essential role in the pathogenesis of transforming growth factor-beta-induced pulmonary fibrosis. *J Biol Chem* 287:41991-42000.

Zhu, P., X. Zhu, J. Wu, L. He, T. Lu, Y. Wang, B. Liu, B. Ye, L. Sun, D. Fan, J. Wang, L. Yang, X. Qin, Y. Du, C. Li, L. He, W. Ren, X. Wu, Y. Tian, and Z. Fan. 2019. IL-13 secreted by ILC2s promotes the self-renewal of intestinal stem cells through circular RNA circPan3. *Nat Immunol* 20:183-194.

9. Acknowledgements

I would first like to express my gratitude to Prof. Dr. Tobias B. Huber for the possibility to perform my doctoral thesis in the III. Department of Medicine in UKE. I would like also to thank Prof. Dr. Ulf Panzer for the possibility to contribute to a participating project in SFB1192 and for his scientific engagement and providing an encouraging environment for young scientists to make academic progress.

I would like to express my heartiest gratitude to my doctoral supervisor Prof. Dr. Jan-Eric Turner for his continued support and guidance throughout my thesis. His mentoring, leadership, and goal-oriented approach to research have greatly shaped my academic development. I also appreciate his enthusiasm for science and for helping students become an independent thinker by providing intellectual discussions and challenging our problem-solving skills.

I would also like to extend my appreciation to Ann-Christin for her mentoring, Gini for her friendship and excellent technical support, and Alex for humouring and dancing with me at any given opportunity. I am grateful for their continuous help and unwavering support as well as encouragement throughout my project. They have provided a fun, relaxed, and comfortable working environment. I would like to also especially mention the other members of Turner Lab (Lena, Malte, Nick and Martina) who have been pivotal toward my project and lab life.

A special thank you to Prof. Dr. Nicola Gagliani and Prof. Dr. Hans-Willi Mittrücker for being my thesis committee members and providing valuable discussion and insights throughout the progress of my thesis.

Lastly, I would like to thank my family and friends, especially Ahmed and Marina, without whom the PhD journey would not have been successful. The emotional and mental support from them has been invaluable to continue moving forward toward completion. Most importantly, with great love and respect in my heart, I would like to dedicate this thesis to my parents and my late grandfather who have always encouraged me to pursue education with their unconditional support even with limited resources and possibilities at hand.

10. Curriculum vitae

Lebenslauf entfällt aus datenschutzrechtlichen Gründen.

10. Curriculum vitae

11. Declaration of own contribution to the publications

Retinoic acid drives intestine-specific adaptation of effector ILC2s originating from distant sites

The project hypothesis was developed by Prof. Jan-Eric Turner as the principal investigator. I carried out the project plan with the guidance of Prof. Jan-Eric Turner. I performed the experiments and analysed them independently and received critical evaluation, direction, and interpretation from Prof. Jan-Eric Turner. For complex experiments, I had help from the other lab members. I also participated in the writing, visualising, revising, and editing of the manuscript along with Prof. Jan-Eric Turner.

Conventional NK cells and type 1 innate lymphoid cells do not influence pathogenesis of experimental glomerulonephritis

The project hypothesis was developed by Prof. Jan-Eric Turner as the principal investigator. Together with Prof. Jan-Eric Turner's advice, I helped establish the panel and perform immunofluorescence staining for confocal microscopy for the study. I also participated during revision and review of the manuscript.

12. Affidavit

Ich versichere ausdrücklich, dass ich die Arbeit selbständig und ohne fremde Hilfe verfasst, andere als die von mir angegebenen Quellen und Hilfsmittel nicht benutzt und die aus den benutzten Werken wörtlich oder inhaltlich entnommenen Stellen einzeln nach Ausgabe (Auflage und Jahr des Erscheinens), Band und Seite des benutzten Werkes kenntlich gemacht habe.

Ferner versichere ich, dass ich die Dissertation bisher nicht einem Fachvertreter an einer anderen Hochschule zur Überprüfung vorgelegt oder mich anderweitig um Zulassung zur Promotion beworben habe.

Ich erkläre mich einverstanden, dass meine Dissertation vom Dekanat der Medizinischen Fakultät mit einer gängigen Software zur Erkennung von Plagiaten überprüft werden kann.

Unterschrift: ....

13. Publications

ARTICLE

Retinoic acid drives intestine-specific adaptation of effector ILC2s originating from distant sites

Nikhat Shaikh[1,2], Alex Waterhölter[1,2], Ann-Christin Gnirck[1,2], Martina Becker[1,2], Virginia Adamiak[1,2], Lena Henneken[1,2], Malte Wunderlich[1,2], Wiebke Hartmann[3], Lara Linnemann[3], Tobias B. Huber[1], Christian F. Krebs[2,4], Ulf Panzer[2,4], Richard M. Locksley[5], Christoph Wilhelm[6], Minka Breloer[3], and Jan-Eric Turner[1,2]

Adaptation of immune cells to tissue-specific microenvironments is a crucial process in homeostasis and inflammation. Here, we show that murine effector type 2 innate lymphoid cells (ILC2s) from various organs are equally effective in repopulating ILC2 niches in other anatomical locations where they adapt tissue-specific phenotypes of target organs. Single-cell transcriptomics of ILC2 populations revealed upregulation of retinoic acid (RA) signaling in ILC2s during adaptation to the small intestinal microenvironment, and RA signaling mediated reprogramming of kidney effector ILC2s toward the small intestinal phenotype in vitro and in vivo. Inhibition of intestinal ILC2 adaptation by blocking RA signaling impaired worm expulsion during *Strongyloides ratti* infection, indicating functional importance of ILC2 tissue imprinting. In conclusion, this study highlights that effector ILC2s retain the ability to adapt to changing tissue-specific microenvironments, enabling them to exert tissue-specific functions, such as promoting control of intestinal helminth infections.

Introduction

Group 2 innate lymphoid cells (ILC2s) have emerged as important regulators of type 2 immune responses in helminth infection and allergic diseases. In the context of tissue injury, ILC2s facilitate repair processes and restoration of homeostasis by producing mediators that instruct other immune cells, directly stimulate proliferation of epithelial cells, and promote extracellular matrix remodeling (Klose and Artis, 2016). Thus, in recent years, therapeutic targeting of ILC2s has been identified as a potential strategy to enhance tissue regeneration in acute and chronic inflammation of various organs, e.g., the lung, kidney, and intestine (Düster et al., 2018; Monticelli et al., 2011, 2015; Riedel et al., 2017; Turner et al., 2013). Uncontrolled activation of ILC2s, however, can have deleterious side effects and result in organ-specific fibrosis (Hams et al., 2014; McHedlidze et al., 2013). With regard to the suitability of ILC2s as a therapeutic target, this dichotomy requires careful evaluation of ILC2 responsiveness and effector mechanisms in different anatomical locations.

ILC2s are equipped with a wide array of receptors to sense, integrate, and respond to local cues provided by other immune cells, epithelial cells, and stromal cells of the tissue niche they reside in (Karagiannis and Wilhelm 2018; Klose and Artis, 2016). Accordingly, recent studies have demonstrated that ILC2s in different non-lymphoid organs are phenotypically and functionally distinct (Gadani et al., 2017; Ricardo-Gonzalez et al., 2018; Simoni et al., 2017). Mature effector ILC2s in peripheral tissues can differentiate locally from progenitor populations (Bando et al., 2015; Zeis et al., 2020) that either seed non-lymphoid organs during fetal development and early postnatal life (Bando et al., 2015; Schneider et al., 2019) or may derive from ILC progenitors recruited from distant sites, such as the bone marrow (Bar-Ephraim et al., 2019; Lim et al., 2017; Zeis et al., 2020). While local intratissue differentiation seems to be the main mechanism for ILC2 renewal and expansion in homeostasis and acute inflammation (Gasteiger et al., 2015; Zeis et al., 2020), in chronic inflammation, ILC progenitors recruited from the circulation, and potentially, interorgan trafficking of mature ILC2s can contribute to replenishment of the ILC2 pool in affected tissues (Huang et al., 2018; Ricardo-Gonzalez et al., 2020).

[1]III. Department of Medicine, University Medical Center Hamburg-Eppendorf, Hamburg, Germany; [2]Hamburg Center for Translational Immunology, University Medical Center Hamburg-Eppendorf, Hamburg, Germany; [3]Helminth Immunology Group, Bernhard Nocht Institute for Tropical Medicine, Hamburg, Germany; [4]Division of Translational Immunology, III. Department of Medicine, University Medical Center Hamburg-Eppendorf, Hamburg, Germany; [5]Department of Medicine, Howard Hughes Medical Institute, University of California, San Francisco, San Francisco, CA, USA; [6]Unit for Immunopathology, Institute of Clinical Chemistry and Clinical Pharmacology, University Hospital Bonn, University of Bonn, Bonn, Germany.

Correspondence to Jan-Eric Turner: j.turner@uke.de

A.-C. Gnirck's current affiliation is Euroimmun, Lübeck, Germany.   M. Becker's current affiliation is Affimed, Heidelberg, Germany.

However, whether mature effector ILC2s in peripheral tissues retain phenotypic flexibility after hematogenous trafficking to other anatomical locations and which microenvironmental factors might shape organ-specific effector ILC2 adaptation and function is still unclear.

Here, we show that upon adoptive transfer into alymphoid recipients, murine effector ILC2s isolated from various non-lymphoid organs are equally effective in repopulating ILC2 niches in other peripheral tissues, arguing against the preferential organ-specific homing of ILC2 populations. Transferred effector ILC2s acquired the tissue-specific phenotype of organs they came to reside in—a process we refer to as "tissue adaptation." Adaptation to the small intestinal microenvironment required retinoic acid (RA) signaling in ILC2s and inhibition of intestinal ILC2 adaptation by blocking RA signaling impaired worm expulsion after *Strongyloides ratti* infection.

In summary, we provide evidence for retained flexibility of mature effector ILC2s to adapt to new tissue microenvironments with important implications for organ-specific ILC2 functions, and potentially, for organ-specific therapeutic targeting of these cells.

Results

Organ-specific subset distribution and phenotype of ILC2s

Therapeutic targeting of ILCs has been identified as a potential strategy to enhance tissue repair in various organs, e.g., the kidney, lung, and intestine (Düster et al., 2018; Monticelli et al., 2011, 2015; Riedel et al., 2017; Turner et al., 2013). To evaluate ILC responsiveness and effector mechanisms in different anatomical locations, we first analyzed organ-specific subset distribution of helper-like ILCs under homeostatic conditions in the kidney, lung, and small intestinal lamina propria (SILP) of naïve C57BL/6 and BALB/c mice by flow cytometry (Fig. 1, A–C; and Fig. S1). These analyses identified GATA3+ ILC2s as a major ILC subset in all the three tissues. As previously described (Penny et al., 2018), RORγt+ ILC3s were abundant in SILP; however, they were scarce in the lungs and kidneys of naïve mice. CD127+NKp46+T-bet+Eomes− ILC1s represented a minor helper-like ILC population in all examined tissues (Fig. 1, A and C); however, low CD127 expression on kidney and lung ILC1s might result in an underestimation of ILC1 abundance in these locations with our gating strategy (Fig. S2, A and B).

In the following, we focused on the ILC2 populations found in all three organs. To explore how tissue-specific factors shape the transcriptome of ILC2s in different anatomical locations at steady state, we next performed bulk RNA sequencing (RNAseq) of ILC2s purified by flow cytometry from kidney, lung, and SILP of naïve mice (Fig. 1, D–F). The sorting strategy was designed based on the ILC2 surface marker expression to exclude potential transcriptional alterations by reporter transgenes (Fig. S2, B–C). To obtain high purity (99%, Fig. S2 C) and coverage (>80%, Fig. S2 D) of the Lin−CD127+GATA3+ ILC2 population, a combination of Sca-1 and CD25 was found to be optimal for ILC2 isolation from kidney and lung, while SILP ILC2s were best identified as CD25+KLRG1+. Unbiased clustering in principal

component analyses revealed a tissue-specific distinct transcriptomic signature of ILC2s (Fig. 1 D). However, a sample distance analysis based on all detected transcripts demonstrated that kidney and lung ILC2s were transcriptionally more closely related compared with SILP ILC2s (Fig. 1 E). Several hundred transcripts were differentially expressed between ILC2s isolated from different locations (Fig. 1 F). Among these, numerous genes regulating responsiveness to environmental stimuli (cytokines and growth factors) and cell migration/adhesion were specifically up- or downregulated in each organ.

To characterize the phenotypic differences of ILC2s in the kidney, lung, and SILP with a second approach, we selected a panel of cytokine receptors and other common ILC2 surface markers and analyzed the ILC2 phenotype by flow cytometry in unchallenged C57BL/6 and BALB/c mice and after activation of ILC2s by i.p. IL-33 injection (Fig. 1, G and H; and Fig. S1, F and G). The comparison of geometric mean fluorescence intensity (MFI) of these surface markers among ILC2 populations confirmed our RNAseq results at protein level (see *Il17rb*, *Il1lr1*, and *Thy1*), e.g., with high expression of IL-17RB and KLRG1 but low expression of IL-33R and CD90.2 in small intestinal ILC2s (Fig. 1 G and Fig. S1). To visualize similarities and differences of the tissue-specific ILC2 phenotypes in an unsupervised approach, we next concatenated the flow cytometry data from different organs followed by dimensionality reduction and clustering using the Uniform Manifold Approximation and Projection (UMAP) algorithm (Fig. 1 H and Fig. S1). In line with the transcriptomic analyses, this approach revealed a substantial phenotypic overlap of kidney and lung ILC2s, while ILC2s from SILP formed a clearly separated cluster, which was preserved after IL-33 treatment.

While SILP ILC2s express much lower levels of IL-33R than kidney and lung ILC2s, they are not completely negative (compare Fig. S1 F). In line, they show accumulation and increased cytokine production in response to systemic IL-33 treatment, as used for in vivo ILC2 expansion in our experiments (Fig. 1, I–M; and Fig. S1 H). Consistent with lower IL-33R expression, IL-33–mediated in vivo ILC2 expansion was less prominent in the SILP (approximately factor 5) compared with lung and kidney (approximately factor 10–20; Fig. 1 I). Although the frequency Ki67 positivity in IL-33–expanded ILC2s at the time of analysis (2–3 wk after the first IL-33 injection) was not increased, the absolute number of Ki67+ ILC2s was significantly higher after IL-33 treatment in all organs, indicating recent proliferation (Fig. 1, J and K). The cytokine production profile differed between the three organs as SILP ILC2s, in general, produced more cytokines compared with kidney and lung ILC2s (Fig. 1, L and M), while lung ILC2s particularly showed lower IL-4 production than the other organs. The distinct surface marker phenotype (e.g., IL-33RloIL-17RBhiCD90.2loKLRG1hiICOSlo in SILP, Fig. 1 G) and cytokine production profile (Fig. 1, L and M) were preserved after application of IL-33, indicating that tissue imprinting of ILC2s is maintained during IL-33–induced ILC2 activation and expansion in the tissues.

Taken together, these data suggest that tissue-specific factors in the small intestine drive a unique ILC2/ILC3 subset distribution and a distinct ILC2 phenotype.
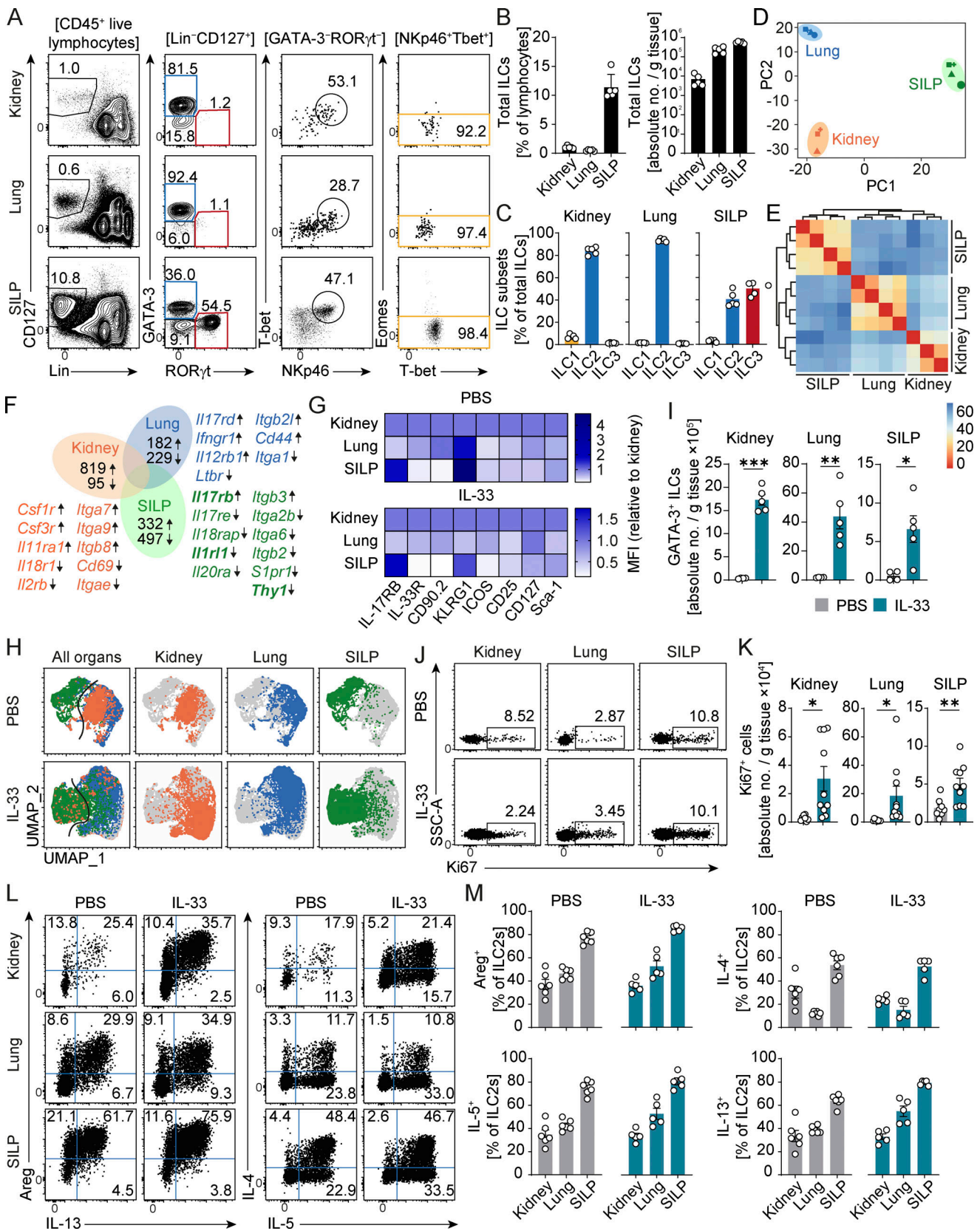
Figure 1. Organ-specific ILC subset distribution and phenotype of ILC2s. (A) Flow cytometric characterization and gating strategy of ILC subsets isolated from kidney, lung, and SILP of naïve C57BL/6 mice (blue = ILC2s, red = ILC3s, and yellow = ILC1s). Numbers indicate the percentage of events in the respective gates. **(B)** Frequencies and absolute numbers of total ILCs in kidney, lung, and SILP. **(C)** Frequencies of ILC subset distribution in the respective organs. Symbols represent individual data points and bars indicate mean ± SEM. **(D)** Principal component analysis of bulk RNAseq data from ILC2s purified from the indicated

organs by flow cytometry. ILC2s from the kidneys and lungs of C57BL/6 mice were sorted as CD45$^+$Lin$^-$CD127$^+$CD25$^+$Sca-1$^+$, whereas ILC2s from SILP were sorted as CD45$^+$Lin$^-$CD127$^+$CD25$^+$KLRG1$^+$. Symbols represent individual ILC2 samples sorted from independent pools of mice (n = 3–4 samples with five mice per pool). **(E)** Sample distance plot based on all detected transcripts in the individual samples of the three organs. **(F)** Venn diagram of differentially expressed transcripts in each tissue compared with the other two tissues (false discovery rate < 0.1 and Log$_2$FC > 1). Numbers indicate the up- (arrow up) or down-regulated (arrow down) transcripts. Selected transcripts are specified for each organ with transcripts of interest marked in bold. **(G)** Flow cytometric analysis of Lin$^-$GATA-3$^+$ ILC2s from PBS- and IL-33–treated (400 ng i.p. injection on four consecutive days) wild type C57BL/6 mice (n = 3–5 mice per group). Analyses were performed at 2–3 wk after the first injection. Heat maps show geometric MFI of various surface markers of ILC2s in the indicated organs normalized to surface marker expression of kidney ILC2s. **(H)** UMAP clustering of the flow cytometry data from G. Lin$^-$GATA-3$^+$ ILC2s of the lung, kidney, and SILP were concatenated (40,000 events for each organ), and unbiased clustering was performed. Plots show combined and single-organ contribution of kidney (orange), lung (blue), and SILP (green) ILC2s to the UMAP clustering. **(I)** Absolute numbers of Lin$^-$GATA-3$^+$ ILC2s analyzed in G. **(J and K)** Representative flow cytometry plots (J) and absolute numbers (K) of ILC2s isolated from the kidney, lung, and SILP of PBS- (n = 8) and IL-33–treated (n = 10) wild type C57BL/6 mice. **(L and M)** Representative flow cytometry plots (L) and frequencies (M) of different cytokines produced by ILC2s of PBS- (n = 6) and IL-33–treated C57BL/6 mice (n = 5). Numbers in the flow cytometry plots indicate the percentage of events in the respective gates. Data in A, B, and G–I are representative of at least two independent experiments with similar results. Data in J and K are pooled from three and in L and M are pooled from two individually performed experiments. Symbols represent individual data points, and bars indicate mean ± SEM. Statistical analysis was performed using unpaired two-tailed Student's t test (*P < 0.05, **P < 0.01, ***P < 0.001).

ILC2 phenotype is dictated by the tissue microenvironment

Next, we asked the question of whether these tissue-specific ILC2 phenotypes are irreversibly imprinted during differentiation or whether ILC2s from peripheral sites retain the ability to adapt to new tissue microenvironments. To address this, we established an adoptive transfer model in which highly purified congenitally marked ILC2s from the kidney, lung, and SILP of IL-33–treated mice were transferred into alymphoid $Rag2^{-/-}Il2rg^{-/-}$ mice, and tissue repopulation was assessed after 3 wk (Fig. 2, A–D). In these experiments, ILC2s were sorted as CD45$^+$Lin$^-$CD127$^+$KLRG1$^+$, allowing for reliable identification and high-purity sorting of ILC2s from all anatomical locations in IL-33–treated mice (Fig. S2 E and Fig. 2 B). Flow cytometric analyses of the recipient mice revealed that CD45.1$^+$ ILC2s repopulated all tissues examined, regardless of the origin of transferred ILC2 populations. The distribution of ILC2 frequencies and numbers in all kidneys, lungs, and SILP was reminiscent of wild type mice (Fig. 2, C and D; and Fig. 1, A and B). Moreover, transferred ILC2s, again regardless of their tissue of origin, adopted the surface marker expression pattern specific for the respective target organ, as seen in wild type mice without cell transfer (Fig. 2, E and F; and Fig. 1 G).

These data argue against tissue-specific homing capacity and irreversible imprinting of ILC2s during differentiation and provide evidence for continuous adaptation of mature effector ILC2s to the tissue microenvironment they reside in.

Effector ILC2s can adapt to new tissue microenvironment

Next, we wanted to investigate whether tissue adaptation of ILC2s was due to true flexibility of mature effector ILC2s rather than a result of tissue ILC progenitors that might contaminate the transferred Lin$^-$CD127$^+$KLRG1$^+$ ILC2 populations, seed the empty niches, and proliferate in target tissues. Since tissue ILC2 progenitors were recently shown to express only intermediate levels of IL-5 (Zeis et al., 2020), we sorted IL-5^{hi} effector ILC2s from the kidney of IL-33–treated IL-5 reporter (Red5) mice to high purity, transferred them into alymphoid $Rag2^{-/-}Il2rg^{-/-}$ mice, and assessed tissue repopulation after 1–6 wk (Fig. 3). In these experiments, ILC2s were sorted as CD45$^+$Lin$^-$CD127$^+$IL-33R$^+$KLRG1$^+$IL-5$^{tdTomato\ hi}$ to exclude IL-5^{lo} ILC2 tissue precursor populations (Fig. S2 F and Fig. 3 C). The IL-5$^{tdTomato+}$GATA3$^+$ ILC2s exhibited similar surface marker expression as seen in the total GATA3$^+$ ILC2s population in wild type mice, with high expression of IL-17RB and KLRG1 and low expression of IL-33R, CD90.2, and ICOS in SILP compared with kidney (Fig. 3, A, B, and G, upper row).

Already at 1 wk after transfer, high-purity Lin$^-$CD127$^+$IL-33R$^+$KLRG1$^+$IL-5$^{tdTomato\ hi}$ effector ILC2s started to repopulate not only kidneys but also SILP. ILC2 numbers and frequencies in tissues further increased over time (Fig. 3, D–F). Of note, the ratios between kidney and SILP ILC2s were comparable with that observed in wild type mice at all time points (Fig. 3, D–F). Irrespective of their kidney origin, within 1 wk, transferred ILC2s adopted the phenotype of the target tissues, as assessed by our defined set of surface markers (Fig. 3, G and H). To visualize ILC2s in their respective tissue niches, we performed immunohistochemistry for tdTomato-positive ILC2s in kidney and SILP. We observed that kidney ILC2s resided in the tubulointerstitial compartment and periglomerular space, and SILP ILC2s were found in villi and close to the crypt bases in both IL-33–treated Red5 mice and $Rag2^{-/-}Il2rg^{-/-}$ mice 3 wk after ILC2 transfer (Fig. 3 I).

While formal proof of mature effector ILC2 adaptation would require clonal single-cell readouts, these data further substantiate that ILC2s seem to retain flexibility even after differentiation to the effector state and indicate that migrating effector ILC2s can occupy the same niche as the resident ILC2 populations.

Adaptable, non-adaptable, and hardwired features of organ-specific ILC2 transcriptional programs

Next, we used an unbiased approach to investigate transcriptional programs specific to kidney and SILP ILC2s, and subsequently, to delineate which features of these programs are flexible during adaptation to the small intestinal microenvironment. To this end, we adoptively transferred kidney ILC2s from IL-33–treated $Il13^{Cre} \times R26r^{eYFP}$ (IL-13 fate mapping mice, IL-13^{fm}) mice to $Rag2^{-/-}Il2rg^{-/-}$ mice and analyzed transferred ILC2s isolated from SILP of recipient mice at two time points after transfer (2 and 8 wk) using single-cell RNAseq (scRNAseq; see Fig. 4 A for experimental setup). In these experiments, ILC2s were sorted as CD45$^+$Lin$^-$CD127$^+$IL-13^{fm+}, which allowed for unequivocal identification of transferred ILC2 populations in
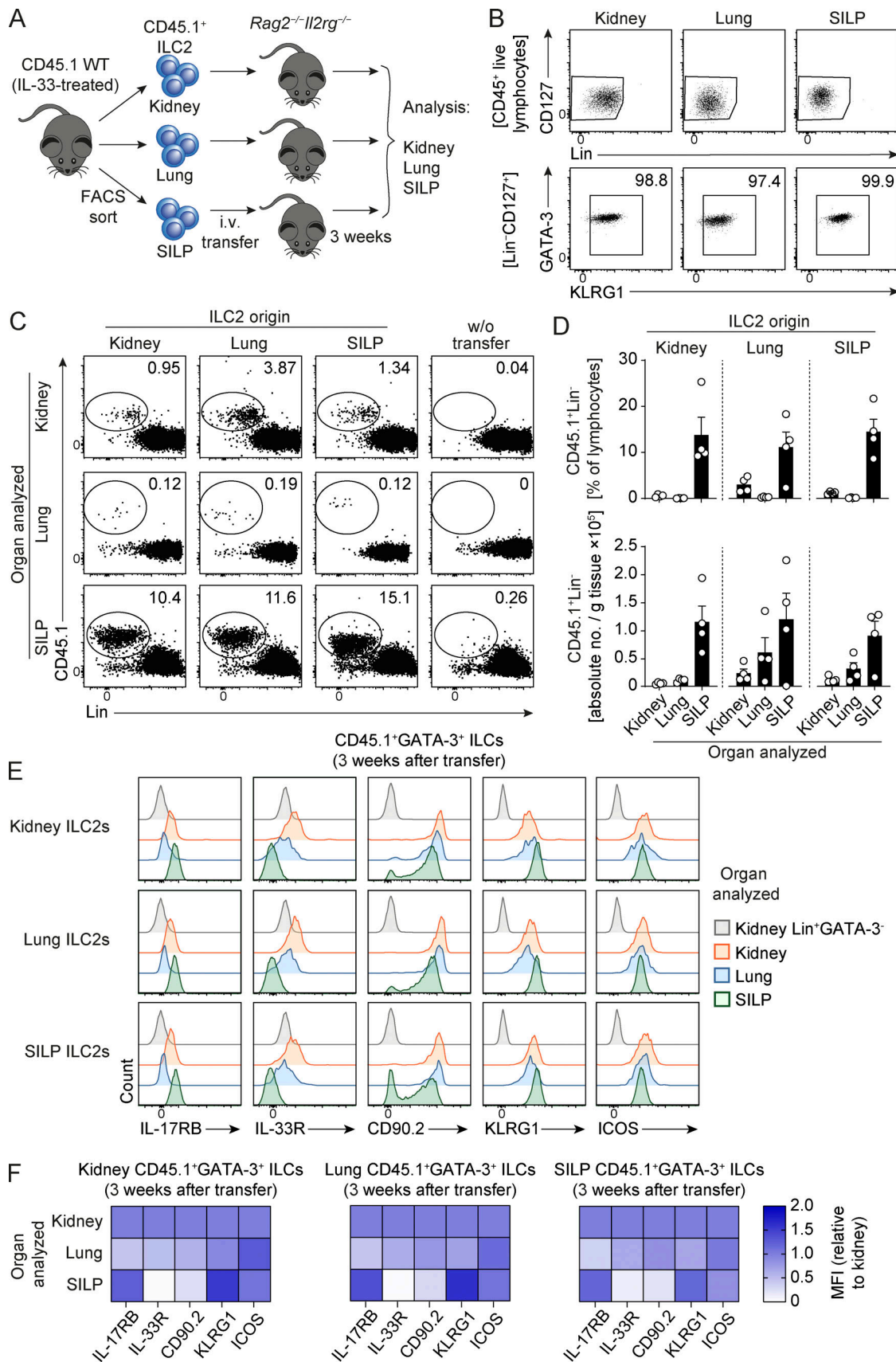
Figure 2. **ILC2 phenotype is dictated by the tissue microenvironment. (A)** Schematic representation of the adoptive transfer model. ILC2s (sorted as CD45+Lin−CD127+KLRG1+) isolated from kidney, lung, and SILP of IL-33–treated (i.p. injection on four consecutive days) C57BL/6 CD45.1 wild type mice were

adoptively transferred i.v. into C57BL/6 $Rag2^{-/-}Il2rg^{-/-}$ mice. Tissues from the recipient mice were analyzed after 3 wk of reconstitution. **(B)** Flow cytometry plots of ILC2 sorting purity from A. The numbers represent frequencies of sorted ILC2s in the total lymphocyte population. **(C–F)** Flow cytometric analysis of leukocytes isolated from the kidney, lung, and SILP of C57BL/6 $Rag2^{-/-}Il2rg^{-/-}$ mice after 3 wk of ILC2 transfer and without transfer. **(C)** Representative plots comparing CD45.1[+] ILC2s isolated from the three indicated organs of recipient mice (rows) with transferred ILC2 populations derived from different organ origins (columns). Numbers indicate the percentage of cells in each gate. **(D)** Frequencies and absolute numbers of CD45.1[+] ILC2s in kidney, lung, and SILP at 3 wk after transfer. Symbols represent individual data points, and bars indicate mean ± SEM (n = 4 per organ analyzed). **(E)** Representative histogram overlays showing surface marker expression of kidney, lung, and SILP CD45.1[+] ILC2s isolated after 3 wk of reconstitution. **(F)** Heat maps of the MFI of various surface markers of ILC2s 3 wk after ILC2 transfer normalized to surface marker expression of kidney ILC2s. All data are representative of two independent experiments with at least three animals per group.

recipient mice, facilitated cell sorting, and thereby minimized contamination in scRNAseq analyses (Fig. S2 G; and Fig. S3, A and B). In addition, kidney and SILP ILC2s from IL-13[fm] donor mice were also subjected to scRNAseq. scRNAseq analysis of IL-13[fm+] donor ILC2s isolated from the kidney again confirmed the mature effector identity of the transferred population with high levels of *Il5*, *Il13*, *Klrg1*, and *Il1rl1* transcripts and minimal (co-)expression of the recently described ILC2 progenitor markers *Tcf7*, *Il18r1*, *Pdcd1* (encoding for PD-1), and *Zbtb16* (encoding for PLZF; Zeis et al., 2020; Fig. S3, C–F).

Unbiased UMAP clustering of the merged scRNAseq data set revealed four distinct clusters, one for each organ analyzed at different time points (Fig. 4 B and Fig. S4 A). As expected, donor kidney and SILP ILC2s clustered separately from each other and from SILP ILC2s of recipient mice, whereas SILP ILC2s obtained 2 and 8 wk after transfer clustered together. Analysis of mRNA expression of the defined surface marker set in the ILC2 clusters confirmed our previous flow cytometry–based findings on mRNA level of the switch of transferred kidney ILC2s to the SILP ILC2 phenotype after transfer (Fig. 4 C). To identify organ-specific ILC2 transcriptional programs, we first performed differential expression (DE) analyses of donor kidneys versus donor SILP ILC2s (Fig. 4 D). The organ-specific upregulated genes in this comparison were defined as the "kidney program" and the "SILP program," respectively, and subjected to HALLMARK pathway gene set enrichment analyses using the Mouse Molecular Signatures Database (Fig. 4 E). These analyses revealed several pathways upregulated in SILP ILC2s (n = 27), some of which were immune cell related, while kidney ILC2s showed upregulation of a smaller number (n = 6) of metabolic and general signaling pathways (Fig. 4 E). In line with rapid ILC2 tissue adaptation, the kidney program was markedly downregulated in adapting kidney ILC2s already at 2 wk and almost completely lost at 8 wk after transfer (Fig. 4 F, right panel). The (partial) upregulation of the SILP program in ex-kidney ILC2s was also already observed at 2 wk after transfer and increased until 8 wk but remained incomplete even at the late time point (Fig. 4 F, left panel). Next, we defined three DE comparisons between the groups (Fig. 4, F and G) that identify differentially regulated gene sets, representing the "adaptable" SILP features (comparison 1), "non-adaptable" SILP features (comparison 2), and "hardwired" kidney features (comparison 3). These gene sets were then subjected to HALLMARK pathway gene set enrichment analyses (Fig. S4 B). However, several of the upregulated pathways seemed to be unspecific (e.g., upregulated in all three comparisons) or related to the adoptive transfer setting into alymphoid $Rag2^{-/-}Il2rg^{-/-}$ mice (upregulated in ex-kidney SILP ILC2s at 8 wk in comparisons to

both non-transfer settings). Thus, we used a Venn diagram of SILP-specific pathways to identify "fully adaptable" SILP features, "partially adaptable" SILP features, and "non-adaptable" SILP features (Fig. 4 H, upper panel). A similar strategy was used for filtering kidney-specific pathways (Fig. 4 H, lower panel). Interestingly, when using these filtering steps, we failed to extract any "hardwired" kidney ILC2 features from the data. In contrast, several immune-related pathways, e.g., TNF/NF-κB signaling, were found among the (partially) adaptable SILP features that were acquired by ex-kidney ILC2s in the small intestine (Fig. 4 I). Non-adaptable SILP features were related to DNA replication, DNA repair, as well as Notch signaling and response to estrogens (Fig. 4 I).

Adapting ILC2s gradually acquire the transcriptional program of small intestinal ILC2

To further investigate the dynamics of intestinal ILC2 adaptation after transfer, we focused on scRNAseq analysis of ex-kidney ILC2s isolated from SILP at 2 wk after transfer. At this time point, adapting kidney ILC2s have acquired a substantial part of the SILP program while still expressing a residual kidney signature (see Fig. 4 F). UMAP clustering of the 2-wk sample revealed three clusters (Fig. 5 A), of which cluster 3 showed substantial upregulation of the SILP program and expressed the kidney program at a low level (Fig. 5, A and B). To identify the dynamics of the adaptation process, we used RNA velocity analysis that, based on the amount of unspliced and spliced mRNAs in each cell, assigns directed, dynamic information to the state of each cell in a transition process (Fig. 5 C; La Manno et al., 2018). The directional information derived from this approach showed a trajectory from cluster 2 with low SILP program expression toward cluster 3 with high SILP program expression (Fig. 5 C). RNA velocity-based pseudotime analyses demonstrated a gradual increase in the SILP program and most of our defined SILP ILC2 surface markers in adapting ex-kidney ILC2s at 2 wk after transfer (Fig. 5, D and E). The residual kidney program (including *Il1rl1*) remained stable over pseudotime, indicating that most kidney features were already downregulated within the first 2 wk of the adaptation process (Fig. 5, D and E; see Fig. 4 F).

Taken together, these data further support the hypothesis that mature effector ILC2s can gradually adapt the tissue-specific ILC2 transcriptional program of a new microenvironment.

RA signaling activity is increased in ILC2s adapting to the small intestine

RA is an important mediator in the intestinal microenvironment and its production by SILP dendritic cells has been shown to
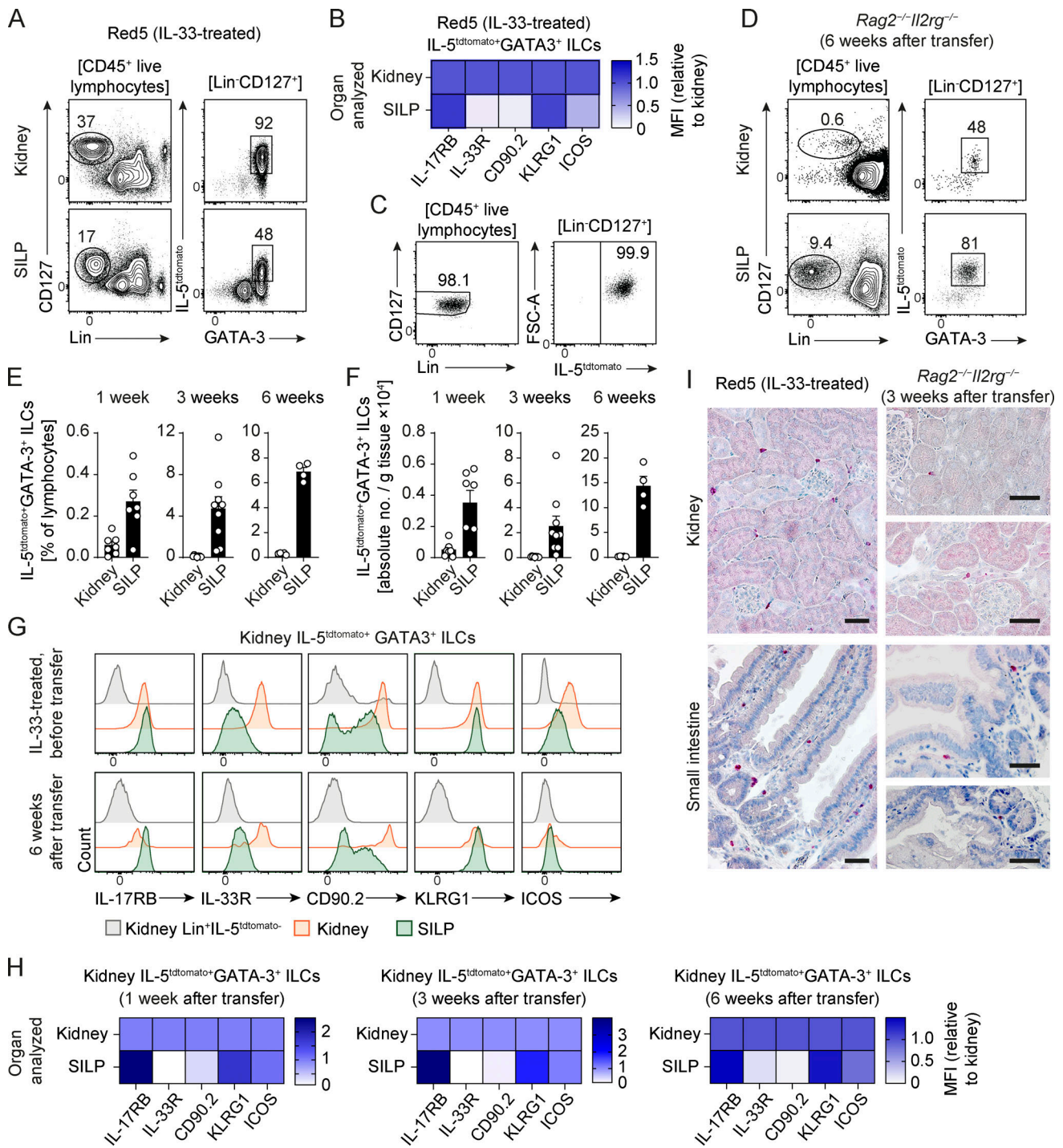
Figure 3. **Effector ILC2s can adapt to new tissue microenvironment. (A)** Flow cytometric analysis of IL-5[tdtomato+]GATA3^{+} ILCs isolated from kidney and SILP of IL-33–treated Red5 mice (i.p. injection on four consecutive days). Numbers indicate the percentage of cells in each gate. **(B)** Heat map of MFI of different surface markers on IL-5[tdtomato+]GATA3^{+} ILCs isolated from kidney and SILP normalized to surface marker expression of kidney ILC2s. **(C)** Representative sorting purity of transferred ILC2s (sorted as CD45^{+}Lin^{−}CD127^{+}IL-33R^{+}KLRG1^{+}IL-5[tdtomato+]) originating from the kidney of IL-33–treated Red5 mice. Sorted kidney ILC2s were transferred to C57BL/6 $Rag2^{−/−}Il2rg^{−/−}$. **(D–F)** Representative flow cytometric plots (D), frequencies (E), and absolute numbers (F) of IL-5[tdtomato+]GATA3^{+} ILC2s obtained from the kidney and SILP (n = 4–7 per organ) of C57BL/6 $Rag2^{−/−}Il2rg^{−/−}$ mice at different time points after transfer. Numbers in D indicate the percentage of events in each gate. Symbols represent individual data points, and bars indicate mean ± SEM. **(G and H)** Representative histogram overlays (G) and heat map of MFI (H) of different surface markers of IL-5[tdtomato+]GATA3^{+} ILCs originating from the kidney of Red5 mice analyzed 1–6 wk after transfer in the kidney and SILP of C57BL/6 $Rag2^{−/−}Il2rg^{−/−}$ mice and normalized to surface marker expression on kidney ILC2s. **(I)** Immunohistochemical staining of tdTomato-positive ILC2s (deep red) in the kidney and SILP tissue of IL-33–treated Red5 mice and in C57BL/6 $Rag2^{−/−}Il2rg^{−/−}$ mice 3 wk after kidney IL-5[tdtomato+] ILC2 transfer. Scale bars, 50 μm. Data in D–H represent five independent experiments.

Shaikh et al.
Retinoic acid mediates intestinal ILC2 adaptation

Journal of Experimental Medicine   7 of 20
https://doi.org/10.1084/jem.20221015
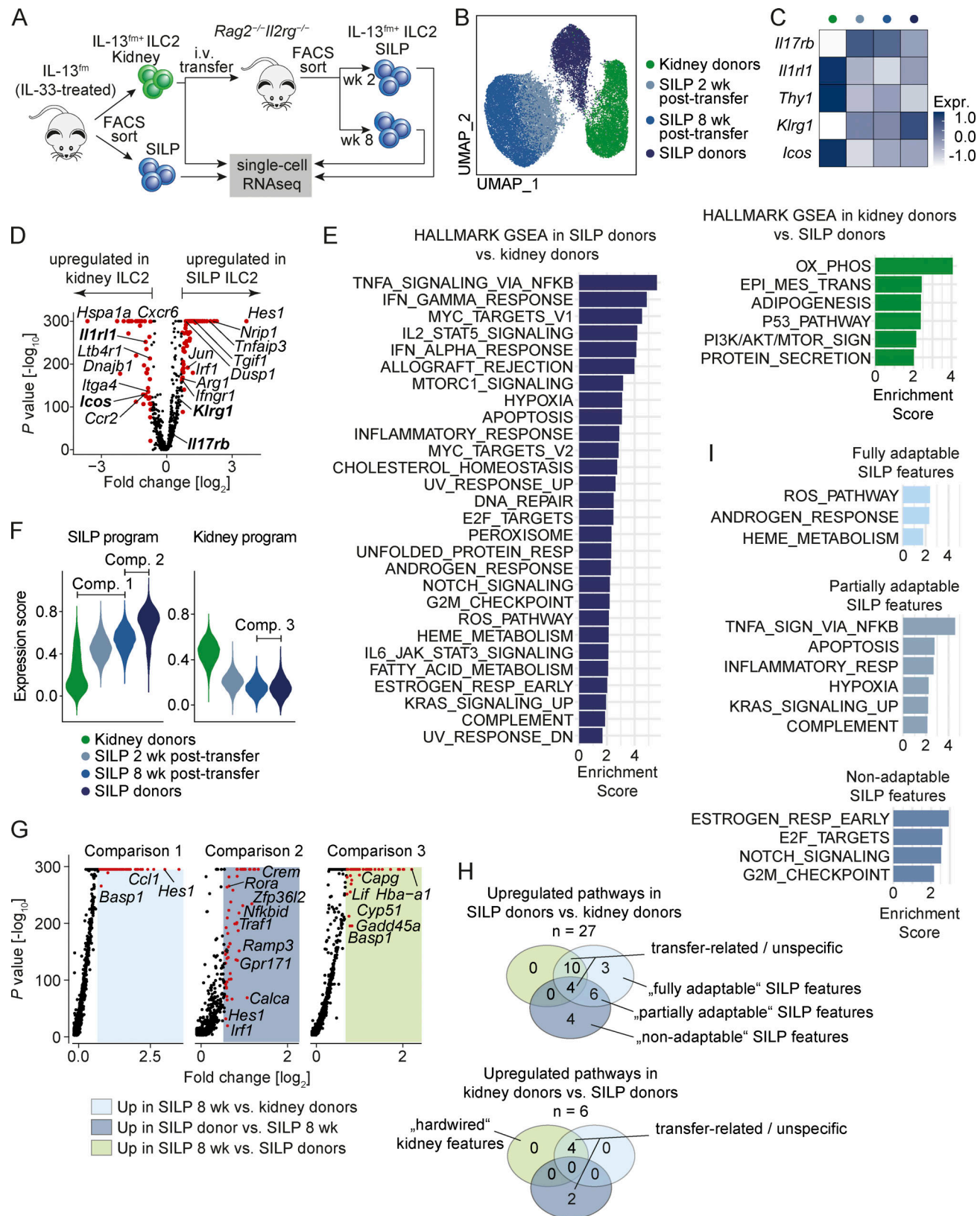
Figure 4. Adaptable and hardwired features of kidney and SILP ILC2s. (A) Schematic representation of the experimental setup for scRNAseq of ILC2 populations. ILC2s from kidney and SILP were isolated from IL-33–treated BALB/c IL-13^fm mice (i.p. injection on four consecutive days) and sorted for scRNA sequencing analysis (donors). The cells were sorted as CD45$^+$Lin$^-$CD127$^+$IL-13^{fm+}. Simultaneously, kidney ILC2s from the same isolated cell pool were adoptively transferred i.v. into BALB/c *Rag2$^{-/-}$Il2rg$^{-/-}$* mice. After 2 and 8 wk, IL-13^{fm+} ILC2s were recovered from SILP and subjected to scRNAseq analysis. **(B)** Unsupervised UMAP clustering of combined scRNAseq data of kidney and SILP ILC2s from donors and of SILP ILC2s after 2 and 8 wk from recipients.

(C) Heat map of differentially expressed ILC2 surface markers in donor and recipient clusters. **(D)** DE analysis between donor kidney and SILP ILC2s. Genes that are significantly upregulated with ≥twofold change are shown as red dots. **(E)** Gene set enrichment analysis (GSEA) for HALLMARK pathways of the Mouse Molecular Signatures Database using the genes significantly upregulated in SILP (left, dark blue) and kidney (right, dark green) ILC2s. **(F)** Violin plots depicting the expression score of SILP program and kidney program, defined as the organ-specific upregulated genes in the DE analyses in D, in the respective conditions. The indicated comparisons represent adaptable SILP features (= comp. 1), non-adaptable SILP features (= comp. 2), and hardwired kidney features (= comp. 3). **(G)** DE expression analysis of the comparisons indicated in F. Significantly upregulated genes (≥twofold) in the indicated samples are shown as red dots. **(H)** Venn diagram of SILP-specific and kidney-specific HALLMARK pathways from E and classification of the pathways as indicated. **(I)** Specific adaptable and non-adaptable HALLMARK pathways in SILP ILC2s identified by filtering as shown in H.

imprint intestine-specific features on T cells (Iwata, 2009). Two RA receptors, *Rara* and *Rxrg*, were among the significantly upregulated genes in bulk-like DE analysis of the scRNAseq data from SILP versus kidney ILC2s. In addition, *Rxrg* was found among the top 10 cluster-defining genes of SILP-adapted ex-kidney ILC2s in the scRNAseq analyses (Fig. S4 A). Expression analyses of all known RA receptors in our single-cell and bulk RNAseq data sets showed that *Rara*, *Rxrb*, and *Rxrg* expression was higher in SILP ILC2s than in kidney ILC2s, while *Rarb*, *Rarg*, and *Rxra* expression was lower in SILP ILC2s (Fig. 6, A and B). In addition, screening of SILP ILC2 program genes (Fig. 4 D) and of the top 30 cluster-defining genes upregulated in the SILP-adapted ex-kidney ILC2 clusters (Fig. S4 A) identified several genes that were previously described to be induced by RA signaling (*Nrip1*, *Tgif1*, *Ctsh*, *Dusp1*, *Irf1*; Fig. 6, C and D). To assess RA signaling in adapting ILC2s in a broader sense, we generated an RA signaling score by combining Gene Ontology (GO) terms for RA receptor binding (GO:0046965), RA receptor signaling pathway (GO:0048384), and response to RA (GO:0032526) in one expression module (Fig. 6 E). This expression score was significantly upregulated in all SILP ILC2 clusters from the transfer experiments compared with kidney ILC2s (Fig. 6 E, see Fig. 4, A and B). In addition, analyses focused on ex-kidney ILC2s isolated from the SILP at 2 wk after transfer (compare Fig. 5) showed upregulation of the RA module in SILP phenotype ILC2s (cluster 3; Fig. 6 F). RNA velocity-based pseudotime analyses of adapting ILC2s demonstrated gradual upregulation

of four out of the five RA signaling genes during acquisition of the SILP ILC2 program (Fig. 6 G and Fig. 5 D), suggesting a role for RA signaling activity in ILC2 adaption to the intestinal microenvironment.

RA signaling drives functional adaptation of ILC2s to the intestinal phenotype in vitro

To validate the hypothesis that RA signaling activity drives phenotypic ILC2s adaptation to the intestinal microenvironment, we next cultured kidney ILC2s with or without RA and analyzed selected surface markers using flow cytometry after 4 d of culture (Fig. 6, H and I). Indeed, we observed that cells treated with RA upregulated IL-17RB and KLRG1 expression while downregulating CD90.2 and ICOS, mimicking the "intestinal" ILC2 phenotype, with the exception that we did not observe RA-mediated downregulation of the IL-33R (Fig. 6, H and I). To further validate whether downregulation of IL-17RB was of functional relevance, we studied the responsiveness of cultured kidney ILC2s to IL-25 and IL-33 after RA-induced switch to the intestinal phenotype. These experiments confirmed that RA treatment not only upregulates IL-17RB expression on ILC2s but also increases their responsiveness to subthreshold IL-25 (1 ng/ml), as measured by enhanced production of IL-5 and IL-13 in RA-preconditioned cells (Fig. 6 J). In line with unchanged receptor expression, responsiveness to IL-33 was unaltered by RA (Fig. 6 J). These data identify RA signaling as one important regulator of the phenotypic switch of ILC2s to the SILP
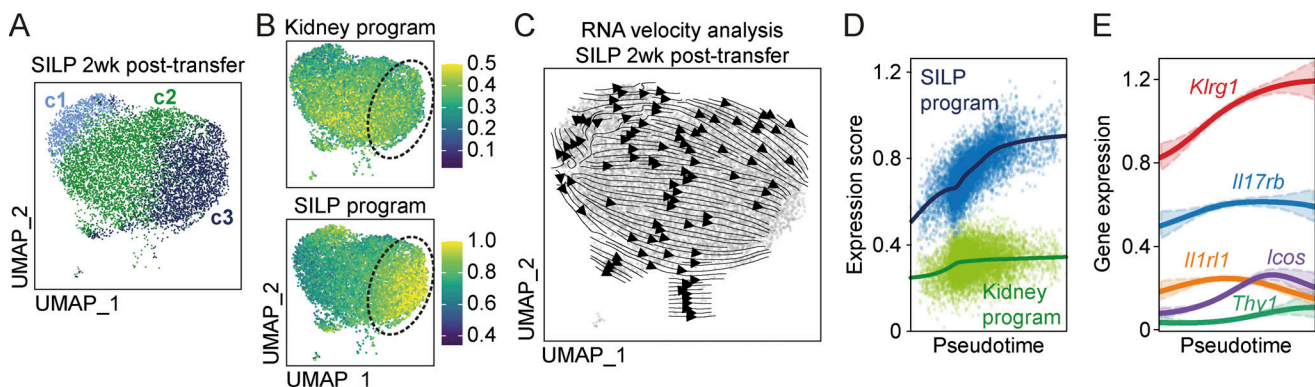
Figure 5. **Gradual acquisition of the SILP ILC2 phenotype by transferred kidney ILC2s. (A)** Unsupervised UMAP subclustering of scRNAseq data of ex-kidney ILC2s isolated from the SILP of recipient BALB/c *Rag2⁻/⁻Il2rg⁻/⁻* mice 2 wk after transfer (see Fig. 4 A for experimental setup). **(B)** Color mapping of kidney and SILP program expression on the UMAP subclustering of adapting ex-kidney ILC2s at 2 wk after transfer. Lowest expression is indicated by blue and highest expression by yellow. **(C)** Dynamic information of cell states in the transition process generated using RNA velocity analysis of adapting ex-kidney ILC2s at 2 wk after transfer. **(D and E)** RNA velocity-based pseudotime analyses of the SILP and kidney programs (D) and selected surface markers (E) in adapting ex-kidney ILC2s at 2 wk after transfer.
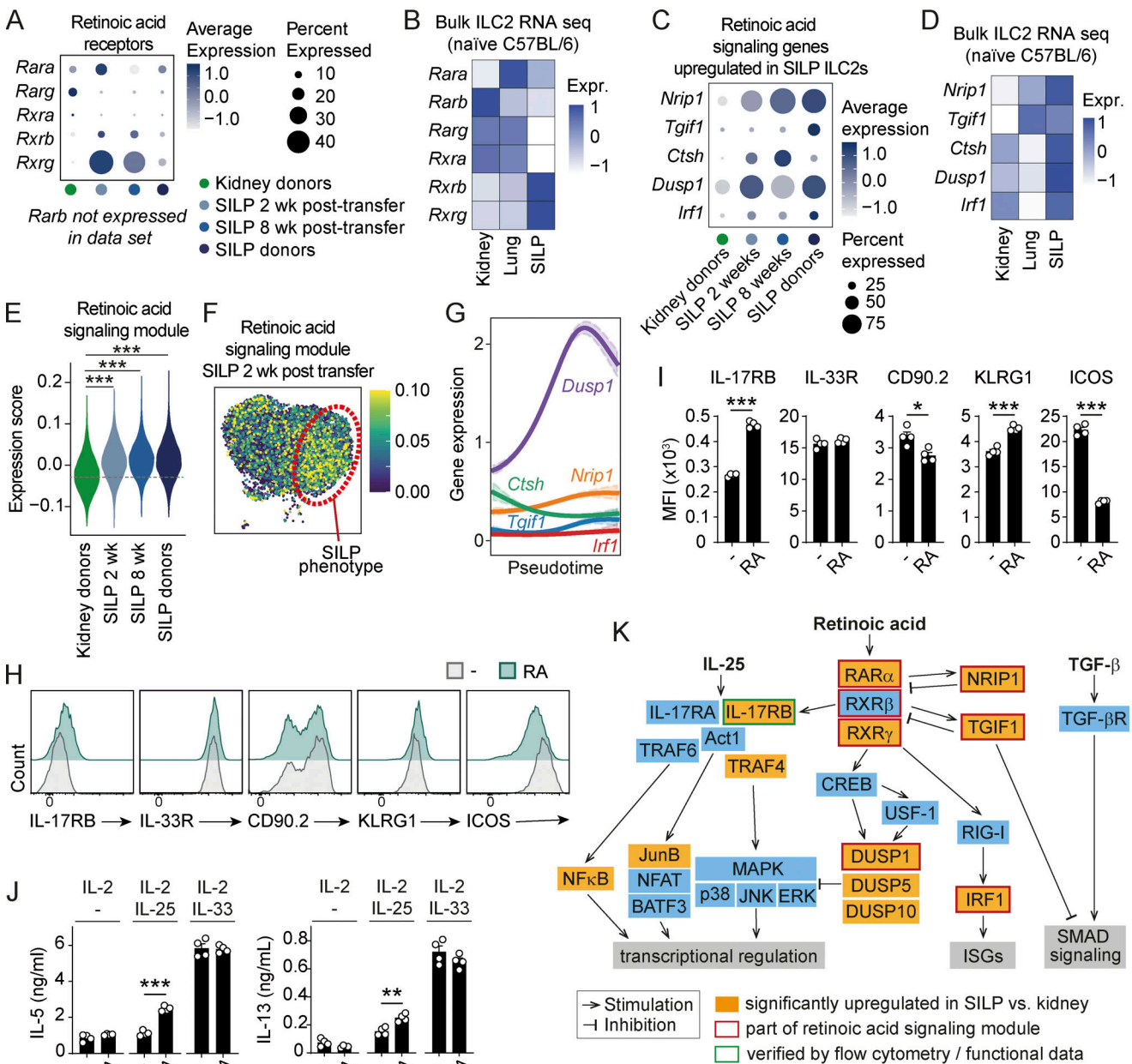
Figure 6. **RA signaling drives functional adaptation of ILC2s to the intestinal phenotype. (A)** Dot plot of RA receptor expression in the scRNAseq data set of kidney and SILP ILC2s from donors and of SILP ILC2s after 2 and 8 wk from recipients of kidney ILC2s (see Fig. 4 A for experimental setup). **(B)** Heat map of RA receptor expression in bulk RNAseq data set of ILC2s isolated from the kidneys, lungs, and SILP of naïve C57BL/6 mice (see Fig. 1). **(C)** Dot plot of RA signaling genes selected from the DE analyses (see Fig. 4 D) and top 30 cluster-defining genes (see Fig. S4 A). **(D)** Heat map of RA signaling genes in the bulk RNAseq data set of ILC2s isolated from naïve C57BL/6 mice (see Fig. 1). **(E)** Violin plots depicting the expression score of RA signaling associated genes in the respective conditions. **(F)** Color mapping of RA expression score on the UMAP subclustering of adapting ex-kidney ILC2s at 2 wk after transfer (see Fig. 5). Lowest expression is indicated by blue and highest expression by yellow. **(G)** RNA velocity-based pseudotime analyses of selected RNA signaling genes in adapting ex-kidney ILC2s at 2 wk after transfer. **(H and I)** Representative histogram overlays (H) and MFI (I) for surface marker expression of sorted kidney ILC2s after culture with IL-2 ($n = 4$ for each condition) in the presence or absence of RA (1 μM). **(J)** Cytokine quantification in the supernatant of the cultured kidney ILC2s stimulated with subthreshold IL-25 or IL-33 (1 ng/ml each; $n = 4$ for each condition). Data in H–J are representative of three individual experiments with similar results. Symbols represent individual data points and bars indicate mean ± SEM. Statistical analysis was performed using unpaired two-tailed Student's t test (*P < 0.05, **P < 0.01, ***P < 0.001). **(K)** Hypothetical model of RA signaling network in SILP ILC2s based on genes upregulated in the RNAseq data sets and a literature review of described downstream pathways. CREB, cAMP response element-binding protein; ISG, interferon-stimulated gene.

microenvironment. Based on the RA-induced genes that were upregulated during intestinal ILC2 adaptation in our RNAseq data sets and a literature review of described downstream pathways (Bartholin et al., 2006; Borowczyk et al., 2021; Jeffrey et al., 2007; Lu et al., 2008; Samarut and Rochette-Egly, 2012; White et al., 2003; Zhuang et al., 2021), we devised a hypothetical model of the broader consequences of RA signaling on intestinal ILC2 biology (Fig. 6 K).

Shaikh et al.
Retinoic acid mediates intestinal ILC2 adaptation

Journal of Experimental Medicine   10 of 20
https://doi.org/10.1084/jem.20221015

Role of Notch signaling for adaptation of ILC2s to the intestinal phenotype in vitro

While we established RA signaling as one driving factor for ILC2 adaptation to the intestinal microenvironment, other tissue cues most likely act in concert with RA to induce their full phenotypic switch (including, e.g., IL-33R downregulation). The central adaptor of the Notch pathway, *Hes1*, was the most upregulated gene in the SILP program (see Fig. 4 D) and was also found among the 10 cluster-defining genes of SILP-adapted ex-kidney ILC2s in the scRNAseq analyses (Fig. S4 A). Although in unbiased analyses, the HALLMARK Notch signaling pathway was identified as one of the non-adaptable SILP features (see Fig. 4 I, lower panel), *Hes1* was strongly upregulated in adapting ex-kidney ILC2s (see Fig. 4 G, comparison 1). In line, an expression score of genes related to Notch signaling (KEGG PATHWAY: hsa04330) was significantly upregulated in all SILP ILC2 clusters compared with kidney ILC2s (Fig. S5 A), pointing to a role of Notch signaling in ILC2 adaptation to the SILP. To address this, we performed another set of in vitro experiments, culturing kidney ILC2s in the absence and presence of the Notch ligand DLL4 (Fig. S5, B and C). Although some features of the intestinal ILC2 phenotype in kidney ILC2s could be induced by activation of Notch signaling (upregulation of IL-17RB, downregulation of IL-33R and CD90.2), other markers remained unchanged (ICOS) or were regulated inversely (downregulation of KLRG1; Fig. S5, B and C). Importantly, despite upregulation of IL-17RB, DLL4 stimulation significantly decreased IL-25 responsiveness of ILC2s, indicating that activation of the Notch pathway might be a general inhibitor of ILC2 function (Fig. S5 D). Finally, a combination of DLL4 and RA treatment was able to induce ICOS downregulation but failed to restore upregulation of KLRG1 and the increased cytokine responsiveness observed with RA treatment alone (Fig. S5, E–G). In conclusion, in addition to RA and Notch signaling, other unknown factors are required to simulate a full phenotypic and functional switch of kidney ILC2s to the intestinal ILC2 program in vitro.

RA is essential for intestinal adaptation of ILC2s in vivo

As RNAseq and in vitro analyses identified RA signaling as one factor for adaptation of intestine-specific ILC2 phenotype, we decided to validate this effect in vivo by blocking RA signaling using a pan-RA receptor inverse agonist (Spencer et al., 2014; BMS493; hereafter referred to as retinoic acid inhibitor [RAi]). For this, we performed an adoptive transfer of IL-13^{fm+} ILC2s into *Rag2*$^{−/−}$*Il2rg*$^{−/−}$ mice and treated the recipients with RAi from 1 d prior to cell transfer for 3 wk. Control recipients received DMSO injections (see Fig. 7 A for experimental setup). As observed in previous analyses, transferred kidney ILC2s occupied the niches in kidney, lung, and SILP in ratios comparable to wild type mice in both groups (Fig. 7, B and C) and adopted the intestinal IL-17RB^{hi}IL-33R^{lo}CD90.2^{lo}KLRG1^{hi}ICOS^{lo} phenotype in the SILP of DMSO-treated mice (Fig. 7 D). In line with our hypothesis, RAi prevented the adaptation of kidney ILC2s to the SILP phenotype, reducing upregulation of IL-17RB and KLRG1, while increasing expression of CD90.2 and ICOS on ex-kidney SILP ILC2s (Fig. 7 D). As observed under in vitro conditions, IL-33R expression remained unchanged between the groups.

As cellular adaptation to tissues should occur constitutively, even at steady state, we next asked the question of whether RA signaling inhibition could also reverse intestinal adaptation of endogenous ILC2s in a non-transfer setting. To address this, we treated T cell–deficient *Rag2*$^{−/−}$ and immunocompetent *Il13*^{fm} mice with RAi for 3 wk and assessed abundance and phenotype of ILC2s in kidney, lung, and SILP (Fig. 7, E–I). As previously observed (Spencer et al., 2014), RAi treatment led to a significant increase in ILC2 abundance in the SILP with a shift in the ILC2/ILC3 ratio (Fig. 7, F and G). Endogenous SILP ILC2s from RAi-treated mice significantly downregulated IL-17RB and KLRG1 expression, while upregulating CD90.2 and ICOS expression (Fig. 8, H and I), indicating a partial reversal of the intestinal ILC2 phenotype, as defined by our surface marker set. Taken together, these data confirm that RA contributes to continuous phenotypic ILC2 adaptation to the small intestinal microenvironment in vivo.

RA signaling inhibition impairs anti-helminth immunity

To study the importance of RA-mediated adaptation on ILC2 functionality in a model that induces a strong intestinal type 2 immune response, we decided to block RA signaling in a helminth infection model. To this end, we applied RAi in *Rag2*$^{−/−}$ and *Rag2*$^{−/−}$*Il2rg*$^{−/−}$ mice for 3 wk before infecting them with *S. ratti*, a model for human gastrointestinal nematode infection (Breloer and Abraham, 2017). Control recipients received DMSO injections (see Fig. 8 A for experimental setup). In these experiments, the small intestine was used for the analysis of worm burden, precluding the analysis of ILC2s from the SILP. Thus, we confirmed the effect of RAi on endogenous ILC2s isolated from the colon of infected *Rag2*$^{−/−}$ mice (Fig. 8, B–D). As observed in uninfected mice (see Fig. 7, E–I), RAi treatment of worm-infected mice resulted in a shift of the ILC2/ILC3 ratio and a change of colonic ILC2 surface marker expression toward a non-intestinal phenotype (e.g., IL-17RB^{lo}CD90^{hi}KLRG1^{lo}ICOS^{hi}; Fig. 8, D and E). In line with a functional relevance of this ILC2 phenotypic switch and despite increased ILC2 frequencies, worm burden in the small intestine was significantly higher in RAi-treated *Rag2*$^{−/−}$ mice than in DMSO controls (Fig. 8 F). In *Rag2*$^{−/−}$*Il2rg*$^{−/−}$ mice, serving as controls for *Rag2*$^{−/−}$ mice since they lack endogenous ILC population, the adult worm burden remained unchanged after RAi treatment. In addition, mast cell activation after *S. ratti* infection, as assessed by serum mouse mast cell protease 1 (mMCPT-1), was significantly reduced in the RAi-treated *Rag2*$^{−/−}$ mice but not in RAi-treated *Rag2*$^{−/−}$*Il2rg*$^{−/−}$ mice compared with their respective controls (Fig. 8 G).

These results are discrepant with a previous report demonstrating that increased ILC2 abundance in conditions of impaired RA signaling improves anti-helminth response in chronic *Trichuris muris* infection of the cecum (Spencer et al., 2014). However, the observation that ILC2 frequencies and phenotype substantially differ between intestinal segments might explain the distinct sensitivity of these two helminths species to interventions targeting ILC2 adaptation, according to their target segment in the intestine (*S. ratti*, small intestine versus *T. muris*, cecum). To formally address this, we analyzed ILC2 abundance and IL-17RB/IL-33R expression in the different intestinal

Shaikh et al.
Retinoic acid mediates intestinal ILC2 adaptation

Journal of Experimental Medicine
https://doi.org/10.1084/jem.20221015

11 of 20
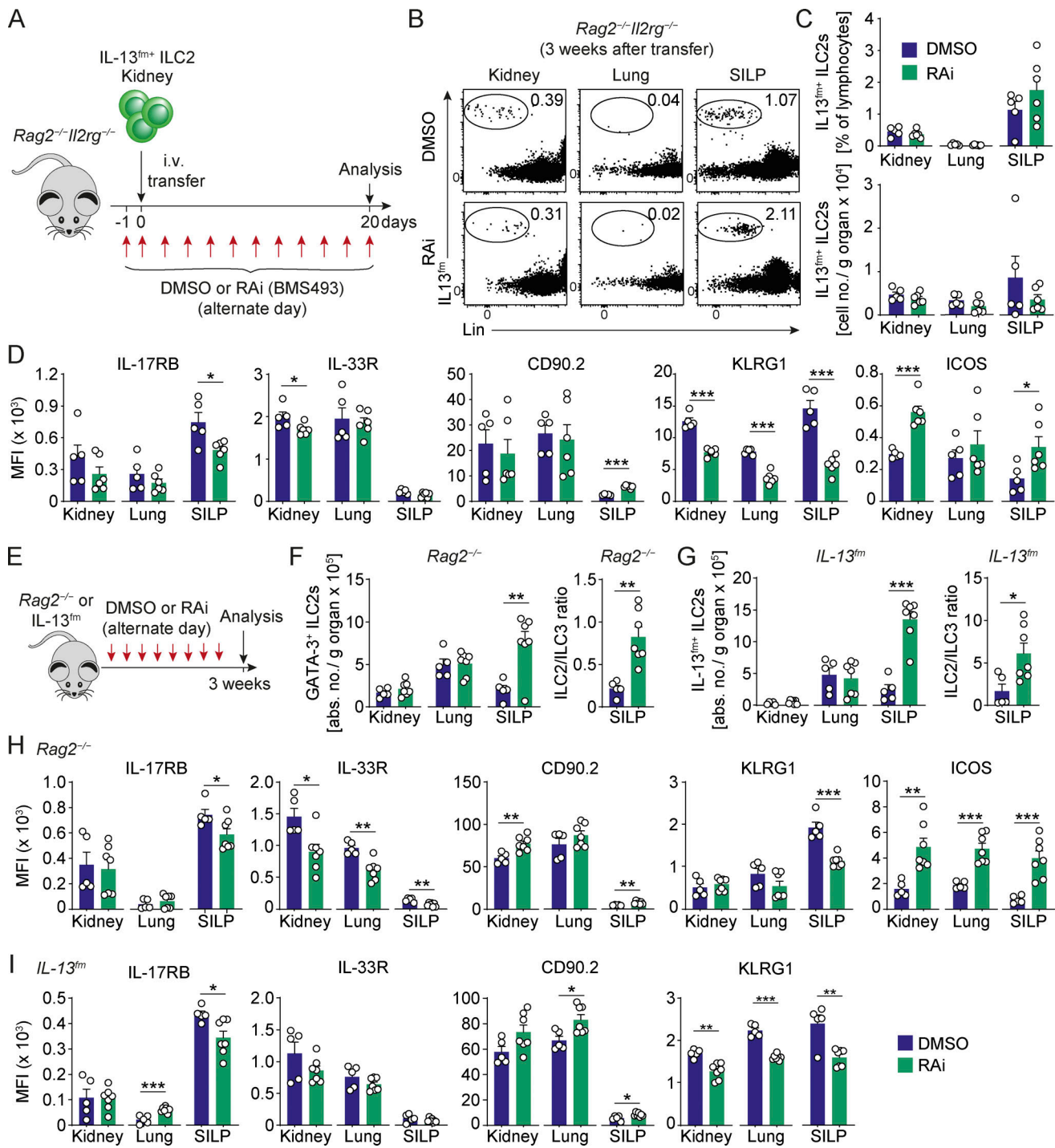
Figure 7. **RA signaling is essential for intestinal adaptation of ILC2s in vivo. (A)** Experimental design of the RAi (BMS493 220 µg) treatment of ILC2-transferred BALB/c *Rag2*^{−/−}*Il2rg*^{−/−} mice. Kidney ILC2s isolated from IL-33–treated BALB/c *IL-13*[fm] mice (i.p. injections on four consecutive days) were adoptively transferred through i.v. injections into BALB/c *Rag2*^{−/−}*Il2rg*^{−/−} recipient mice (*n* = 11). The recipient mice received either DMSO (*n* = 5) or RAi (*n* = 6) treatment at the indicated time points. **(B)** Representative FACS plots of Lin⁻IL-13[fm+] ILC2s isolated from the kidneys, lungs, and SILP of BALB/c *Rag2*^{−/−}*Il2rg*^{−/−} mice after 3 wk of transfer and treatment with either DMSO or RAi. Numbers indicate the percentage of cells in each gate. **(C)** Frequencies and absolute numbers of IL-13[fm+] ILC2s isolated from the kidney, lung, and SILP of BALB/c *Rag2*^{−/−}*Il2rg*^{−/−} mice treated with either DMSO or RAi. **(D)** MFI of different surface marker expressions of ILC2s isolated from the respective organs. **(E)** Experimental design of the RAi treatment of BALB/c *Rag2*^{−/−} and BALB/c IL-13[fm] mice. The mice received either DMSO (*n* = 5) or RAi (*n* = 7) treatment for 3 wk, and ILC2s from the kidney, lung, and SILP were analyzed. **(F and G)** Absolute numbers and ILC2/ILC3 ratio of Lin⁻GATA-3⁺ ILC2s, Lin⁻IL-13[fm+] ILC2s, and Lin⁻RORγt⁺ ILC3s isolated from the kidney, lung, and SILP of BALB/c *Rag2*^{−/−} (F) and BALB/c IL-13[fm] (G) mice. **(H and I)** MFI of different surface marker expression of ILC2s isolated from the respective organs of BALB/c *Rag2*^{−/−} (H) and BALB/c IL-13[fm] mice (I). Data are pooled from two individually performed experiments. Symbols represent individual data points and bars indicate mean ± SEM. Statistical analysis was performed using unpaired two-tailed Student's *t* test (*P < 0.05, **P < 0.01, ***P < 0.001).

Shaikh et al.
Retinoic acid mediates intestinal ILC2 adaptation

Journal of Experimental Medicine   12 of 20
https://doi.org/10.1084/jem.20221015
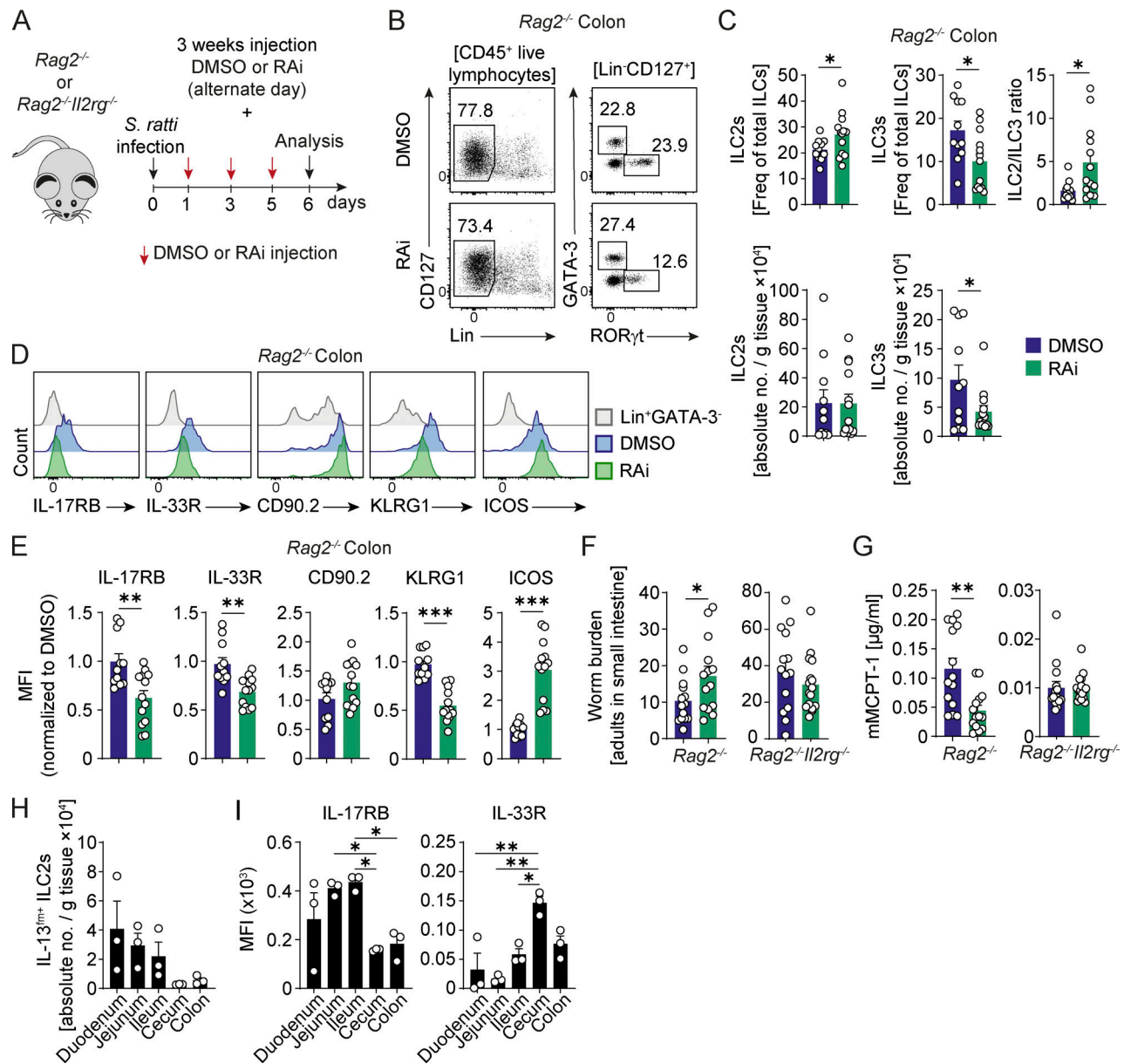
Figure 8. RA signaling inhibition reverses intestinal ILC2 adaptation and impairs anti-helminth immunity. (A) Experimental setup of RAi treatment and subsequent *S. ratti* infection in BALB/c *Rag2⁻/⁻* and BALB/c *Rag2⁻/⁻Il2rg⁻/⁻* mice. **(B)** Representative flow cytometric plots of ILC2 and ILC3 populations isolated from the colon of BALB/c *Rag2⁻/⁻* mice treated with either DMSO or RAi and infected with *S. ratti*. In *S. ratti* experiments, colon was analyzed for the RAi effect on ILC2s because the small intestine was needed for worm counting. Gating strategy is indicated in brackets and numbers indicate the percentage of cells in each gate. **(C)** Frequencies (upper panel) and absolute numbers (lower panel) of GATA-3⁺ ILC2s and RORγt⁺ ILC3s populations as well as their proportional shift (right panel) in the colon of BALB/c *Rag2⁻/⁻* mice infected with *S. ratti* after 3 wk of DMSO or RAi treatment. **(D and E)** Representative histogram overlays (D) and MFI (E) of the surface marker expression in the two groups. **(F)** Worm burden in the small intestine of *Rag2⁻/⁻* and *Rag2⁻/⁻Il2rg⁻/⁻* mice 6 d after infection with *S. ratti*. **(G)** Mast cell activity assessed as mMCPT-1 serum concentration in *Rag2⁻/⁻* and *Rag2⁻/⁻Il2rg⁻/⁻* mice infected with *S. ratti*. Data are pooled from two (*Rag2⁻/⁻*) or three (*Rag2⁻/⁻Il2rg⁻/⁻*) individually performed experiments with three to five mice per group. **(H and I)** Absolute numbers (H) and MFI (I) of IL-17RB and IL-33R of Lin⁻IL-13fm⁺ ILC2s isolated from different intestinal segments of naïve BALB/c IL-13fm mice. Data represent at least two individually performed experiments with three mice per group. Symbols represent individual data points and bars indicate mean ± SEM. Statistical analysis was performed using unpaired two-tailed Student's *t* test (C–G) or one-way ANOVA with Tukey's post-hoc test (H and I); *P < 0.05, **P < 0.01, ***P < 0.001.

segments of IL-13fm mice (Fig. 8, H and I). Indeed, the abundance of ILC2s in the cecum was much lower than that in small intestinal segments. In addition, IL-17RB expression was substantially lower on cecal than on small intestinal ILC2s, while IL-33R expression was higher. This supports the hypothesis that the expulsion of *T. muris* from the cecum is less sensitive to RAi-

induced perturbations in ILC2 tissue adaptation, e.g., impaired upregulation of IL-17RB, as IL-17RB expression is already low on cecal ILC2s in steady state. Increases in ILC2 abundance under RAi treatment, on the other hand, are likely to improve worm expulsion in *T. muris* infection as steady-state ILC2 levels are low in the cecum.

Shaikh et al.
Retinoic acid mediates intestinal ILC2 adaptation

Journal of Experimental Medicine 13 of 20
https://doi.org/10.1084/jem.20221015

In summary, these data confirm that blocking RA signaling can partially reverse the small intestinal ILC2 phenotype, impairing the immune response against *S. ratti*.

Discussion

Tissue-specific phenotype adaptation is a process widely studied for various immune cell types. The dogma that organ-specific microenvironments dictate phenotype and functionality of immune cells has been long-established for cells of the myeloid lineage (Lavin et al., 2014; Roquilly et al., 2022). In contrast, lymphocyte residency and adaptation in non-lymphoid tissues is an emerging concept that has recently been brought forward by landmark studies on tissue-resident memory T cells and ILCs (Masopust and Soerens, 2019; Meininger et al., 2020). With respect to the ILC2 subset, several recent reports have demonstrated that these tissue-resident lymphocytes exhibit substantial heterogeneity between tissues, and it is presumed that this heterogeneity is imprinted by local niches with their specific microenvironmental cues (Ricardo-Gonzalez et al., 2018; Spits and Mjösberg, 2022).

Using an adoptive transfer model, we show here that murine effector ILC2s originating from non-lymphoid organs could effectively repopulate their niche in various peripheral tissues of alymphoid mice, arguing against an imprinted homing capacity at developmental stages determining the fate of ILC2 localization, as has been previously suggested (Kim et al., 2015; Yang et al., 2016). ILC2s, regardless of their tissue of origin, adapted the phenotype of the tissue they came to reside in, which is in line with previous studies on macrophages and ILC3s that were also capable of adapting to different tissue niches after transfer (Lavin et al., 2014; Nussbaum et al., 2017). In the present study, we observed flexible phenotypic adaptation of the transferred effector ILC2 populations isolated from the kidney, lung, and SILP. We used several strategies in combination to minimize the probability that the effects observed here are due to expansion and differentiation of transferred ILC2 tissue precursor populations: (1) sorting of IL-33R+KLRG1+IL-5hi ILC2s to a high purity (99.9%, see Fig. 3 C) minimizes ILC2 tissue progenitor contamination; (2) scRNAseq of ILC2 populations before transfer shows absence of TCF-7+IL-18R+ ILC2 tissue progenitors in the transferred ILC2 population (see Fig. S3); and (3) RNA velocity analyses of adapting kidney ILC2s in the small intestine supports continuous adaptation of effector ILC2s from the "kidney program" toward the "small intestinal program" (see Fig. 5). However, formal proof of mature effector ILC2 adaptation would require clonal single-cell readouts, which is extremely challenging in innate cells that cannot be tracked using rearranged antigen receptors for endogenous single-cell barcoding. In the future, somatic mitochondrial DNA mutations might offer a possibility for endogenous barcoding of innate lymphoid cell populations to address these questions on a clonal level (Rückert et al., 2022). Moreover, further investigations will be required to assess the ability of mature ILC2s from other tissues (e.g., skin, meninges, and adipose tissue) to replicate these findings.

ILC2s are believed to be distributed to tissues during the perinatal window. Here, they undergo proliferation and expansion and maintain residency in homeostatic conditions, replenishing through tissue precursor expansion (Gasteiger et al., 2015; Huang et al., 2018; Moro et al., 2016; Schneider et al., 2019). However, under inflammatory conditions, such as allergic lung inflammation and prolonged helminth infection, ILC2s from non-lymphoid organs or their precursors from bone marrow have been reported to undergo hematogenous trafficking to affected organs where they contribute to the tissue ILC2 pool (Gasteiger et al., 2015; Huang et al., 2018; Karta et al., 2018; Ricardo-Gonzalez et al., 2020; Stier et al., 2018; Zeis et al., 2020). Collectively, these data suggest that interorgan trafficking of effector ILC2s, as modeled in our adoptive transfer experiments, and our finding of their retained capacity for tissue-specific adaptation is relevant, especially under inflammatory conditions.

Although distinct ILC2 phenotypes have been well recognized in various tissues, the signaling pathways that define tissue-specific ILC2 programs remain poorly understood, and it remains unclear to which extent these tissue signatures can be adapted by ILC2s originating from distant sites. Here, we applied scRNAseq to ex-kidney ILC2s adapting to the small intestinal microenvironment to extract fully adaptable, partially adaptable, and non-adaptable features of the SILP ILC2 transcriptional program, as well as "hardwired" kidney ILC2 features that would not adapt to the new location. Interestingly, we failed to extract any hardwired kidney features from the data, which might indicate that kidney ILC2s exhibit a minimum of tissue-specific adaptation and express a "core ILC2 signature" that is shared with ILC2s in SILP (and presumably other locations). In contrast, several immune-related pathways, such as TNF/NF-κB, ROS, and complement signaling, were identified in the adaptable SILP-specific ILC2 signature and were (partially) acquired by kidney ILC2s in the small intestine.

Using the scRNAseq data set, we then identified RA signaling as one potential mediator of intestine-specific adaptation of effector ILC2s. A prominent feature of successful ILC2 adaptation to the SILP was upregulation of the IL-25 receptor (IL-17RB) and downregulation of the IL-33 receptor (IL-33R), a phenotype that has been observed in previous studies (Huang et al., 2018; Ricardo-Gonzalez et al., 2018; von Moltke et al., 2016). Our in vitro analysis confirmed that RA was sufficient to drive ILC2 upregulation of IL-17RB, as well as changes in other surface markers indicative of the intestine-specific phenotype (CD90.2loKLRG1hiICOSlo). In line with IL-17RB upregulation, RA increased responsiveness of ILC2s to subthreshold IL-25 stimulation, indicating functional importance of this phenotypic switch. In contrast, IL-33R expression was unaltered, and sensitivity of ILC2s to IL-33 stimulation was maintained in the presence of RA in vitro, which was in line with a previous study examining the effect of RA on lung ILC2s (Seehus et al., 2017). Importantly, blocking of RA signaling in vivo after adoptive ILC2 transfer partially inhibited the intestine-specific adaptation of ILC2s, again with the exception of IL-33R downregulation. Our scRNAseq analyses pointed at Notch signaling as another potential pathway involved, a pathway that has been implicated in ILC2 development (Wong et al., 2012) and may also play a role in ILC2 to ILC3 plasticity (Zhang et al., 2017). However, our in vitro

validation of this candidate pathway indicated that Notch activation, despite upregulation of IL-17RB and downregulation of IL-33R, acted as a general inhibitor of IL-25– and IL-33–stimulated cytokine production by ILC2s. Although combined activation of the RA and Notch pathways in vitro recapitulated most surface markers defining the intestinal ILC2 phenotype, RA was not able to functionally rescue the general inhibitory effect of Notch ligands on ILC2 cytokine responsiveness (see Fig. S5). Thus, while we established RA signaling as one driving factor for ILC2 adaptation to the intestinal microenvironment, it is evident that a complex combination of signals through various pathways (e.g., RA, Notch, and others) are integrated by SILP ILC2s to shape their full intestine-specific phenotype and function.

As tissue-specific surface receptor expression of ILC2s impacts their functional response in the lung and skin (Ricardo-Gonzalez et al., 2018; Zhang et al., 2022), we hypothesized that RA-mediated ILC2 adaptation to the intestinal environment is required for an optimal type 2 immune response against helminths in which ILC2s play an important role (Meiners et al., 2020; Neill et al., 2010). In line with this hypothesis, we observed that inhibition of RA signaling in $Rag2^{-/-}$ mice leads to reversal of the intestinal phenotype of endogenous ILC2s, which was accompanied by reduced mast cell activation and impaired worm expulsion in acute S. ratti infection. Importantly, this effect depended on the presence of ILCs since it was not observed in ILC-deficient $Rag2^{-/-}Il2rg^{-/-}$ mice. One potential explanation for this finding could be that failed phenotypic ILC2 adaptation impairs their IL-9 production, resulting in suboptimal mast cell activation that is instrumental in S. ratti elimination from the small intestine (Meiners et al., 2020; Reitz et al., 2018). In such a setting, impaired ILC2 activation could be due to a reduced responsiveness of ILC2s to IL-25, caused by a failure to upregulate IL-17RB in the intestine under conditions of impaired RA signaling. This hypothesis is supported by several landmark studies demonstrating that IL-25 is constitutively produced by tuft cells in the small intestine, and a tuft cell/ILC2 feed-forward loop is crucial to mount an efficient anti-helminth immune response (Gerbe et al., 2016; Howitt et al., 2016; von Moltke et al., 2016). In this context, it would also be important to study the effect of IL-25 stimulation on expansion and phenotypic adaptation of ILC2s from the SILP. However, despite extensive efforts, we were unable to retrieve cells from the SILP of mice for several weeks after IL-25 application (200–400 ng per mouse i.p. for four consecutive days), presumably because of intense intestinal inflammation and mucus production induced by IL-25 treatment. Interestingly, detailed literature research revealed a lack of studies on IL-25–expanded murine SILP ILC2s, indicating that other research groups face similar technical challenges.

As previously described (Spencer et al., 2014), RA inhibition also affected ILC2/ILC3 subset distribution, resulting in a significant increase of the ILC3/ILC2 ratio in the small intestine and colon (see Fig. 7, F and G; and Fig. 8, B and C). However, while increased ILC2 abundance in conditions of impaired RA signaling was shown to improve anti-helminth response in chronic T. muris infection of the cecum (Spencer et al., 2014), we observed the opposite effect in acute S. ratti infection. This discrepancy might be explained by considerable differences in these two

helminth infection models, regarding the route of infection (S. ratti, subcutaneous versus T. muris, oral), the infection dynamics (S. ratti, acute, self-limiting infection versus T. muris, chronic infection), and probably the most important, the target segment in the intestine (S. ratti, small intestine versus T. muris, cecum). Our data indeed showed low abundance and low IL-17RB expression of ILC2s in the cecum as compared with the SILP (see Fig. 8, H and I). This supports the hypothesis that an increase in ILC2 abundance under RAi treatment (Spencer et al., 2014) is likely to have a positive impact on worm expulsion in cecal T. muris infection, while IL-17RB upregulation is less relevant (as IL-17RB levels are generally low on cecal ILC2s). In S. ratti infection of the small intestine, in contrast, impaired expression of IL-17RB (and potentially other functional markers) under RA signaling inhibition is functionally relevant (as IL-17RB levels are high at steady state), and hence, impaired ILC2 adaptation results in impaired control of helminth infections.

In conclusion, the results presented here attribute an important role to RA signaling in ILC2 adaptation to the small intestine, a mechanism that had not been demonstrated before. However, the study must be considered in the context of several limitations. First, to definitively prove the cell-intrinsic role of RA signaling in intestinal adaptation of ILC2s, transfer experiments with ILC2s deficient in RA signaling would be required. However, owing to the complexity of RA signaling pathway and potential involvement of several RA receptors (e.g., $Rara$, $Rxrb$, and $Rxrg$ were expressed in SILP ILC2s), this would require targeting multiple receptors or their downstream signaling components in mice by complex genetic modifications. Second, although demonstrated by ex vivo ILC2 culture experiments, the direct in vivo link between RA-mediated upregulation of IL-17RB expression on SILP ILC2s, increased IL-25 sensitivity, and consequently, alteration of ILC2 in vivo function (e.g., increased cytokine production) has not been shown here. In addition, the predicted RA-induced modulation of IL-17RB downstream signaling (see Fig. 6 K) awaits further exploration to substantiate its mechanistic basis. Finally, we propose a differential response of ILC2s in different intestinal segments (e.g., small versus large intestine) which might offer an explanation for the opposing effects of RA inhibition on defense against different helminth species (Spencer et al., 2014). While the segment-specific ILC2 abundance and expression pattern of IL-17RB and IL-33R (Fig. 8, H and I) suggests differential in vivo functions, a formal proof of this hypothesis is still lacking and warrants further investigations.

Regardless of these limitations, our study highlights that effector ILC2s, after hematogenous trafficking, retain the capacity to adapt to new tissue-specific microenvironments, which may enable them to exert tissue-specific functions, such as promoting control of intestinal helminth infections.

Materials and methods
Animals
C57BL/6 wild type, BALB/c wild type, C57BL/6 $Rag2^{-/-}Il2rg^{-/-}$, C57BL/6 CD45.1, BALB/c $Rag2^{-/-}Il2rg^{-/-}$, BALB/c $Rag2^{-/-}$, and C57BL/6 $IL5^{tdTomato}$ (Red5) mice were bred in the animal

Shaikh et al.
Retinoic acid mediates intestinal ILC2 adaptation

Journal of Experimental Medicine   15 of 20
https://doi.org/10.1084/jem.20221015

facility of the University Medical Centre Hamburg-Eppendorf under specific pathogen–free conditions. BALB/c *Il13*[YFP/Cre] were purchased from the Jackson Laboratory and crossed with BALB/c LSL-*R26r*[tdTomato] mice to generate IL13[fm] mice and bred in the animal facility of the University Medical Centre Hamburg-Eppendorf under specific pathogen–free conditions. Adult male and female mice with the appropriate sex- and age-matched controls were used in all experiments. All animal experiments were performed according to national and institutional animal care and ethical guidelines and were approved by the local committees (approval number: N054/2020; Behörde für Gesundheit und Verbraucherschutz, Freie und Hansestadt Hamburg).

In vivo treatments
For ILC2 activation and expansion, mice received injections of 200 or 400 ng recombinant mouse (rm) IL-33 (BioLegend) in 200 µl PBS i.p. on four consecutive days. Controls received 200 µl PBS. ILC2s were isolated at 2–3 wk after the first IL-33 injection. To block RA signaling, a pan-RAi (BMS493; R&D) was dissolved in DMSO (final conc. 29.3 µg/µl). 220 µg RAi/animal (diluted in PBS) was administered i.p. every second day. The same DMSO concentration was administered to control animals.

S. ratti infection, adult worm count, and mast cell activation
The *S. ratti* cycle was maintained in Wistar rats, and stage 3 larvae were isolated from their charcoal feces culture 1 d before infection using the Baermann technique. Infection of BALB/c *Rag2*^{−/−}*Il2rg*^{−/−} and BALB/c *Rag2*^{−/−} mice was performed by s.c. injection of 2,000 stage 3 larvae in 30 µl PBS into the hind footpad, as described earlier (Eschbach et al., 2010). To count the adult worms on day 6 after infection, the small intestine was cut open longitudinally, washed to remove feces, and tissue was incubated for 3 h at 37°C in tap water while thoroughly shaking every hour for 10 s by hand. After allowing the worms to settle down (~30 min at room temperature), supernatant was removed and adult worms were counted under a bright-field microscope in a double-blinded fashion. For mast cell activation analysis, blood was collected on day 6 after infection. Serum was analyzed using the MCPT-1 Uncoated ELISA Kit (Thermo Fisher Scientific) according to the manufacturer's instructions.

Cell isolation
For the isolation of renal leukocytes, mouse kidneys were cut into small pieces and digested in complete medium (RPMI 1640, 10% fetal bovine serum, 1% Hepes, 1% penicillin/streptomycin; all Gibco) supplemented with collagenase D (0.4 mg/ml; Roche) and DNase I (100 µg/ml; Roche) for 45 min at 37°C while rotating on a MACSmix tube rotator (Miltenyi) and subsequently further shred using gentleMACS dissociation (Miltenyi). Lungs were cut into small pieces and digested in a complete medium supplemented with Liberase (0.42 mg/ml; Roche) and DNase I (100 µg/ml; Roche) for 45 min at 37°C while rotating. Afterward, the suspension was mashed through a 70-µm nylon strainer. For the isolation of leukocytes from the SILP, cecum, and colon, Peyer's patches were removed, the intestine was opened longitudinally, and washed in PBS supplemented with 1% FCS, 5 mM EDTA

(Sigma-Aldrich), and 1 mM dithiothreitol (Sigma-Aldrich) for 7 min at 37°C on the shaker. After a second round of shaking (without dithiothreitol), epithelial cells were discarded while the remaining intestinal tissue was minced and incubated in complete medium supplemented with 500 µg/ml collagenase VIII (Sigma-Aldrich) and 20 µg/ml DNAse I (Roche) on a shaker for 30 min at 37°C. Then, cells were mashed through a 70-µm nylon strainer. Further, leukocyte purification was achieved by Percoll gradient centrifugation (37.5%; GE Healthcare). After subsequent erythrocyte lysis with ammonium chloride (kidney and lung only), cell suspensions were filtered through a 50-µm nylon strainer and used for further analyses.

Flow cytometry
Nonspecific antibody binding was prevented by incubation with 10% normal mouse serum (Jackson ImmunoResearch Laboratories). To characterize ILC subsets, cell suspensions of mouse kidneys, lungs, and SILP were stained with fluorochrome-coupled antibodies (all from BioLegend, unless otherwise indicated) against CD45 (30-F11), IL-7Rα (CD127; A7R34), Thy1.2 (CD90.2; 30-H12), and a combination of lineage markers (Lin), including CD3 (145-2C11), CD4 (RM4-5), CD5 (53-7.3), CD8 (53-6.7), CD11b (M1/70), CD11c (HL-3; BD), CD19 (6D5), CD49b (HMα2), TCR-β (H57-597), TCR-γδ (GL3), GR-1 (RB6-8C5), and Ter119 (Ter119). For further characterization of ILC surface marker expression, antibodies against CD25 (PC61.5), IL-33R (RMST2-33; Invitrogen), IL-17RB (CD335; 752101; R&D), KLRG1 (2F1/KLRG1), Ly6A/E (Sca-1; D7), ICOS (C398.4A), NKp46 (29A1.4), and CD117 (c-kit; 2B8) were used. Intranuclear staining (INS), using antibodies against GATA-3 (L50-823; BD), T-bet (4B10), ROR-γt (B2D; BD), Eomes (Dan11mag; eBioscience), and Ki67 (B56; eBioscience), was generally performed with the Transcription Factor Staining Buffer Set (eBioscience) according to the manufacturer's instruction. INS of leukocytes isolated from reporter mice was performed with a special protocol. After staining of the surface markers, isolated leukocytes were fixed with 3.7% paraformaldehyde (Sigma-Aldrich) for 25 min at room temperature and subsequently resuspended in Perm Wash buffer from the above-mentioned Transcription Factor Staining Set supplemented with INS antibodies and incubated overnight at 4°C. For intracellular cytokine staining, isolated leukocytes were restimulated with phorbol 12-myristate 13-acetate (1 µg/ml; Sigma-Aldrich) and ionomycin (1 µg/ml; Calbiochem) in the presence of brefeldin A (10 µg/ml; Sigma-Aldrich) and β-mercaptoethanol (0.05 mM; Thermo Fisher Scientific) for 2.5 h, stained for surface markers as described above, fixed with fixation/permeabilization buffer from the abovementioned Transcription Factor Staining Buffer Set for 25 min at room temperature, and permeabilized with IGEPAL CA-630 (0.1%; Sigma-Aldrich) for 4 min at room temperature. Subsequently, cells were resuspended in Perm Wash buffer for staining with a combination of fluorochrome-coupled antibodies against IL-13 (eBio13A; eBioscience), IL-5 (TRFK5; BioLegend), amphiregulin (Areg; polyclonal Goat IgG; R&D Systems), and IL-4 (11B11; BD) overnight at 4°C. Dead-cell staining was performed using LIVE/DEAD Fixable Read Dead Stain Kit (Invitrogen) or Zombie Dye (BioLegend). The absolute numbers of CD45^{+} cells in cell

Shaikh et al.
Retinoic acid mediates intestinal ILC2 adaptation

Journal of Experimental Medicine
https://doi.org/10.1084/jem.20221015

16 of 20

suspension were determined by staining with fluorochrome-coupled anti-CD45 combined with cell-count beads (Countbright; Invitrogen). All samples were acquired on a Becton Dickinson LSRII flow cytometer (BD) using the Diva software and analyzed with the FlowJo Software (Treestar, Inc.). Dimensionality reduction and visualization of high-dimensional flow cytometry data were performed using the UMAP plugin of the FlowJo software v10.

Cell sorting
For sorting of ILC2s from the kidneys, cells were isolated as described above. Instead of using a Percoll gradient, leukocytes were enriched with the CD45 microbeads MACS Cell separation technology (Miltenyi) according to the manufacturer's instruction. For the isolation of lung ILC2s, the EasySep Mouse ILC2 Enrichment Kit (Stemcell) was used prior to flow cytometry–based cell sorting. ILC2s from the small intestine were isolated as described above. For adoptive cell transfer experiments, in vivo IL-33–expanded ILC2s from kidney, lung, and SILP were defined as CD45+Lin−CD127+KLRG1+ and FACS purified from wild type C57BL/6 CD45.1 mice. Transfer of effector ILC2s was performed using IL-33–activated CD45+Lin−CD127+IL-33R+KLRG1+Red5+ ILC2s sorted from the kidneys of C57BL/6 Red5 mice. For adoptive transfers, 5–10 × 10^4 ILC2s were administered i.v. into Rag2$^{−/−}$Il2rg$^{−/−}$ recipient mice. For scRNAseq of ILC2s from the kidneys and SILP from BALB/c IL13^{fm} mice, CD45+Lin−CD127+IL13^{fm+} ILC2s were sorted and further processed. All samples were sorted on a BD FACSAria Fusion.

Bulk RNAseq
RNA from 2 to 3 × 10^4 ILC2s was isolated using the RNeasy Plus Micro Kit (QIAGEN) according to the manufacturer's instructions. The quality of prepared RNA was assessed using the Agilent 2100 Bioanalyzer (Agilent Technologies). After library construction, quality control with Qubit 2.0 fluorometer (Life Technologies) was applied. Sequencing was performed by Novogene using the HiSeq 4000 platform with paired-end of 150 bp (PE 150) sequencing strategy (Illumina). Sequence reads were trimmed to remove sequencing adapters by Trimmomatic 0.38 (Bolger et al., 2014), discarding sequences shorter than 36 bps. Trimmed reads were then aligned to the mouse reference assembly (GRCM38.92) using STAR (v2.5.4b; Dobin et al., 2013). Differential expression analysis was carried out using DESeq2 (Love et al., 2014) and R. Significantly differentially expressed genes (false discovery rate < 0.1 and abs. Log$_2$FC > 1) were used in further analysis. Processed and raw data files of the bulk RNAseq data are available from the Gene Expression Omnibus (https://www.ncbi.nlm.nih.gov/geo/) under the accession number GSE242571.

scRNAseq
Single-cell libraries of sorted cells were generated with the 10X Genomics Chromium Single Cell 5′v1.1 reagents kit according to the manufacturer's protocol. The libraries were sequenced on Illumina NovaSeq 6000 with 150 base pairs and paired-end configurations. Cell Ranger (version 4.0.0) was used to demultiplex cellular barcodes and map reads to the reference

genome (mm10-Ensemble 98). Transcriptomic data were added into a single Seurat object (v.4.0.2). After exclusion of low-quality cells (<500 or >2,500 genes expressed), low expressed genes (<3 genes per cell), and cells with high mitochondrial gene number (>8% of all genes), unsupervised clustering was performed using standard workflow by Seurat. UMAP calculated for the first five principal components was used for dimensionality reduction and plotting. Clusters were assigned according to the sample of origin. DE analyses between cell clusters were performed with the FindAllMarkers function of Seurat. For RNA velocity analysis, a loom-file containing the splicing information was generated using velocyto. Using the python (V3.8.8) package "scVelo" (V0.2.5), the data was preprocessed with the function scv.pp.filter_and_normalize() with standard parameters. Then, first- and second-order moments were computed with scv.pp.moments(). RNA velocity was estimated with scv.tl.velocity in the stochastic mode. Plots were generated using the scv.tl.velocity_graph() and then the scv.pl.velocity_embedding_stream() function. To plot gene expression over pseudotime, pseudotime information was calculated with the scv.tl.velocity_pseudotime function. Then, terminal and initial cell states were determined using the cr.tl.terminal_states() and cr.tl.initial_states() function of the "CellRank" package (V1.5.1). Then, general additive models were fitted on gene expression data and transcripts were plotted using the cr.pl.gene_trends() function. The expression modules (SILP program, kidney program) were plotted using the geom_smooth function of the R package ggplot2 with the pseudotime and score values. For GO term analysis, we compared the gene expression of two clusters with a wilcoxauc() test of the presto library (V1.0.0), arranged the genes according to their area under the curve, and performed gene set enrichment using the fgsea() function of the R library fgsea (V. 1.16.0) with nperm = 1,000. Gene sets were downloaded using the msigdbr function of the msigdbr R library (V7.5.1). RA signaling score was generated by combining GO terms for RA receptor binding (GO:0046965), RA receptor signaling pathway (GO:0048384), and response to RA (GO:0032526), and used for analysis within the AddModuleScore function with default parameters. The Notch signaling score was generated similarly using the Notch signaling pathway (KEGG PATHWAY: hsa04330). Overlay of the Tcf7 and Il18r1 mRNA expression was performed using the Seurat FeaturePlot function using the blend parameter. Processed and raw data files of the scRNAseq data are available from the Gene Expression Omnibus (https://www.ncbi.nlm.nih.gov/geo/) under the accession number GSE242571.

Immunohistochemistry
For staining of tdTomato-positive ILC2s in Red5 mice, 2.5-μm-thick paraffin sections from kidney and SILP were heated at 98°C for 40 min in DAKO antigen retrieval buffer (pH 9; Agilent Technologies). Unspecific binding was blocked with 5% horse serum (Vector Laboratories) and 0.05% triton-X100 in PBS. The sections were then incubated with goat anti-tdTomato (1:2,000, orb182397; Biorbyt) in 5% horse serum overnight at 4°C. Next, the sections were incubated with biotinylated rabbit anti-goat antibody (BA-5000; Vector Laboratories) followed by incubation

with anti-rabbit polymer (POLAP-006; Zytomed Systems). Finally, the development and nuclear staining of stained sections were performed with New Fuchsin and Hemalaun, respectively. Tissue slices were evaluated with an Axioskop light microscope (Zeiss) and photographed with an Axiocam HRc camera (Zeiss).

Cell culture and cytokine quantification

FACS-purified kidney ILC2s (defined as CD45$^+$Lin$^-$CD127$^+$KLRG1$^+$) from IL-33–treated mice were cultured (~10,000 cells/well) in a 96-well U-bottom plate in Iscove's Modified Dulbecco's Medium containing 5% FCS, 1% penicillin/streptomycin, and 50 μM 2-mercaptoethanol (all Gibco) in the presence of rmIL2 (10 ng/ml, BioLegend) with or without all trans RA (1 μM; Enzo Life Sciences). In some experiments, the plate was precoated with the Notch ligand DLL4 (2.5 μg/ml; R&D) for at least 3 h at 37°C. Cells were cultured for 4 d and analyzed for surface marker expression using flow cytometry. In some experiments, cells were stimulated with either rmIL-25 (1 ng/ml; R&D) or rmIL-33 (1 ng/ml) on day 3 and culture supernatants were collected 24 h later and analyzed for IL-5 and IL-13 protein with the LEGENDplex bead-based immunoassay according to the manufacturer's instructions (BioLegend).

Statistics

The two-tailed parametric t test was used for comparison between two groups. In case of three or more groups, ordinary one-way ANOVA with Tukey's post hoc test was used. A P value of <0.05 was considered to be statistically significant.

Online supplemental material

Fig. S1 characterizes ILC subsets and ILC2s in different organs. Fig. S2 shows gating and sorting strategies for analysis and purification of ILCs from different organs. Fig. S3 depicts the sorting purity and scRNAseq analysis of kidney ILC2s. Fig. S4 illustrates cluster-defining genes and pathway analysis of scRNAseq data. Fig. S5 shows Notch signaling in intestine-specific adaptation of kidney ILC2s in vitro.

Data availability

All the data in the figures are available in the published article and its online supplemental material. Bulk RNAseq and scRNAseq dataset (raw and processed data) are available from the Gene Expression Omnibus (https://www.ncbi.nlm.nih.gov/geo/) under the accession number GSE242571.

Acknowledgments

References

Bando, J.K., H.E. Liang, and R.M. Locksley. 2015. Identification and distribution of developing innate lymphoid cells in the fetal mouse intestine. Nat. Immunol. 16:153–160. https://doi.org/10.1038/ni.3057

Bar-Ephraim, Y.E., J.J. Koning, E. Burniol Ruiz, T. Konijn, V.P. Mourits, K.A. Lakeman, L. Boon, M. Bögels, J.P. van Maanen, J.M.M. Den Haan, et al. 2019. CD62L is a functional and phenotypic marker for circulating innate lymphoid cell precursors. J. Immunol. 202:171–182. https://doi.org/10.4049/jimmunol.1701153

Bartholin, L., S.E. Powers, T.A. Melhuish, S. Lasse, M. Weinstein, and D. Wotton. 2006. TGIF inhibits retinoid signaling. Mol. Cell. Biol. 26:990–1001. https://doi.org/10.1128/MCB.26.3.990-1001.2006

Bolger, A.M., M. Lohse, and B. Usadel. 2014. Trimmomatic: A flexible trimmer for Illumina sequence data. Bioinformatics. 30:2114–2120. https://doi.org/10.1093/bioinformatics/btu170

Borowczyk, J., M. Shutova, N.C. Brembilla, and W.H. Boehncke. 2021. IL-25 (IL-17E) in epithelial immunology and pathophysiology. J. Allergy Clin. Immunol. 148:40–52. https://doi.org/10.1016/j.jaci.2020.12.628

Breloer, M., and D. Abraham. 2017. Strongyloides infection in rodents: Immune response and immune regulation. Parasitology. 144:295–315. https://doi.org/10.1017/S0031182016000111

Dobin, A., C.A. Davis, F. Schlesinger, J. Drenkow, C. Zaleski, S. Jha, P. Batut, M. Chaisson, and T.R. Gingeras. 2013. STAR: Ultrafast universal RNA-seq aligner. Bioinformatics. 29:15–21. https://doi.org/10.1093/bioinformatics/bts635

Düster, M., M. Becker, A.C. Gnirck, M. Wunderlich, U. Panzer, and J.E. Turner. 2018. T cell-derived IFN-γ downregulates protective group 2 innate lymphoid cells in murine lupus erythematosus. Eur. J. Immunol. 48:1364–1375. https://doi.org/10.1002/eji.201747303

Eschbach, M.L., U. Klemm, J. Kolbaum, B. Blankenhaus, N. Brattig, and M. Breloer. 2010. Strongyloides ratti infection induces transient nematode-specific Th2 response and reciprocal suppression of IFN-gamma production in mice. Parasite Immunol. 32:370–383. https://doi.org/10.1111/j.1365-3024.2010.01199.x

Gadani, S.P., I. Smirnov, A.T. Wiltbank, C.C. Overall, and J. Kipnis. 2017. Characterization of meningeal type 2 innate lymphocytes and their response to CNS injury. J. Exp. Med. 214:285–296. https://doi.org/10.1084/jem.20161982

Shaikh et al.
Retinoic acid mediates intestinal ILC2 adaptation

Journal of Experimental Medicine
https://doi.org/10.1084/jem.20221015

18 of 20

Gasteiger, G., X. Fan, S. Dikiy, S.Y. Lee, and A.Y. Rudensky. 2015. Tissue residency of innate lymphoid cells in lymphoid and nonlymphoid organs. *Science*. 350:981–985. https://doi.org/10.1126/science.aac9593

Gerbe, F., E. Sidot, D.J. Smyth, M. Ohmoto, I. Matsumoto, V. Dardalhon, P. Cesses, L. Garnier, M. Pouzolles, B. Brulin, et al. 2016. Intestinal epithelial tuft cells initiate type 2 mucosal immunity to helminth parasites. *Nature*. 529:226–230. https://doi.org/10.1038/nature16527

Hams, E., M.E. Armstrong, J.L. Barlow, S.P. Saunders, C. Schwartz, G. Cooke, R.J. Fahy, T.B. Crotty, N. Hirani, R.J. Flynn, et al. 2014. IL-25 and type 2 innate lymphoid cells induce pulmonary fibrosis. *Proc. Natl. Acad. Sci. USA*. 111:367–372. https://doi.org/10.1073/pnas.1315854111

Howitt, M.R., S. Lavoie, M. Michaud, A.M. Blum, S.V. Tran, J.V. Weinstock, C.A. Gallini, K. Redding, R.F. Margolskee, L.C. Osborne, et al. 2016. Tuft cells, taste-chemosensory cells, orchestrate parasite type 2 immunity in the gut. *Science*. 351:1329–1333. https://doi.org/10.1126/science.aaf1648

Huang, Y., K. Mao, X. Chen, M.A. Sun, T. Kawabe, W. Li, N. Usher, J. Zhu, J.F. Urban Jr, W.E. Paul, and R.N. Germain. 2018. S1P-dependent interorgan trafficking of group 2 innate lymphoid cells supports host defense. *Science*. 359:114–119. https://doi.org/10.1126/science.aam5809

Iwata, M. 2009. Retinoic acid production by intestinal dendritic cells and its role in T-cell trafficking. *Semin. Immunol.* 21:8–13. https://doi.org/10.1016/j.smim.2008.09.002

Jeffrey, K.L., M. Camps, C. Rommel, and C.R. Mackay. 2007. Targeting dual-specificity phosphatases: Manipulating MAP kinase signalling and immune responses. *Nat. Rev. Drug Discov.* 6:391–403. https://doi.org/10.1038/nrd2289

Karagiannis, F., and C. Wilhelm. 2018. Innate lymphoid cells-key immune integrators of overall body homeostasis. *Semin. Immunopathol.* 40:319–330. https://doi.org/10.1007/s00281-018-0684-y

Karta, M.R., P.S. Rosenthal, A. Beppu, C.Y. Vuong, M. Miller, S. Das, R.C. Kurten, T.A. Doherty, and D.H. Broide. 2018. β₂ integrins rather than β₁ integrins mediate Alternaria-induced group 2 innate lymphoid cell trafficking to the lung. *J. Allergy Clin. Immunol.* 141:329–338.e12. https://doi.org/10.1016/j.jaci.2017.03.010

Kim, M.H., E.J. Taparowsky, and C.H. Kim. 2015. Retinoic acid differentially regulates the migration of innate lymphoid cell subsets to the Gut. *Immunity*. 43:107–119. https://doi.org/10.1016/j.immuni.2015.06.009

Klose, C.S.N., and D. Artis. 2016. Innate lymphoid cells as regulators of immunity, inflammation and tissue homeostasis. *Nat. Immunol.* 17:765–774. https://doi.org/10.1038/ni.3489

La Manno, G., R. Soldatov, A. Zeisel, E. Braun, H. Hochgerner, V. Petukhov, K. Lidschreiber, M.E. Kastriti, P. Lönnerberg, A. Furlan, et al. 2018. RNA velocity of single cells. *Nature*. 560:494–498. https://doi.org/10.1038/s41586-018-0414-6

Lavin, Y., D. Winter, R. Blecher-Gonen, E. David, H. Keren-Shaul, M. Merad, S. Jung, and I. Amit. 2014. Tissue-resident macrophage enhancer landscapes are shaped by the local microenvironment. *Cell*. 159:1312–1326. https://doi.org/10.1016/j.cell.2014.11.018

Lim, A.I., Y. Li, S. Lopez-Lastra, R. Stadhouders, F. Paul, A. Casrouge, N. Serafini, A. Puel, J. Bustamante, L. Surace, et al. 2017. Systemic human ILC precursors provide a substrate for tissue ILC differentiation. *Cell*. 168:1086–1100.e10. https://doi.org/10.1016/j.cell.2017.02.021

Love, M.I., W. Huber, and S. Anders. 2014. Moderated estimation of fold change and dispersion for RNA-seq data with DESeq2. *Genome Biol.* 15:550. https://doi.org/10.1186/s13059-014-0550-8

Lu, T.C., Z. Wang, X. Feng, P. Chuang, W. Fang, Y. Chen, S. Neves, A. Maayan, H. Xiong, Y. Liu, et al. 2008. Retinoic acid utilizes CREB and USF1 in a transcriptional feed-forward loop in order to stimulate MKP1 expression in human immunodeficiency virus-infected podocytes. *Mol. Cell. Biol.* 28:5785–5794. https://doi.org/10.1128/MCB.00245-08

Masopust, D., and A.G. Soerens. 2019. Tissue-resident T cells and other resident leukocytes. *Annu. Rev. Immunol.* 37:521–546. https://doi.org/10.1146/annurev-immunol-042617-053214

McHedlidze, T., M. Waldner, S. Zopf, J. Walker, A.L. Rankin, M. Schuchmann, D. Voehringer, A.N.J. McKenzie, M.F. Neurath, S. Pflanz, and S. Wirtz. 2013. Interleukin-33-dependent innate lymphoid cells mediate hepatic fibrosis. *Immunity*. 39:357–371. https://doi.org/10.1016/j.immuni.2013.07.018

Meiners, J., M. Reitz, N. Rüdiger, J.E. Turner, L. Heepmann, L. Rudolf, W. Hartmann, H.J. McSorley, and M. Breloer. 2020. IL-33 facilitates rapid expulsion of the parasitic nematode *Strongyloides ratti* from the intestine via ILC2- and IL-9-driven mast cell activation. *PLoS Pathog.* 16: e1009121. https://doi.org/10.1371/journal.ppat.1009121

Meininger, I., A. Carrasco, A. Rao, T. Soini, E. Kokkinou, and J. Mjösberg. 2020. Tissue-specific features of innate lymphoid cells. *Trends Immunol.* 41:902–917. https://doi.org/10.1016/j.it.2020.08.009

Monticelli, L.A., L.C. Osborne, M. Noti, S.V. Tran, D.M.W. Zaiss, and D. Artis. 2015. IL-33 promotes an innate immune pathway of intestinal tissue protection dependent on amphiregulin-EGFR interactions. *Proc. Natl. Acad. Sci. USA*. 112:10762–10767. https://doi.org/10.1073/pnas.1509070112

Monticelli, L.A., G.F. Sonnenberg, M.C. Abt, T. Alenghat, C.G.K. Ziegler, T.A. Doering, J.M. Angelosanto, B.J. Laidlaw, C.Y. Yang, T. Sathaliyawala, et al. 2011. Innate lymphoid cells promote lung-tissue homeostasis after infection with influenza virus. *Nat. Immunol.* 12:1045–1054. https://doi.org/10.1038/ni.2131

Moro, K., H. Kabata, M. Tanabe, S. Koga, N. Takeno, M. Mochizuki, K. Fukunaga, K. Asano, T. Betsuyaku, and S. Koyasu. 2016. Interferon and IL-27 antagonize the function of group 2 innate lymphoid cells and type 2 innate immune responses. *Nat. Immunol.* 17:76–86. https://doi.org/10.1038/ni.3309

Neill, D.R., S.H. Wong, A. Bellosi, R.J. Flynn, M. Daly, T.K.A. Langford, C. Bucks, C.M. Kane, P.G. Fallon, R. Pannell, et al. 2010. Nuocytes represent a new innate effector leukocyte that mediates type-2 immunity. *Nature*. 464:1367–1370. https://doi.org/10.1038/nature08900

Nussbaum, K., S.H. Burkhard, I. Ohs, F. Mair, C.S.N. Klose, S.J. Arnold, A. Diefenbach, S. Tugues, and B. Becher. 2017. Tissue microenvironment dictates the fate and tumor-suppressive function of type 3 ILCs. *J. Exp. Med.* 214:2331–2347. https://doi.org/10.1084/jem.20162031

Penny, H.A., S.H. Hodge, and M.R. Hepworth. 2018. Orchestration of intestinal homeostasis and tolerance by group 3 innate lymphoid cells. *Semin. Immunopathol.* 40:357–370. https://doi.org/10.1007/s00281-018-0687-8

Reitz, M., W. Hartmann, N. Rüdiger, Z. Orinska, M.L. Brunn, and M. Breloer. 2018. Interleukin-9 promotes early mast cell-mediated expulsion of *Strongyloides ratti* but is dispensable for generation of protective memory. *Sci. Rep.* 8:8636. https://doi.org/10.1038/s41598-018-26907-2

Ricardo-Gonzalez, R.R., C. Schneider, C. Liao, J. Lee, H.E. Liang, and R.M. Locksley. 2020. Tissue-specific pathways extrude activated ILC2s to disseminate type 2 immunity. *J. Exp. Med.* 217:e20191172. https://doi.org/10.1084/jem.20191172

Ricardo-Gonzalez, R.R., S.J. Van Dyken, C. Schneider, J. Lee, J.C. Nussbaum, H.E. Liang, D. Vaka, W.L. Eckalbar, A.B. Molofsky, D.J. Erle, and R.M. Locksley. 2018. Tissue signals imprint ILC2 identity with anticipatory function. *Nat. Immunol.* 19:1093–1099. https://doi.org/10.1038/s41590-018-0201-4

Riedel, J.H., M. Becker, K. Kopp, M. Düster, S.R. Brix, C. Meyer-Schwesinger, L.A. Kluth, A.C. Gnirck, M. Attar, S. Krohn, et al. 2017. IL-33-mediated expansion of type 2 innate lymphoid cells protects from progressive glomerulosclerosis. *J. Am. Soc. Nephrol.* 28:2068–2080. https://doi.org/10.1681/ASN.2016080877

Roquilly, A., J.D. Mintern, and J.A. Villadangos. 2022. Spatiotemporal adaptations of macrophage and dendritic cell development and function. *Annu. Rev. Immunol.* 40:525–557. https://doi.org/10.1146/annurev-immunol-101320-031931

Rückert, T., C.A. Lareau, M.F. Mashreghi, L.S. Ludwig, and C. Romagnani. 2022. Clonal expansion and epigenetic inheritance of long-lasting NK cell memory. *Nat. Immunol.* 23:1551–1563. https://doi.org/10.1038/s41590-022-01327-7

Samarut, E., and C. Rochette-Egly. 2012. Nuclear retinoic acid receptors: Conductors of the retinoic acid symphony during development. *Mol. Cell. Endocrinol.* 348:348–360. https://doi.org/10.1016/j.mce.2011.03.025

Schneider, C., J. Lee, S. Koga, R.R. Ricardo-Gonzalez, J.C. Nussbaum, L.K. Smith, S.A. Villeda, H.E. Liang, and R.M. Locksley. 2019. Tissue-resident group 2 innate lymphoid cells differentiate by layered ontogeny and in situ perinatal priming. *Immunity*. 50:1425–1438.e5. https://doi.org/10.1016/j.immuni.2019.04.019

Seehus, C.R., A. Kadavallore, B.d. l. Torre, A.R. Yeckes, Y. Wang, J. Tang, and J. Kaye. 2017. Alternative activation generates IL-10 producing type 2 innate lymphoid cells. *Nat. Commun.* 8:1900. https://doi.org/10.1038/s41467-017-02023-z

Simoni, Y., M. Fehlings, H.N. Kløverpris, N. McGovern, S.L. Koo, C.Y. Loh, S. Lim, A. Kurioka, J.R. Fergusson, C.L. Tang, et al. 2017. Human innate lymphoid cell subsets possess tissue-type based heterogeneity in phenotype and frequency. *Immunity*. 46:148–161. https://doi.org/10.1016/j.immuni.2016.11.005

Spencer, S.P., C. Wilhelm, Q. Yang, J.A. Hall, N. Bouladoux, A. Boyd, T.B. Nutman, J.F. Urban Jr, J. Wang, T.R. Ramalingam, et al. 2014. Adaptation of innate lymphoid cells to a micronutrient deficiency promotes type 2 barrier immunity. *Science*. 343:432–437. https://doi.org/10.1126/science.1247606

Spits, H., and J. Mjösberg. 2022. Heterogeneity of type 2 innate lymphoid cells. *Nat. Rev. Immunol.* 22:701–712. https://doi.org/10.1038/s41577-022-00704-5

Stier, M.T., J. Zhang, K. Goleniewska, J.Y. Cephus, M. Rusznak, L. Wu, L. Van Kaer, B. Zhou, D.C. Newcomb, and R.S. Peebles Jr. 2018. IL-33 promotes the egress of group 2 innate lymphoid cells from the bone marrow. *J. Exp. Med.* 215:263–281. https://doi.org/10.1084/jem.20170449

Turner, J.E., P.J. Morrison, C. Wilhelm, M. Wilson, H. Ahlfors, J.C. Renauld, U. Panzer, H. Helmby, and B. Stockinger. 2013. IL-9-mediated survival of type 2 innate lymphoid cells promotes damage control in helminth-induced lung inflammation. *J. Exp. Med.* 210:2951–2965. https://doi.org/10.1084/jem.20130071

von Moltke, J., M. Ji, H.E. Liang, and R.M. Locksley. 2016. Tuft-cell-derived IL-25 regulates an intestinal ILC2-epithelial response circuit. *Nature.* 529:221–225. https://doi.org/10.1038/nature16161

White, K.A., M.M. Yore, S.L. Warburton, A.V. Vaseva, E. Rieder, S.J. Freemantle, and M.J. Spinella. 2003. Negative feedback at the level of nuclear receptor coregulation. Self-limitation of retinoid signaling by RIP140. *J. Biol. Chem.* 278:43889–43892. https://doi.org/10.1074/jbc.C300374200

Wong, S.H., J.A. Walker, H.E. Jolin, L.F. Drynan, E. Hams, A. Camelo, J.L. Barlow, D.R. Neill, V. Panova, U. Koch, et al. 2012. Transcription factor RORα is critical for nuocyte development. *Nat. Immunol.* 13:229–236. https://doi.org/10.1038/ni.2208

Yang, J., S. Hu, L. Zhao, D.H. Kaplan, G.H. Perdew, and N. Xiong. 2016. Selective programming of CCR10(+) innate lymphoid cells in skin-draining lymph nodes for cutaneous homeostatic regulation. *Nat. Immunol.* 17:48–56. https://doi.org/10.1038/ni.3312

Zeis, P., M. Lian, X. Fan, J.S. Herman, D.C. Hernandez, R. Gentek, S. Elias, C. Symowski, K. Knöpper, N. Peltokangas, et al. 2020. In situ maturation and tissue adaptation of type 2 innate lymphoid cell progenitors. *Immunity.* 53:775–792.e9. https://doi.org/10.1016/j.immuni.2020.09.002

Zhang, J., J. Qiu, W. Zhou, J. Cao, X. Hu, W. Mi, B. Su, B. He, J. Qiu, and L. Shen. 2022. Neuropilin-1 mediates lung tissue-specific control of ILC2 function in type 2 immunity. *Nat. Immunol.* 23:237–250. https://doi.org/10.1038/s41590-021-01097-8

Zhang, K., X. Xu, M.A. Pasha, C.W. Siebel, A. Costello, A. Haczku, K. MacNamara, T. Liang, J. Zhu, A. Bhandoola, et al. 2017. Cutting edge: Notch signaling promotes the plasticity of group-2 innate lymphoid cells. *J. Immunol.* 198:1798–1803. https://doi.org/10.4049/jimmunol.1601421

Zhuang, X., J. Ma, S. Xu, M. Zhang, G. Xu, and Z. Sun. 2021. All-trans retinoic acid attenuates blue light-induced apoptosis of retinal photoreceptors by upregulating MKP-1 expression. *Mol. Neurobiol.* 58:4157–4168. https://doi.org/10.1007/s12035-021-02380-3

Supplemental material
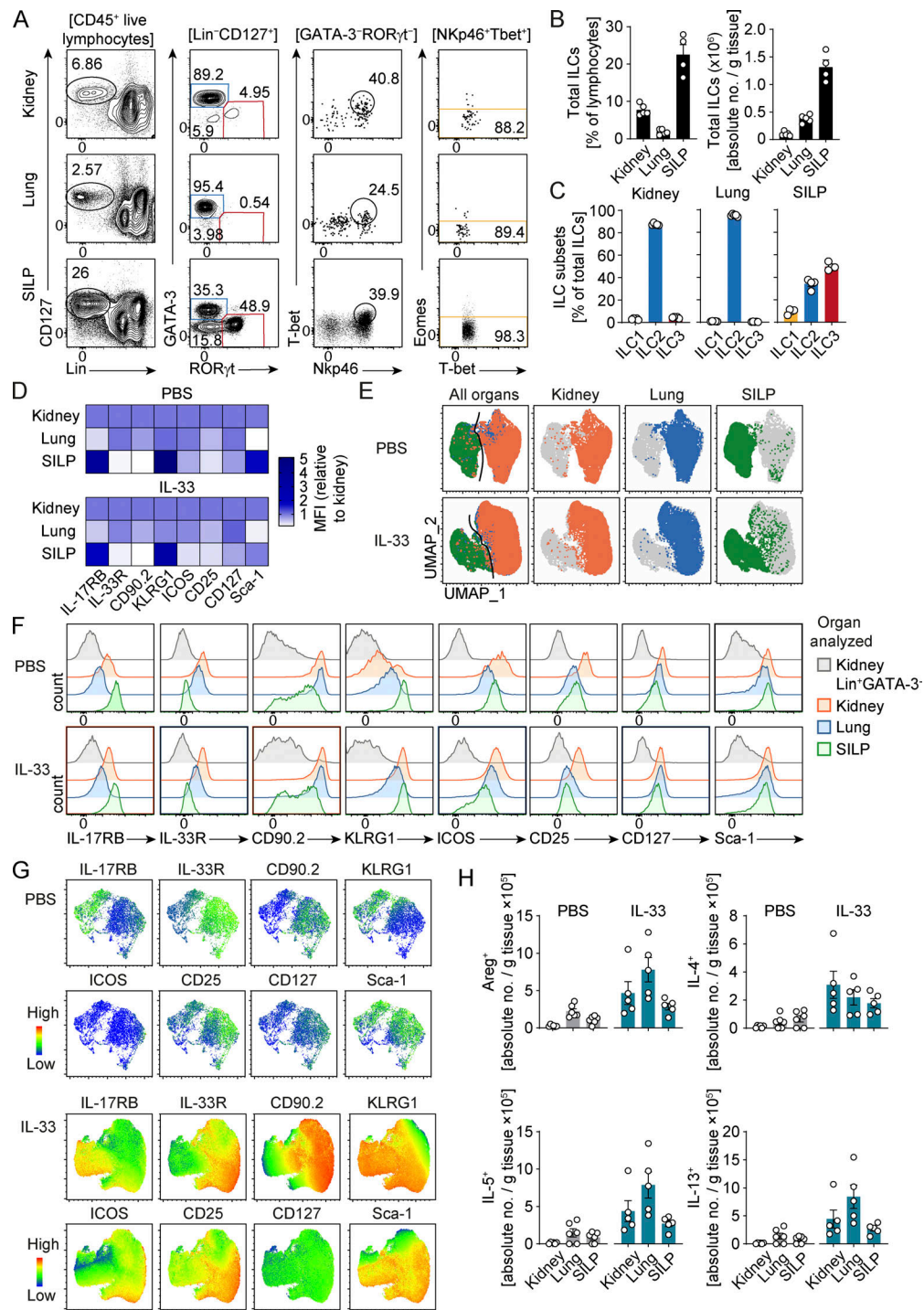
Figure S1. **Characterization of ILC subsets and ILC2s in different organs in BALB/c and C57BL/6 mice. (A)** Flow cytometric characterization and gating strategy of ILC subsets isolated from kidney, lung, and SILP of naïve BALB/c mice (blue = ILC2s, red = ILC3s, and yellow = ILC1s). Numbers indicate the percentage of events in the respective gates. **(B)** Frequencies and absolute numbers of total ILCs in kidney, lung, and SILP. **(C)** Frequencies of ILC subset distribution in the respective organs. Symbols represent individual data points, and bars indicate mean ± SEM. **(D)** Flow cytometric analysis of Lin⁻GATA-3⁺ ILC2s from PBS- or IL-33–treated (i.p. injection on four consecutive days) wild type BALB/c mice at day 12–14 after the first injection. Heat maps show MFI of various surface markers of ILC2s in the indicated organs normalized to surface marker expression of kidney ILC2s. **(E)** Unbiased UMAP clustering of the flow cytometry data from D. Plots show combined and single-organ contribution of kidney (orange), lung (blue), and SILP (green) ILC2s to the UMAP clustering. Data are representative of at least two independent experiments with similar results with n = 3–5 mice per group. **(F)** Representative histogram overlays showing surface marker expression on Lin⁻GATA-3⁺ ILC2s isolated from kidney (orange), lung (blue), and SILP (green) of PBS- or IL-33–treated (i.p. injection on four consecutive days) wild type C57BL/6 mice. **(G)** Concatenated flow cytometry data from A shown in an unbiased UMAP clustering along with multigraph color mapping of cell surface markers on UMAP projection. Lowest expression is indicated by blue and highest expression by red. **(H)** Absolute numbers of different cytokine-producing ILC2s (see Fig. 1, L and M) isolated from the kidney, lung, and SILP of PBS- (n = 6) or IL-33–treated (n = 5) wild type C57BL/6 mice. Data are pooled from two individually performed experiments.
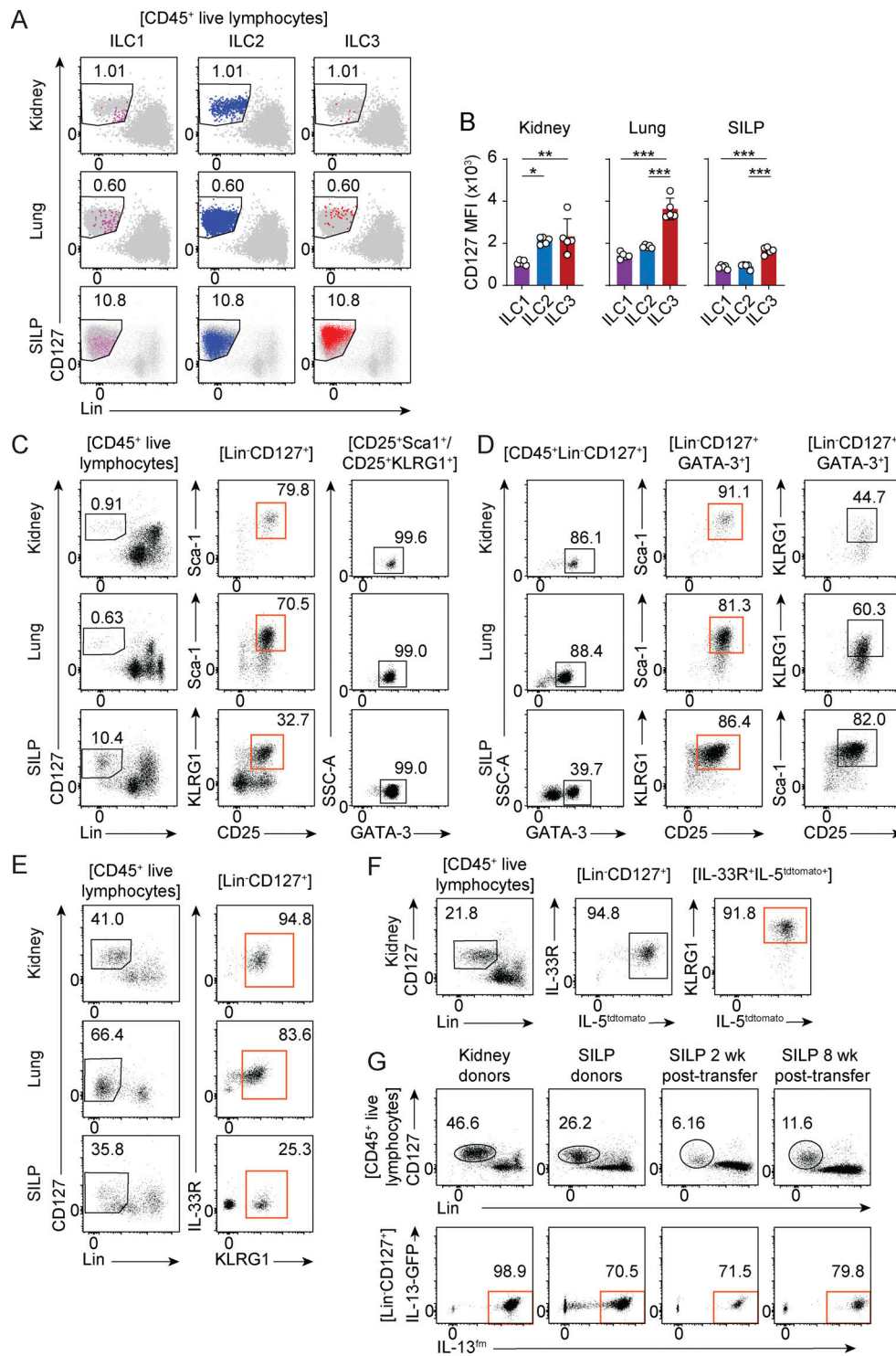
Figure S2. Gating and sorting strategies for analysis and purification of ILCs from different organs. (A) Backgating of ILC populations on the CD45+ live lymphocyte gate in naïve C57BL/6. **(B)** MFI for CD127 expression on the different ILC populations in kidney, lung, and SILP. Data are representative of at least two independent experiments with similar results with n = 3–5 mice per group. **(C)** Sorting strategy for kidney, lung, and SILP ILC2s from naïve C57BL/6 mice without using genetically modified fluorescent reporter mice for RNAseq analyses (see Fig. 1). While the Lin−CD127+CD25+Sca-1+ gate reliably identified GATA-3+ ILC2s in the kidney and lung, SILP ILC2s were better identified by the Lin−CD127+CD25+KLRG1+ gate. **(D)** Gating on all GATA-3+ ILC2s showed that the gating strategy depicted in C represents >80% of the total ILC2 population in naïve C57BL/6 mice. **(E)** Sorting strategy for IL-33–expanded ILC2s from CD45.1 BALB/c mice (see Fig. 2, A and B, for experimental setup and sorting purity). **(F)** Sorting strategy for IL-33–expanded effector ILC2s from C57BL/6 Red5 mice (see Fig. 3 for sorting purity). **(G)** Sorting strategy for IL-33–expanded ILC2s from BALB/c IL-13fm donor mice and BALB/c Rag2−/−Il2rg−/− mice recipient mice (see Fig. 4 A for experimental setup and Fig. S3, A and B, for sorting purity). Numbers in flow cytometry plots indicate the percentage of events in the repective gates. Symbols in B represent individual data points and bars indicate mean ± SEM. Statistical analysis was performed using one-way ANOVA with Tukey's post-hoc test (*P < 0.05, **P < 0.01, ***P < 0.001).
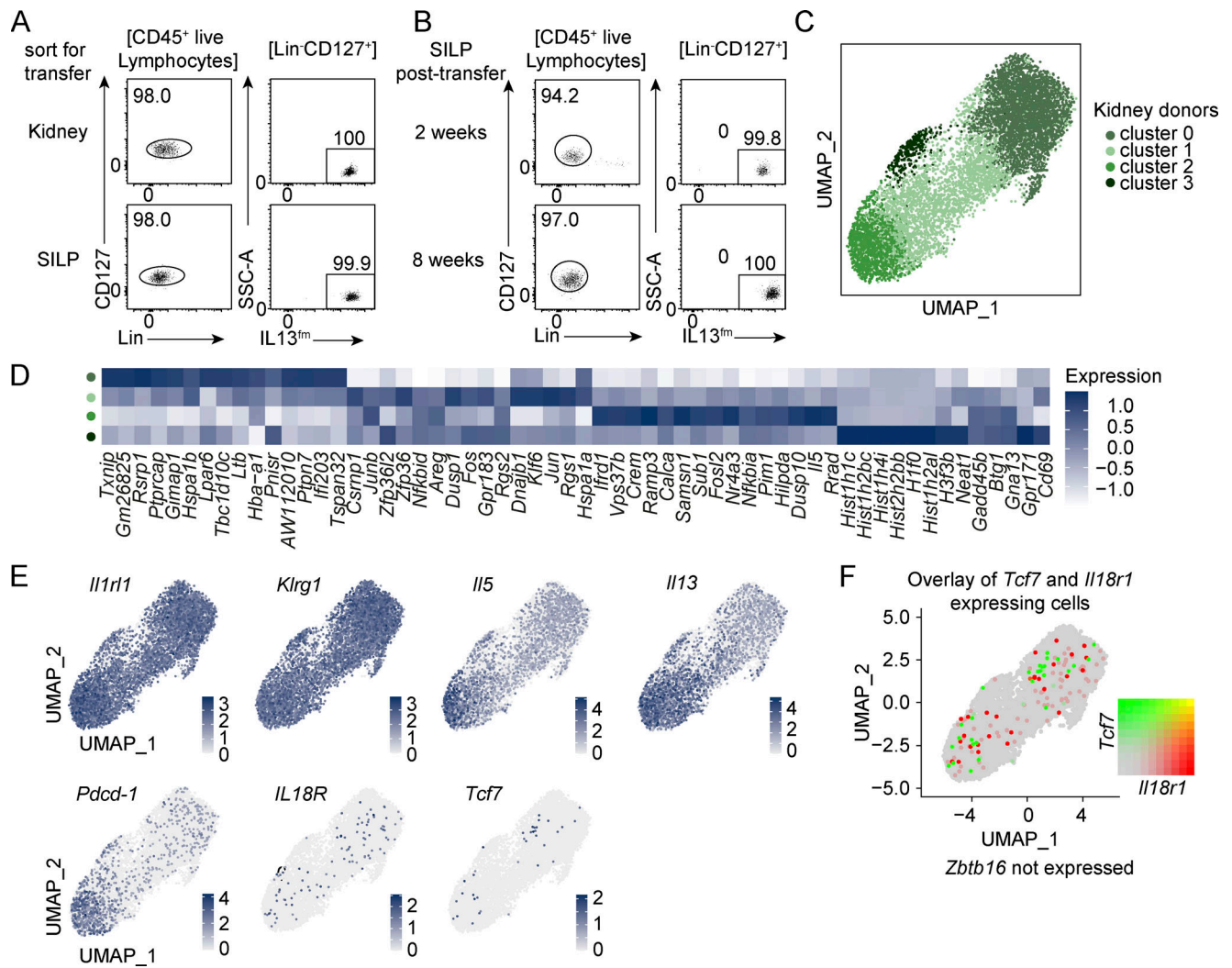
Figure S3. **Sorting purity and scRNAseq analysis of ILC2s. (A)** Representative sorting purity of ILC2s (sorted as Lin⁻CD127⁺IL-13^fm+) isolated from the kidney and SILP of IL-33–treated BALB/c IL-13^fm mice (donors) for scRNAseq. **(B)** Representative sorting purity of ILC2s (sorted as Lin⁻CD127⁺IL-13^fm+) isolated from the SILP (2 and 8 wk after transfer) of BALB/c $Rag2^{-/-}Il2rg^{-/-}$ mice that received adoptive i.v. transfer of kidney ILC2s. **(C)** Unsupervised UMAP clustering of kidney ILC2s from donor mice. **(D)** Heat map of top 15 cluster-defining genes obtained from C. **(E)** Feature plots depicting expression of key markers on the UMAP of the kidney ILC2 dataset from C. **(F)** Overlay of $Tcf7$ and $Il18r1$ genes known to be co-expressed in ILC precursors.
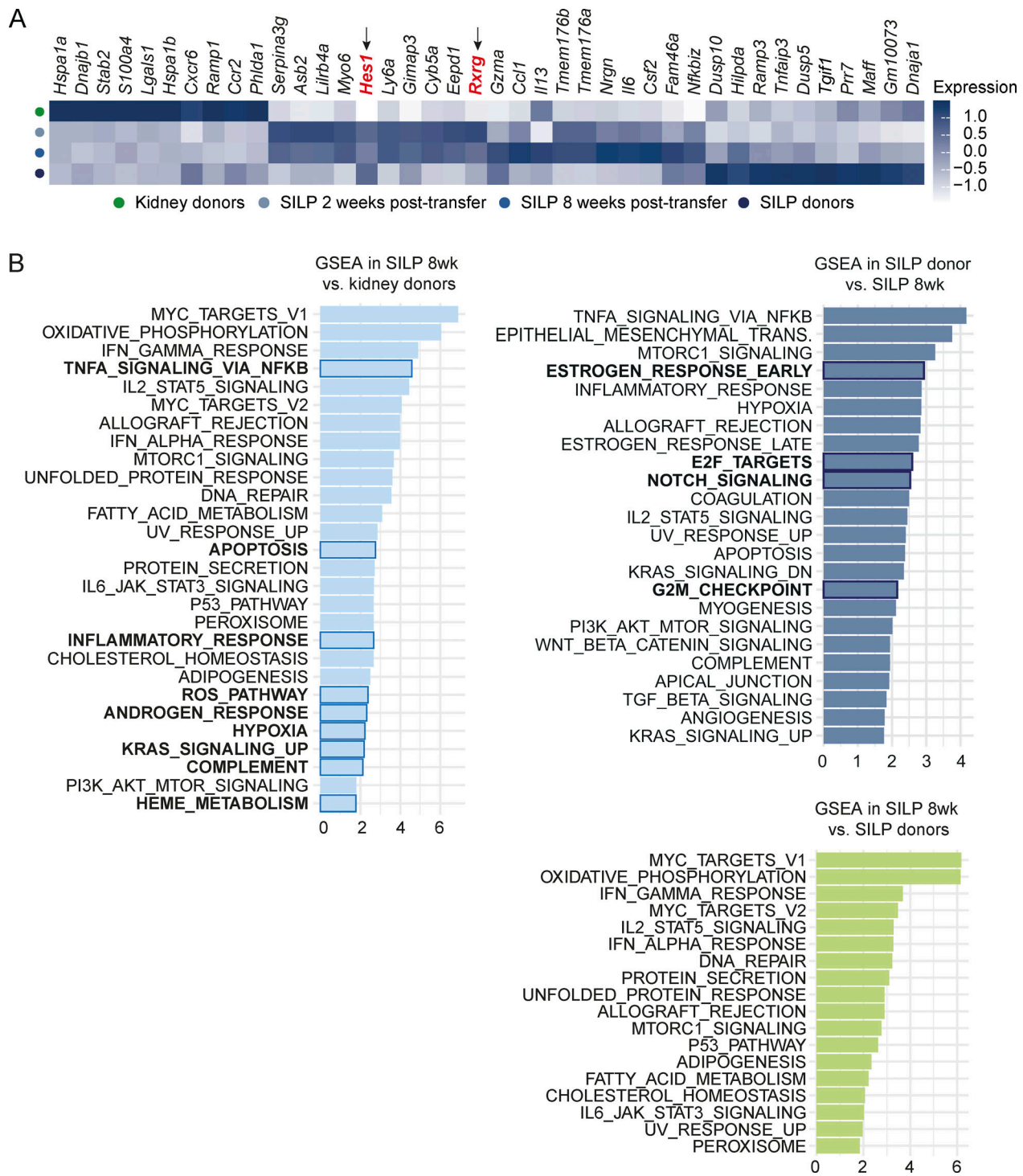
Figure S4. **Cluster-defining genes and pathway analysis of scRNAseq data. (A)** Heat map depicting top 10 cluster-defining genes for each cluster obtained from scRNAseq analysis of donor kidney and SILP ILC2s as well as recipient SILP ILC2s (see Fig. 4 A for experimental setup). Genes associated with RA and Notch signaling are marked with an arrow and labeled in red. **(B)** Gene set enrichment analysis (GSEA) for HALLMARK pathways of the Mouse Molecular Signatures Database using the genes significantly upregulated in the indicated comparisons between ILC2 populations (see Fig. 4 A for experimental setup). Specific pathways identified by further filtering (see Fig. 4, G and H) are indicated by blue boxes and marked in bold.
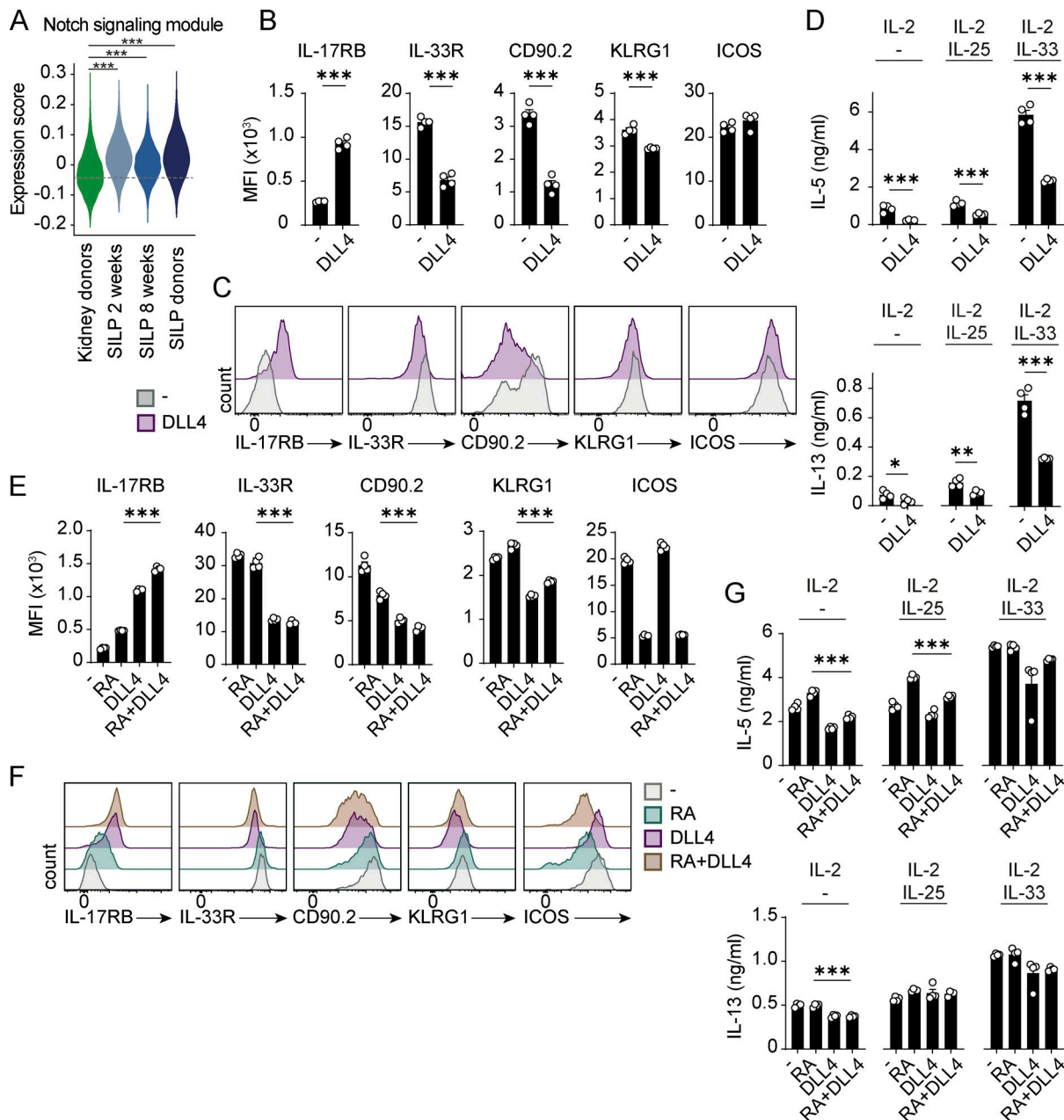
Figure S5. Notch signaling in intestine-specific adaptation of kidney ILC2s in vitro. (A) Violin plots depicting Notch signaling score in the scRNAseq data of kidney and SILP donors and recipient mice (see Fig. 4 A for experimental setup). **(B and C)** MFI (B) and representative histogram overlays (C) of surface marker expression of sorted kidney ILC2s after in vitro culture with IL-2 in the presence or absence of the Notch ligand DLL4 (2.5 µg/ml). Cells were sorted as CD45+Lin−CD127+IL-33R+KLRG1+ from the kidney of IL-33–treated C57BL/6 mice and cultured for 4 d in a 96-well plate (∼10,000 cells/well; n = 4 for each condition). **(D)** Cytokine quantification in the supernatant of the cultured kidney ILC2s stimulated with subthreshold IL-25 or IL-33 (1 ng/ml each). Cells were stimulated on day 3 for 24 h. **(E and F)** MFI (E) and representative histogram overlays (F) for surface marker expression of kidney ILC2s after culture with IL-2 in the presence or absence of RA (1 µM) and DLL4 (n = 4 for each condition). **(G)** Cytokine quantification in the supernatant of the cultivated kidney ILC2s stimulated as in E. Data are representative of three individual experiments with similar results. Symbols represent individual data points and bars indicate mean ± SEM. Statistical analysis was performed using unpaired two-tailed Student's t test (B and D) or one-way ANOVA with Tukey's post-hoc test (E and G); *P < 0.05, **P < 0.01, ***P < 0.001.

The Journal *of* Immunology

Conventional NK Cells and Type 1 Innate Lymphoid Cells Do Not Influence Pathogenesis of Experimental Glomerulonephritis

Constantin Rickassel, Ann-Christin Gnirck, Nikhat Shaikh, Virginia Adamiak, Alex Waterhölter, Yakup Tanriver, Katrin Neumann, Tobias B. Huber, Georg Gasteiger, Ulf Panzer and Jan-Eric Turner

---

Why *The JI*? Submit online.

- **Rapid Reviews! 30 days*** from submission to initial decision

- **No Triage!** Every submission reviewed by practicing scientists

- **Fast Publication!** 4 weeks from acceptance to publication

*average

Subscription   Information about subscribing to *The Journal of Immunology* is online at:
http://jimmunol.org/subscription

Permissions   Submit copyright permission requests at:
http://www.aai.org/About/Publications/JI/copyright.html

Email Alerts   Receive free email-alerts when new articles cite this article. Sign up at:
http://jimmunol.org/alerts

Conventional NK Cells and Type 1 Innate Lymphoid Cells Do Not Influence Pathogenesis of Experimental Glomerulonephritis

Constantin Rickassel,[*,†,1] Ann-Christin Gnirck,[*,†,1] Nikhat Shaikh,[*,†] Virginia Adamiak,[*,†] Alex Waterhölter,[*,†] Yakup Tanriver,[‡] Katrin Neumann,[§] Tobias B. Huber,[*,†] Georg Gasteiger,[¶] Ulf Panzer,[*,†,‖] and Jan-Eric Turner[*,†]

Innate lymphoid cells (ILCs) that express NK cell receptors (NCRs) and the transcription factor T-bet populate nonlymphoid tissues and are crucial in immune responses against viral infections and malignancies. Recent studies highlighted the heterogeneity of this ILC population and extended their functional spectrum to include important roles in tissue homeostasis and autoimmunity. In this article, we provide detailed profiling of NCR⁺T-bet⁺ ILC populations in the murine kidney, identifying conventional NK (cNK) cells and type 1 ILCs (ILC1s) as the two major subsets. Induction of renal inflammation in a mouse model of glomerulonephritis did not substantially influence abundance or phenotype of cNK cells or ILC1s in the kidney. For functional analyses in this model, widely used depletion strategies for total NCR⁺ ILCs (anti-NK1.1 Ab application) and cNK cells (anti-asialoGM1 serum application) were unreliable tools, because they were accompanied by significant off-target depletion of kidney NKT cells and CD8⁺ T cells, respectively. However, neither depletion of cNK cells and ILC1s in NKT cell–deficient mice nor specific genetic deletion of cNK cells in $Ncr1^{Cre/wt} \times Eomes^{fl/fl}$ mice altered the clinical course of experimental glomerulonephritis. In summary, we show in this article that cNK cells and ILC1s are dispensable for initiation and progression of immune-mediated glomerular disease and advise caution in the use of standard Ab depletion methods to study NCR⁺ ILC function in mouse models. *The Journal of Immunology*, 2022, 208: 1–10.

Following the discovery of the NK cell >40 y ago (1, 2), extensive research has unveiled numerous important functions of this first member of the innate lymphoid cell (ILC) family (3). In addition to their well-established role in antitumor responses (4) and defense against viral infections (5), it has become evident that NK cells play a pivotal role in immune-regulatory processes and autoimmune diseases (6).

These diverse functions of NK cells are mediated by various effector mechanisms, including target cell lysis via secretion of cytotoxic molecules (e.g., granzymes or perforin) and induction of apoptosis by death receptors, such as Fas ligand or TRAIL. In addition, NK cells have the ability to produce significant amounts of cytokines, such as IFN-γ and TNF-α, various ILs, and a broad range of chemokines that orchestrate the local immune response (4–6).

In recent years, extensive studies revealed that the NK cell population consists of diverse subpopulations with significant differences regarding phenotype, function, and distribution in peripheral blood, lymphoid organs, and nonlymphoid tissues (7). Traditionally, human NK cells are defined as CD3⁻CD56⁺ lymphocytes and then, based

on their expression level of CD56, further divided into the two major subsets of CD56^bright and CD56^dim NK cells, respectively. It is now well established that CD56^bright NK cells represent the majority of tissue-resident NK (trNK) cells, capable of producing large amounts of cytokines and regulating immune processes, while CD56^dim NK cells are the predominant subset in peripheral blood and are mainly associated with mediating cytotoxicity (7, 8).

In mice, NK cells are defined as CD3⁻NK1.1⁺ and/or NKp46⁺ lymphocytes (9). In analogy to the aforementioned NK cell subsets in humans, murine NK1.1⁺NKp46⁺CD3⁻ cells were further divided into phenotypically and functionally diverse subsets of circulating CD49b⁺Eomes⁺T-bet⁺ conventional NK (cNK) cells and CD49a⁺ Eomes⁻T-bet⁺ cells that are largely tissue resident and have been termed trNK cells by some authors (10). In recent years, the identification and detailed characterization of "helper-like" type 1 ILCs (ILC1s), which share the expression of NK cell receptors (NCRs) and the transcriptions factor T-bet with cNK cells, but do not express Eomes and exhibit less cytotoxicity, have resulted in reclassification of trNK cells in some anatomical locations as ILC1s (11–13). The relationship

*III. Department of Medicine, University Medical Center Hamburg-Eppendorf, Hamburg, Germany; †Hamburg Center for Translational Immunology, University Medical Center Hamburg-Eppendorf, Hamburg, Germany; ‡Department of Internal Medicine IV, Medical Center-University of Freiburg, University of Freiburg, Freiburg, Germany; §Institute of Experimental Immunology and Hepatology, University Medical Center Hamburg-Eppendorf, Hamburg, Germany; ¶Würzburg Institute of Systems Immunology, Julius-Maximilians-University Würzburg, Würzburg, Germany; and ‖Division of Translational Immunology, III. Department of Medicine, University Medical Center Hamburg-Eppendorf, Hamburg, Germany

[1]C.R. and A.-C. G. contributed equally to this work.

ORCIDs: 0000-0002-7582-3605 (A.-C.G.); 0000-0002-0913-1766 (N.S.); 0000-0002-4806-2548 (Y.T.); 0000-0002-3858-3171 (K.N.); 0000-0001-6986-127X (G.G.).

Received for publication October 21, 2021. Accepted for publication January 23, 2022.

Address correspondence and reprint requests to Dr. Jan-Eric Turner, III. Department of Medicine, University Medical Center Hamburg-Eppendorf, Martinistrasse 52, D-20246 Hamburg, Germany. E-mail address: j.turner@uke.de

The online version of this article contains supplemental material.

Abbreviations used in this article: asGM1, asialoGM1; cGN, crescentic glomerulonephritis; cNK, conventional NK; eYFP, enhanced yellow fluorescent protein; GN, glomerulonephritis; GO, Gene Ontology; ILC, innate lymphoid cell; ILC1, type 1 innate lymphoid cell; NCR, NK cell receptor; PAS, periodic acid–Schiff; trNK, tissue-resident NK; UKE, Universitätsklinikum Hamburg-Eppendorf; UMAP, Uniform Manifold Approximation and Projection; wt, wild-type; YFP, yellow fluorescent protein.

between circulating cNK cells, trNK cells, and ILC1s in different organs is at present still ill-defined and an area of active research (14).

Glomerulonephritides are a heterogeneous group of immune-mediated diseases that lead to inflammation of the renal glomeruli and account for up to 20% of patients with chronic kidney disease in industrialized countries (15). Among these, crescentic glomerulonephritis (cGN) is the most severe form. cGN can develop in systemic vasculitis, anti−glomerular basement membrane disease, or systemic lupus erythematosus and frequently leads to a rapid loss of kidney function, resulting in requirement of dialysis or kidney transplantation with considerable morbidity and mortality. The contribution of NK cells to immune-mediated glomerular disease is largely unknown and has been debated controversially (16). Although some early immunohistochemical studies reported the presence of NK cells in a rat glomerular disease model (17) and human GN (18), others did not observe significant NK cell accumulation in rat anti−glomerular basement membrane nephritis (19). Intriguingly, a recent study, addressing the subset-specific roles of cNK cells and trNK cells/ILC1s in a murine kidney ischemia-reperfusion injury model of acute kidney injury, suggested a relevant role of trNK in disease progression (20). However, detailed profiling of murine kidney NK cell/ILC1 subsets and analyses of their functional role in cGN are missing so far.

In this study, we provide a detailed expression profile of NK cell/ILC1 subsets in the murine kidney by RNA sequencing and evaluate their subset-specific role in a well-established model of experimental cGN in mice. We observed that widely used depletion strategies for total NK cells (anti-NK1.1 Ab application) and cNK cells (anti-asialoGM1 [anti-asGM1] serum application) were unreliable tools, because they were accompanied by significant off-target depletion of kidney NKT cells and CD8^{+} T cells, respectively. However, neither depletion of cNK cells and ILC1 in NKT cell−deficient mice nor specific deletion of cNK cells in $Ncr1^{Cre} \times Eomes^{fl/fl}$ mice altered the clinical course of experimental cGN. In summary, we show in this study that cNK cells and ILC1s are dispensable for initiation and progression of immune-mediated glomerular disease and advise caution in the use of standard Ab depletion methods to study NK cell/ILC1 function in mouse models.

Materials and Methods

Animals

C57BL/6J wild-type (wt) animals were ordered from Charles River Laboratories. $Cd8a^{-/-}$, TCR-Jα18$^{-/-}$, $Eomes^{fl/fl}$, and NKp46^{iCre} ($Ncr1^{Cre/wt}$) mice were bred in the animal facility of the University Medical Center Hamburg-Eppendorf (Universitätsklinikum Hamburg-Eppendorf [UKE], Hamburg, Germany) under specific pathogen-free conditions. TCR-Jα18$^{-/-}$ mice were kindly provided by N. Gagliani (UKE), and NKp46^{iCre} mice were kindly provided by E. Vivier (University of Marseille, Marseille, France). $Ncr1^{Cre/wt}$ mice were crossed to $Eomes^{fl/fl}$ mice or LSL-$R26r^{eYFP}$ mice to generate mice with conditional Eomes knockout in NKp46$^+$ cells and NKp46$^+$ cell fate reporter mice (21), respectively. All animal experiments were performed according to national and institutional animal care and ethical guidelines and were approved by the local committees.

Induction of experimental GN and functional analyses

cGN was induced by i.p. injection of nephrotoxic sheep serum (2.5 mg/g body weight) in 8- to 12-wk-old mice as previously described (22). For urine sample collection, mice were housed in metabolic cages for 5 h. Urinary albumin excretion was determined by standard ELISA (Bethyl Laboratories, Montgomery, TX). Urinary creatinine levels were measured with the Creatinine Jaffé Fluid (Hengler Analytik, Steinbach, Germany).

Histopathology and immunohistochemistry

Formalin-fixed, paraffin-embedded kidney sections were stained with periodic acid−Schiff (PAS) reagent according to standard laboratory procedures. Crescent formation in the cGN model was assessed in 30 glomeruli per mouse. Tubular injury was assessed by using photographs of nonoverlapping cortical areas from PAS-stained kidney sections. In the cGN model, the percentage of interstitial area was determined by superimposition of the photographs with 40 apportioned dots, and subsequently interstitially located dots were counted. Tissue slices were evaluated with an Axioskop light microscope (Zeiss, Jena, Germany) and photographed with an AxioCam HRc camera (Zeiss). All histological quantifications were performed in a blinded fashion.

Immunofluorescence

For immunofluorescence staining, 2.5-μm-thick paraffin sections were boiled at 98°C for 20 min in citric acid citrate buffer (pH 6) for Ag retrieval. Because fluorescence intensity of yellow fluorescent protein (YFP) after formalin fixation and embedding in paraffin was not sufficient to visualize YFP$^+$ cells, detection of YFP by immunofluorescence staining was necessary. Unspecific binding was blocked with 5% horse serum (vector) and 0.05% Triton X-100 in PBS. Then, the sections were incubated with rabbit anti-GFP (cross-reactive to YFP; 1:1000, clone ab290; Abcam) and rat anti-Eomes Abs (1:200, clone Dan11mag; eBioscience) in 5% horse serum overnight at 4°C. The staining was visualized using Alexa Fluor 488− (anti-rabbit) and Cy3 (anti-rat)-conjugated secondary Abs (1:100; Jackson ImmunoResearch Laboratories, West Grove, PA) incubated for 1 h at room temperature. DNA was counterstained with Hoechst (1:1000; Molecular Probes). Images of the stained slides were acquired with an LSM 510 Meta confocal microscope using the LSM software (Zeiss).

Cell isolation

For isolation of renal leukocytes, mouse kidneys were cut into small pieces and enzymatically digested in complete medium (RPMI 1640, 10% FBS, 1% HEPES, 1% penicillin/streptomycin; all Life Technologies) supplemented with collagenase D (0.4 mg/ml; Roche, Basel, Switzerland) and DNase I (100 μg/ml; Roche) for 45 min at 37°C while rotating on a MACSmix tube rotator (Miltenyi, Bergisch Gladbach, Germany). After further dispersion with the gentleMACS dissociator (Miltenyi), leukocytes were purified by Percoll gradient centrifugation (37.5%) (GE Healthcare, Chicago, IL) and further enriched by subsequent erythrocyte lysis with ammonium chloride. After filtration through a 50-μm strainer, cell suspension was ready for further analyses. Leukocytes from the liver were isolated by mashing the tissue through a 100-μm strainer and were further purified by subsequent Percoll gradient centrifugation (37.5%) and erythrocyte lysis. Isolation of splenocytes was performed by mashing through a 70-μm strainer and subsequent erythrocyte lysis.

Depletion Abs

For depletion of total NCR$^+$ ILC cell populations, mAb targeting NK1.1 (200 μg per injection) (clone PK136; BioXCell) was i.p. administered 1 day before and at days 2, 5, and 8 after induction of the cGN model. IgG2a (200 μg per injection) (clone C1.18.4; BioXCell) was used as isotype control and was administered in the same manner. To deplete the subpopulation of cNK cells, we used the anti-asGM1 serum (20 μl per injection) (rabbit) (986-10001; Fujifilm Wako Pure Chemical Cooperation) and rabbit serum (20 μl per injection) (140-06571; Fujifilm Wako Pure Chemical Cooperation) as control serum, administered at the same time points.

Flow cytometry

To characterize leukocyte subsets, we stained cell suspensions with fluorochrome-coupled Abs against CD45 (30-F11), CD3 (145-2C11), CD4 (RM4-5), CD8 (53-6.7), TCR-γδ (H57-597), CD11b (M1/70), Ly6G (1A8), SiglecF (E50-2440), F4/80 (BM8), CD69 (H1.2F3), CD127 (A7R34), NKp46 (29A1.4), NK1.1 (PK136), CD49a (Hma1), CD49b (Hma2), and IL-18R (REA947). PE-labeled PBS-57 (α-galactosylceramide analog)-loaded CD1d tetramer was received from the National Institutes of Health Tetramer Facility (Emory University, Atlanta, GA) titrated before use (final concentration, 1:800) and incubated 20 min on ice together with the other Abs for surface marker staining. For labeling of CD45.2$^+$ intravascular cells, fluorochrome-coupled CD45.2 Abs (clone 104) were i.v. injected (2 μg per animal) 5 min prior to sacrifice. To detect transcription factors, we used the Transcription Factor Staining Buffer Set (eBioscience), and staining was performed according to the manufacturer's instructions using fluorochrome-coupled Abs against Eomes (Dan11mag), T-bet (4B10), and RORγt (Q31-378). For intracellular cytokine staining, isolated leukocytes were restimulated with PMA (50 ng/ml; Sigma) and ionomycin (1 μg/ml; Calbiochem) in the presence of brefeldin A (10 μg/ml; Sigma) for 2.5 h at 37°C. After subsequent surface staining, cells were fixed with formalin (3.7%; Sigma), permeabilized with IGEPAL CA-630 (0.1%; Sigma), and stained with IFN-γ (XMG1.2). All Abs were purchased from BioLegend, eBioscience, or BD Biosciences. Nonspecific staining was blocked by incubation with 10% normal mouse serum (Jackson ImmunoResearch Laboratories). Dead cells were stained by using LIVE/DEAD Fixable Read Dead Stain Kit (Invitrogen) or Zombie Dye (BioLegend). Absolute numbers of CD45$^+$ cells in cell suspension were determined by

staining with fluorochrome-coupled anti-CD45 combined with cell count beads (CountBright; Invitrogen). All samples were acquired on a LSRII flow cytometry (BD Biosciences) and analyzed with the FlowJo Software (Tree Star).

Flow cytometry sorting, bulk RNA sequencing, and bioinformatic analyses

For bulk RNA sequencing, leukocytes were isolated from kidneys of naive mice and stained with surface Abs as described earlier. CD49a$^+$ and CD49b$^+$ NK cells were sorted with the FACSAria Fusion Cell Sorter (BD Biosciences). Subsequently, RNA was isolated using the RNeasy Plus Micro Kit (QIAGEN) according to the manufacturer's instructions. Quality control of prepared RNA was performed using the Agilent 2100 Bioanalyzer (Agilent Technologies). After library construction, quality control with Qubit 2.0 fluorometer (Life Technologies) was applied. Sequencing was performed by Novogene Europe (Cambridge, UK) using the HiSeq 4000 platform with paired end of 150 bp (PE 150) sequencing strategy (Illumina). After trimming the reads using Trimmomatic (Version 0.38) (23), data were aligned on the Mus_musculus.GRCm38.95 reference genome using STAR aligner (version 2.6.1) (24). A transcript database was generated by using the same reference genome and counting reads per gene with the summarizeOverlaps function from GenomicAlignments package (Bioconductor Version 3.12) (25) in R (version 4.03). Genes with less than five reads in total were filtered out, and differential expression analysis was performed by using the DESeq function of R package DEseq2 (version 1.30.0) (26). Gene Ontology (GO) term analysis was performed with significantly upregulated genes (Fisher test) of either CD49a$^+$ (ILC1) or CD49b$^+$ (cNK cell) samples on the PANTHER Classification System (http://www.pantherdb.org/) using biological processes of the GO database (released February 1, 2021). Processed and raw data files of the RNA sequencing data are available from the Gene Expression Omnibus (https://www.ncbi.nlm.nih.gov/geo/) under the accession number GSE193001.

Statistics

The Student *t* test was used for comparison between two groups. In case of three or more groups, one-way ANOVA was used followed by a post hoc analysis with Newman–Keuls test for multiple comparisons. A p value <0.05 was considered to be statistically significant.

Results

The kidney harbors two distinct populations of NK1.1$^+$ NKp46$^+$ CD3$^-$ cells that differ in phenotype and tissue localization

A recent study demonstrated that the murine kidney harbors two NK1.1$^+$CD3$^-$ cell populations that can be distinguished by expression of the surface markers CD49a and CD49b and differ in their surface phenotype and migratory behavior (20). For a more detailed characterization of these renal NCR-positive ILC populations, we identified NK1.1$^+$NKp46$^+$CD3$^-$ cells in the kidney of naive mice by flow cytometry and analyzed their abundance, surface phenotype, and transcription factor expression in comparison with liver and spleen (Fig. 1A–D). NK1.1$^+$NKp46$^+$CD3$^-$ cells comprised a
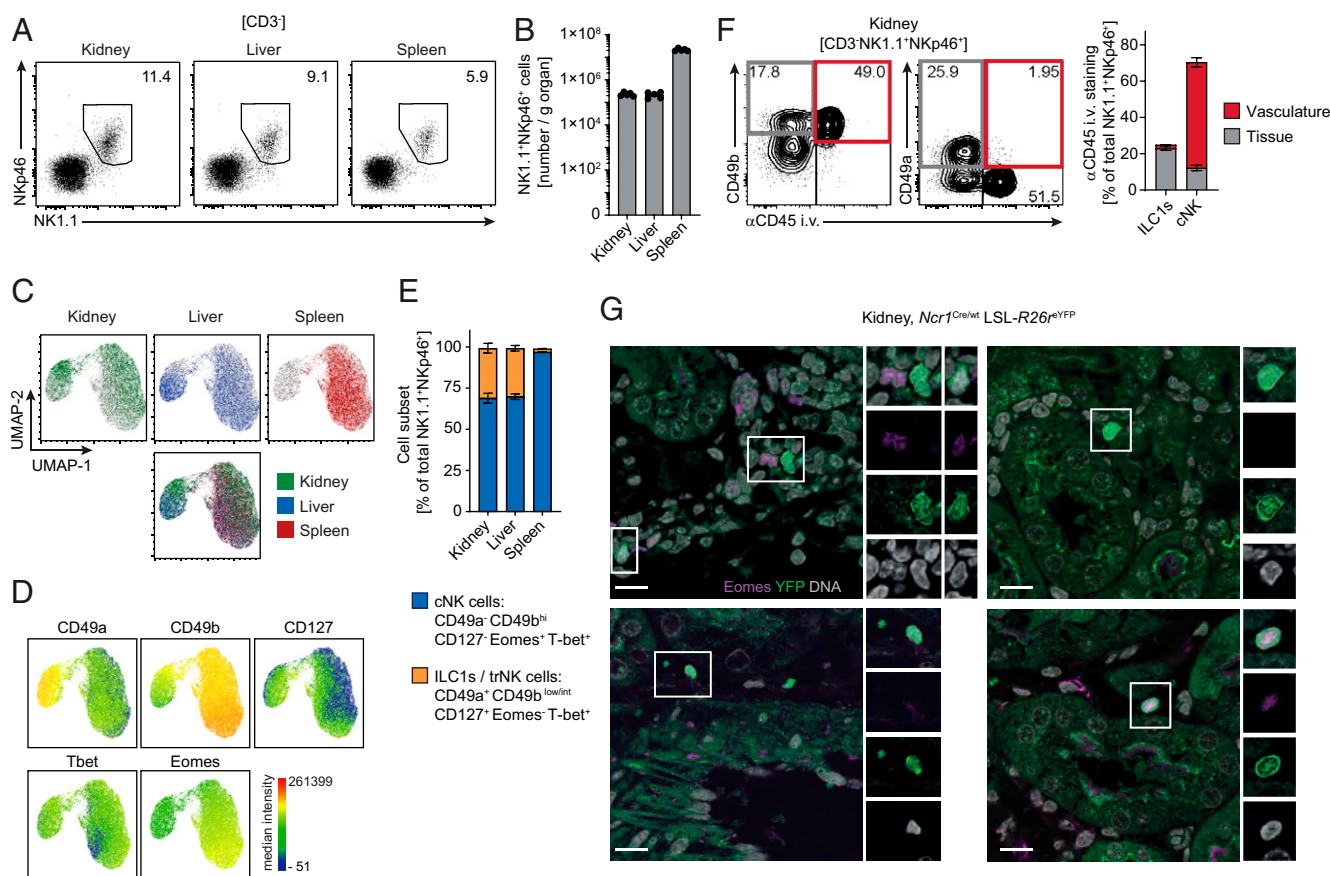
FIGURE 1. Distinct populations of NK1.1$^+$NKp46$^+$CD3$^-$ cells in the murine kidney. (**A**) Representative flow cytometry plots of leukocytes isolated from kidney, liver, and spleen and gated on CD45$^+$CD3$^-$ live lymphocytes. Numbers represent percentage of cells in the gate. (**B**) Quantification of NK1.1$^+$NKp46$^+$CD3$^-$ cells in kidney, liver, and spleen of naive wt mice ($n = 5$). Symbols represent individual animals, and bars represent mean $\pm$ SEM. (**C**) UMAP clustering based on flow cytometric markers of NK1.1$^+$NKp46$^+$ cells concatenated from all organs. Distribution of cells from the respective organs among the UMAP clusters is color coded. (**D**) Expression heatmap for subset-defining markers overlaid on the UMAP plots (blue = low expression, orange = high expression). Analyses in (C) and (D) were performed on pooled data from wt mice ($n = 5$). (**E**) Frequencies of CD49b$^+$ cNK cell and CD49a$^+$ ILC1s in the total NK1.1$^+$NKp46$^+$CD3$^-$ cell population in kidney, liver, and spleen of wt mice ($n = 5$). Bars represent mean $\pm$ SEM. (**F**) Representative flow cytometry plots and quantification of CD49a$^+$ and CD49b^{hi}NK1.1$^+$NKp46$^+$CD3$^-$ cells after in vivo staining with i.v. anti-CD45 antibody. Positivity for anti-CD45 i.v. staining marks intravascular cells, while anti-CD45 i.v. negativity indicates localization in the parenchyma. Bars represent mean $\pm$ SEM (wt mice, $n = 5$). (**G**) Representative confocal images of kidney slices of naive *Ncr1*^{Cre} $\times$ LSL-*R26r*^{eYFP} fate reporter mice after immunofluorescence staining for Eomes (magenta) and NKp46 (YFP, green). Single YFP$^+$ cells are Eomes$^-$ ILC1, while YFP$^+$Eomes$^+$ cells represent cNK cells. Original magnification $\times$630; scale bar: 15 μm. All experiments have been performed twice with similar results.

substantial fraction of lymphocytes (~6%) in the kidney and showed comparable absolute numbers per gram of tissue as in the liver (Fig. 1A, 1B). Concatenation and dimensionality reduction of multi-parameter flow cytometry data with the Uniform Manifold Approximation and Projection (UMAP) algorithm of all three organs clearly confirmed two distinct NK1.1⁺NKp46⁺CD3⁻ populations in the kidney and liver, characterized as CD49b^{hi}CD49a⁻CD127⁻Eomes⁺T-bet⁺ cNK cells and CD49a⁺CD49b$^{low/int}$CD127⁺Eomes⁻T-bet⁺ cells that have previously been termed as trNK cells in the kidney (20) and ILC1s in the liver (11). As expected, NK1.1⁺NKp46⁺CD3⁻ cells in the spleen mainly showed the cNK cell phenotype (Fig 1C, 1D).

As indicated by transcriptomic analyses (see Fig. 2), CD49a⁺ CD49b$^{low/int}$CD127⁺Eomes⁻T-bet⁺ cells in the kidney showed an ILC1 signature, and we therefore use the term ILC1, rather than trNK cell, for the rest of this article.

In vivo labeling with an anti-CD45 Ab revealed that ILC1s were exclusively located in the kidney parenchyma, while the majority of cNK cells had an intravascular location, confirming that they mainly comprise a circulating subset (Fig. 1E) (20). To further study the localization of these subsets in the kidney tissue, we generated NKp46 fate reporter mice (Ncr1$^{Cre/wt}$ × LSL-R26r^{eYFP}) in which all

cells that have at some point expressed the natural cytotoxicity triggering receptor 1 (Ncr1, encoding for NKp46) are marked by constant expression of enhanced YFP (eYFP). Immunofluorescence costaining of YFP (NKp46) and Eomes in kidney slices of these reporter mice allowed for the identification of NKp46⁺Eomes⁺ cells and NKp46⁺Eomes⁻ cells that represent cNK cells and ILC1s, respectively, with a minor contribution of other NKp46⁺ cell populations in both cases (Fig. 1F). Both cNK cells and ILC1s were found in the tubulointerstitial area of the naive mouse kidney (Fig. 1G, upper left and both right panels). Interestingly, in contrast with cNK cells, ILC1s were also found in perivascular spaces (Fig. 1G, lower left panel), which have recently been described as a niche that is populated by ILC2s, e.g., in the kidney and lung (27). This suggests that cNK cells and ILC1s, in addition to their distinct phenotype, might occupy specific niches within the kidney microarchitecture.

RNA sequencing of CD49a⁺ and CD49b^{hi} subsets reveals distinct transcriptomic profiles

To provide an unbiased view of the transcriptomic profile of kidney CD49b^{hi}NK1.1⁺NKp46⁺CD3⁻ cells and CD49a⁺CD49b$^{low/int}$ NK1.1⁺NKp46⁺CD3⁻ cells, we performed bulk mRNA sequencing of these subsets purified by flow cytometry from the kidney of
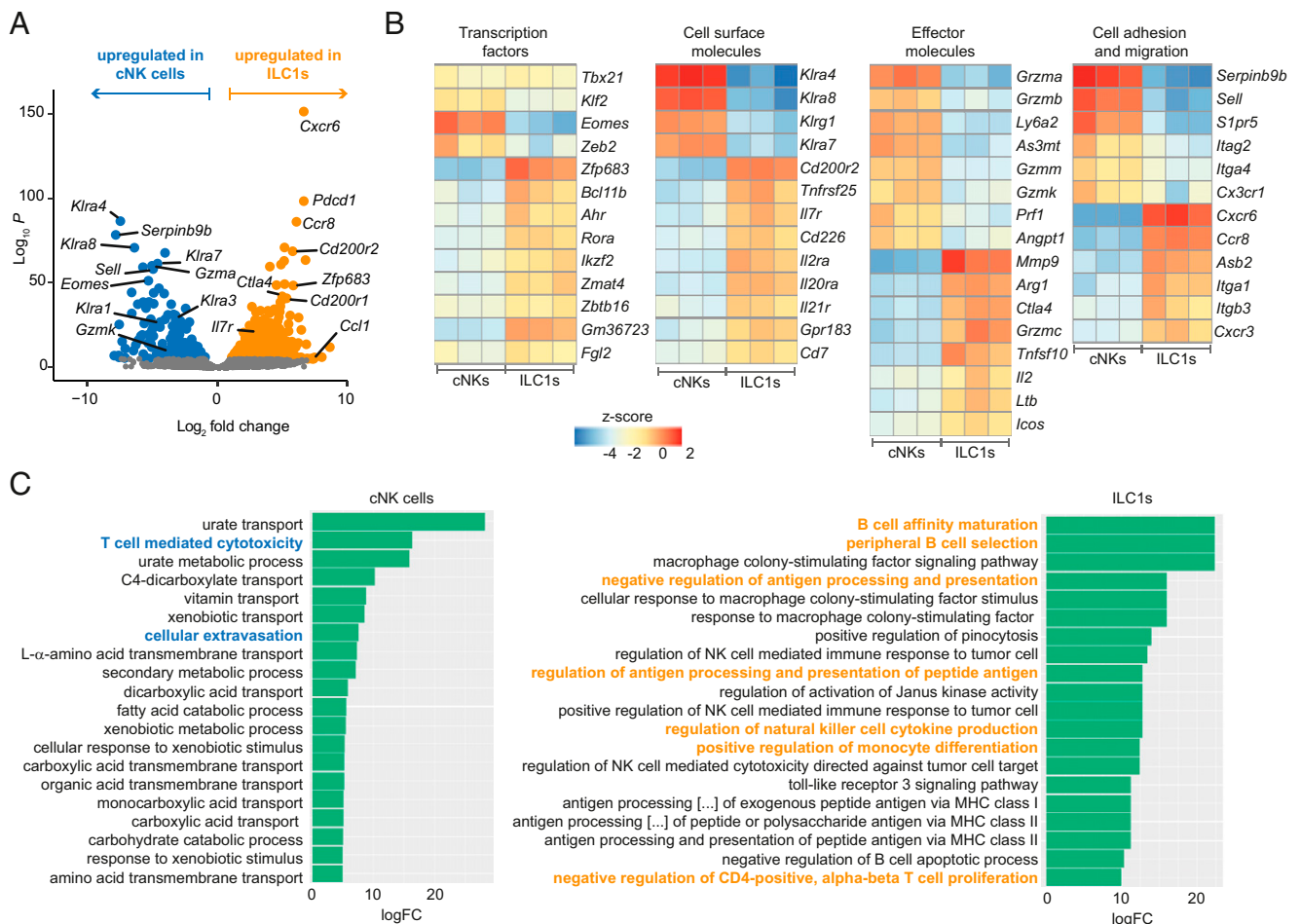
FIGURE 2. RNA sequencing of cNK cells and ILC1s reveals distinct transcriptomic profiles. (**A**) Volcano plot of differential mRNA expression analysis comparing cNK cells (gating strategy: CD45⁺CD19⁻F4/80⁻GR-1⁻CD3⁻NK1.1⁺CD49b^{hi}CD49a⁻ live lymphocytes) and ILC1s (gating strategy: CD45⁺CD19⁻F4/80⁻GR-1⁻CD3⁻NK1.1⁺CD49a⁺CD49b$^{low/int}$ live lymphocytes) purified from the kidney by flow cytometry−based cell sorting and subjected to bulk RNA sequencing (~30,000 cells for each sample). Genes that are not differentially expressed are shown in gray. Data are pooled from n = 3 samples per cell subset. Kidneys from n = 5−8 naive wt mice were pooled for each sample. (**B**) Heatmap of selected genes (z scores) of the respective categories, illustrating differential expression of marker genes and low sample variability. (**C**) GO term analyses of differentially regulated genes in cNK cells and ILC1s showing the top 20 upregulated pathways (sorted for fold change) in each subset. Pathways of special interest are marked in blue and orange, respectively. Sorting was performed in two independent experiments, and data were pooled for analysis.

naive C57BL6/J mice (Fig. 2). The sorting strategy and purity for the cell subsets are depicted in Supplemental Fig. 1. Differential expression analyses comparing the two subsets revealed upregulation of genes in the CD49a$^+$CD49b$^{low/int}$ population that have been associated with a transcriptional ILC1 identity in other organs (11, 12, 28), e.g., Zfp683 (encoding for the transcription factor Hobit), Rora, Bcl11b, Ahr, and Cd200r1, as well as low expression of Gzma and Gzmb, confirming their designation as ILC1s. The cNK cell profile of the CD49b^{hi}CD49a$^-$ population, in contrast, was confirmed by high expression of Eomes, killer cell lectin-like receptor genes, as well as Grzma and Prf1, encoding for granzyme A and perforin, respectively (Fig. 2A, 2B). Interestingly, several chemokine receptor genes (Cxcr6, Ccr8, Cxcr3) and several genes encoding for proteins involved in cell-to-cell contact-dependent regulation of immune cells (e.g., Pdcd1, Ctla4, Icos, Tnfsf10) were highly expressed in the ILC1 population, suggesting that localization within the tissue is key to the function of these cells, and that they might be involved in regulating immune responses by targeting other immune cells (Fig. 2A, 2B). This notion was further supported by GO term analyses based on the differentially upregulated genes (Fig. 2C). In this analysis, the top 20 upregulated pathways in ILC1s included various pathways involved in regulation of B cells, macrophages, APCs, and T cells (Fig. 2C, right panel). The top 20 upregulated pathways in cNK cells, in contrast, were indicative of their cytotoxic function and their intravascular localization (i.e., need for cellular extravasation), because cellular extravasation was the seventh most upregulated GO term (Fig. 2C,

left panel). In addition, several pathways involved in transportation and processing of nutrients and metabolites were upregulated in cNK cells, suggesting a high metabolic activity in this cytotoxic cell type (Fig. 2C, left panel).

In summary, our data confirm the presence of distinct populations of cNK cells and ILC1s in the murine kidney and support the hypothesis that especially ILC1s might have important immune regulatory functions in kidney parenchyma in homeostasis and inflammation.

cNK cell and ILC1 abundance is unaltered by induction of cGN

We next assessed whether an inflammatory environment results in changes in distribution or phenotype of cNK cells or ILC1s in the kidney. To study renal inflammation, we used a well-established experimental model for cGN (nephrotoxic serum nephritis) in mice that is induced by injection of sheep IgG directed against components of the mouse glomerular basement membrane, resulting in glomerular inflammation with crescent formation, proteinuria, and secondary tubulointerstitial inflammation (29). Analysis of ILC1s and cNK cells at different time points after cGN induction did not show substantial changes in total abundance or subset distribution (Fig. 3A). T-bet expression tended to be increased in both ILC1s and cNK cells at later time points, but this increase was moderate and reached significance only in cNK cells. A similar expression increase at later time points was observed for Eomes in the cNK cell subset (Fig. 3B). Interestingly, expression of the IL-7R in ILC1 was increased at 12 h after induction of cGN but had returned to baseline already at day 3 (Fig. 2B). IFN-γ expression in both
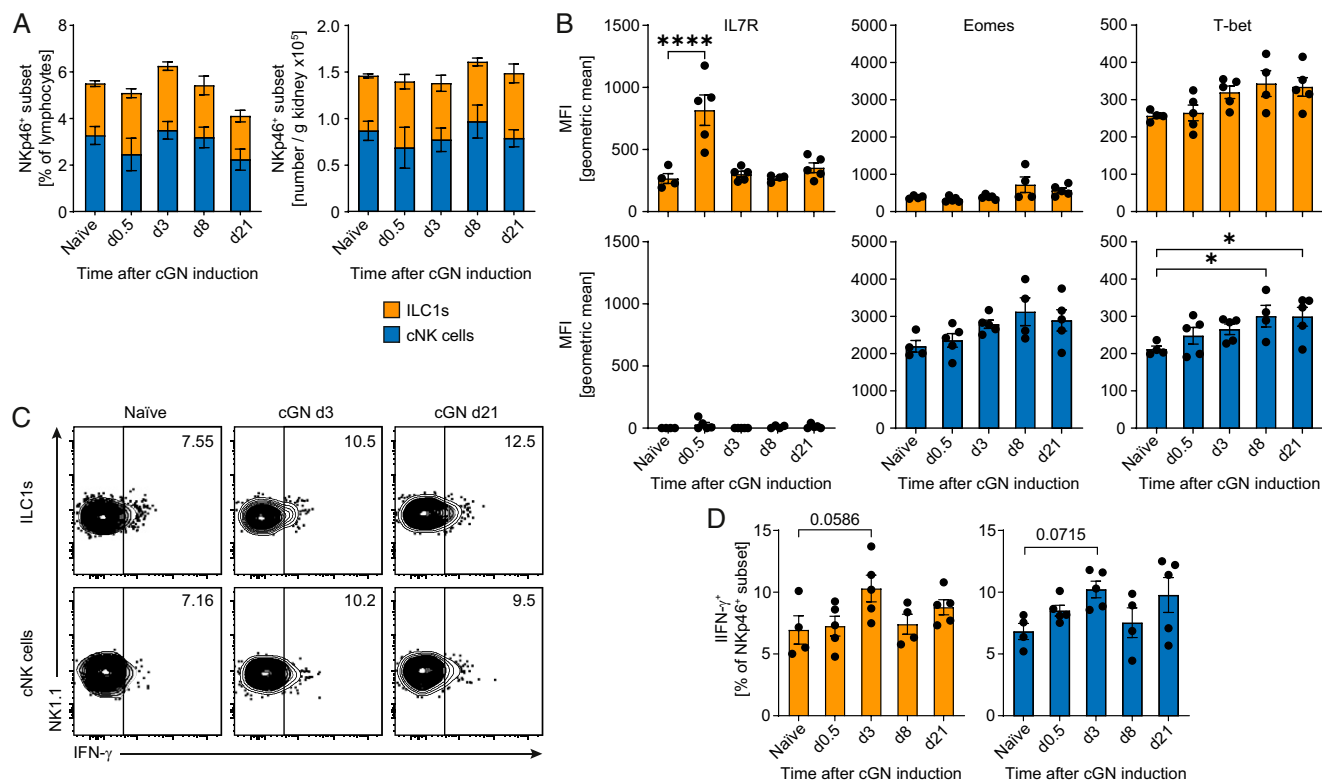
FIGURE 3. cNK cell and ILC1 abundance is unaltered by induction of cGN. (**A**) Frequencies and numbers of NCR$^+$ ILC subsets in the kidney at different time points after induction of experimental cGN. (**B**) Flow cytometric expression analysis of selected parameters in ILC1s and cNK cells at different time points after induction of experimental cGN. (**C**) Representative flow cytometry plots of IFN-γ production assessed by intracellular staining after restimulation with PMA/ionomycin in naive and nephritic wt mice at the designated time points of cGN. Numbers represent percentage of cells in the gate. (**D**) Frequency of IFN-γ$^+$ cells among NCR$^+$ ILC subsets at different time points. Experiments in (A)–(D) were performed with at least four mice per experimental group. Analyses in naive mice, as well as at days 3 and 8, were confirmed in at least two independent experiments. Isolated kidney leukocytes were gated on CD45$^+$CD3$^-$NK1.1$^+$NKp46$^+$ live lymphocytes and then subdivided in CD49b$^+$ cNK cells or CD49a$^+$ ILC1s. Bars represent mean ± SEM. Filled circles represent individual animals. *$p < 0.05$, ****$p < 0.0001$. MFI, mean fluorescence intensity.

subsets showed a slight increase at days 3 and 21 of cGN without reaching statistical significance (Fig. 3C, 3D). In summary, induction of cGN did not substantially alter subtype distribution or basic phenotypic parameters of NCR$^+$ ILCs in the kidney, except for a marked but transient increase of IL-7R expression on ILC1s in the very early phase of inflammation.

Depletion of NK1.1$^+$ and asGM1$^+$ cells leads to aggravation of kidney damage in cGN

In the next step, we aimed to address the functional role of these NCR$^+$ ILC populations in renal inflammation. To this end, we used injection of anti-NK1.1 and anti-asGM1 Abs during the course of cGN as standard methods of NK cell depletion in murine models (experimental setup in Supplemental Fig. 2). Intriguingly, a recent study in a model of acute kidney injury reported cNK/ILC1 subset-specific differences in the susceptibility to anti-asGM1 Ab depletion, with effective depletion of most cNK cells, but a failure to deplete ILC1s because of their low expression of the target molecule asGM1 (20). These findings suggested a suitable method to compare the effect of depletion of total NCR$^+$ ILCs by injecting

anti-NK1.1 with a "specific" depletion of asGM1^{hi} cNK cells by anti-asGM1 Ab treatment.

First, we applied anti-NK1.1 to target the total NCR$^+$ ILCs population, which successfully depleted both CD49a$^+$ and CD49b$^+$ subsets (Fig. 4A). At day 9 after cGN induction, this treatment resulted in increased glomerular crescent formation, a robust and sensitive marker of glomerular damage in cGN, in anti-NK1.1−treated as compared with isotype-treated control mice (Fig. 4B, 4C). However, parameters for tubulointerstitial damage and proteinuria were not different between the nephritic groups (Fig. 4B, 4C). In the second set of experiments, we used anti-asGM1 Ab treatment to preferentially deplete cNK cells, while leaving the ILC1 population intact (Fig. 4D, 4E). This resulted in a similar phenotype as anti-NK1.1 treatment, with increased crescent formation in cNK cell−depleted animals compared with isotype-treated controls (Fig. 4F, 4G), suggesting a potential protective role of cNK in the mouse model for cGN.

NCR$^+$ ILC-depleting Abs show substantial off-target effects

Because NK1.1 and asGM1 expression on non-NK cells has been described before (30), we assessed the effect of both Abs on other
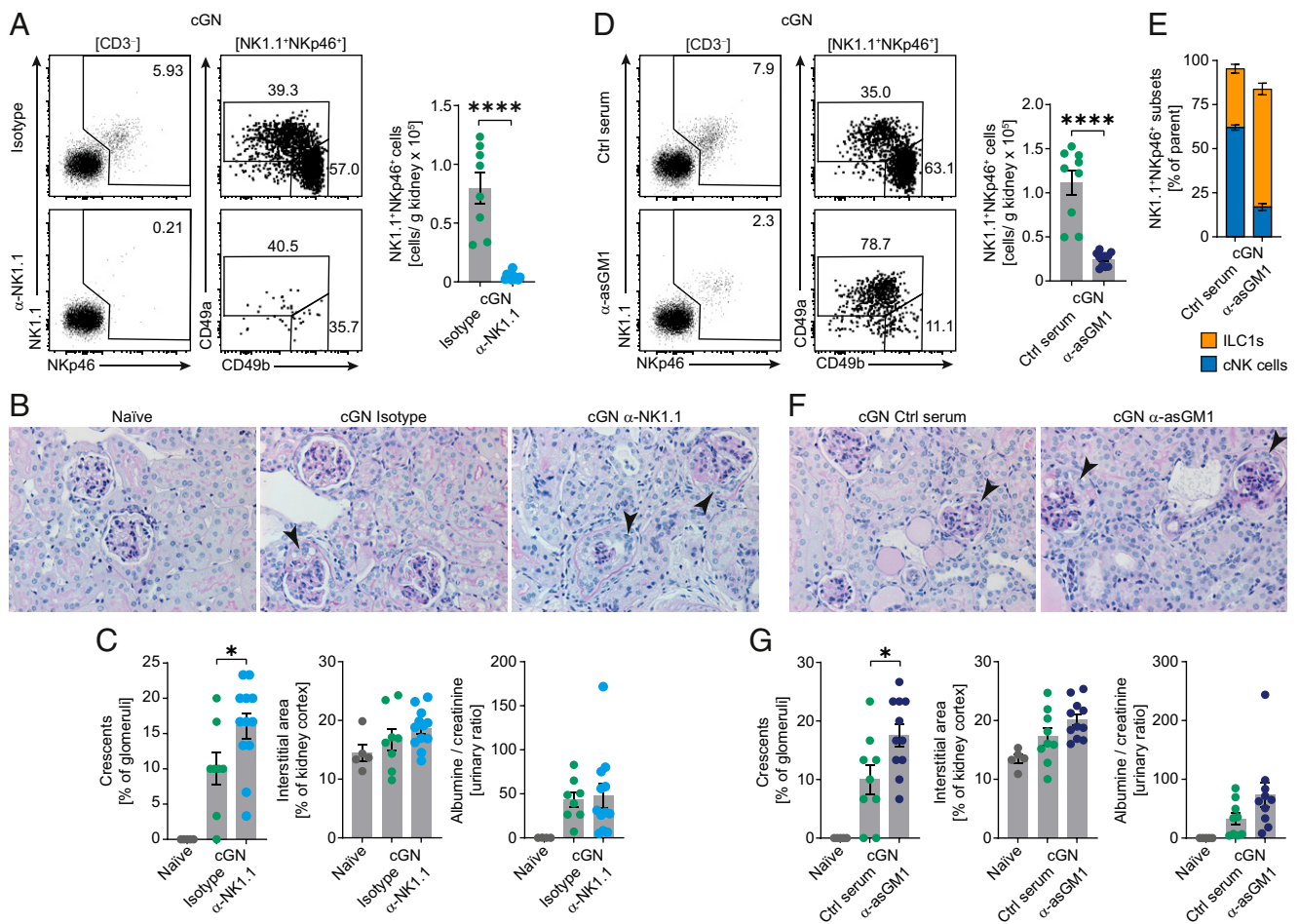
FIGURE 4. Depletion of NK1.1$^+$ and asGM1$^+$ cells leads to aggravation of kidney damage in cGN. (A, D, and E) Representative flow cytometry plots and quantification of NCR$^+$ ILC subsets in the kidney of wt mice at day 9 after induction of cGN. NCR$^+$ ILC depletion was achieved by repeated i.p. injection of anti-NK1.1 antibodies (4 × 200 μg) (**A**) or anti-asGM1 serum (4 × 20 μl) (**D** and **E**). Control mice received injections of IgG2a isotype control (4 × 200 μg) (A) or control serum (4 × 20 μl) (D and E). See Supplemental Fig. 2 for experimental setup. Plots are pregated on CD45$^+$ live lymphocytes. Further gating is specified in brackets. Numbers represent percentage of cells in the gate. (**B** and **F**) Representative PAS staining of kidney tissue obtained from naive wt mice and from wt mice at day 9 after induction of experimental cGN (groups as in A and D). Arrowheads mark crescent formation in the glomeruli. (**C** and **G**) Histopathological quantification of tissue damage (glomerular crescents, interstitial area) and albuminuria of the respective groups on day 9 after induction of experimental cGN. Filled circles represent individual animals. Bars represent mean ± SEM. Data are pooled from two individual experiments with similar results. (A and C) $n = 5$ for naive wt; $n = 12$ for anti-NK1.1−treated wt; $n = 8$ for isotype-treated wt. (D, E, and G) $n = 5$ naive wt; $n = 11$ for anti-asGM1−treated wt; $n = 9$ for control serum-treated wt. *$p < 0.05$, ****$p < 0.0001$.
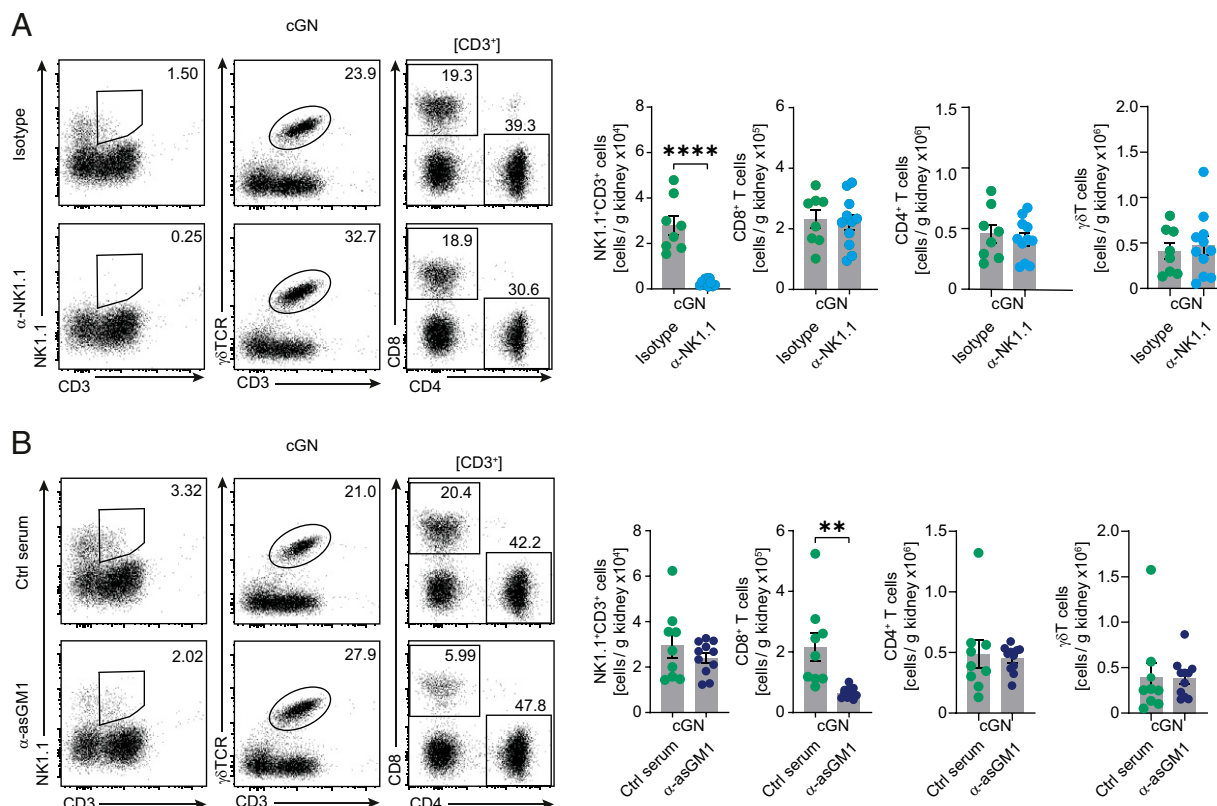
FIGURE 5. NCR$^+$ ILC-depleting Abs show substantial off-target effects. (**A** and **B**) Representative flow cytometry plots and quantification of NK1.1$^+$CD3$^+$ cells, γδ T cells, and CD4$^+$ and CD8$^+$ T cells in the kidney on day 9 of cGN in wt mice treated with either anti-NK1.1 antibody, IgG2a isotype control, anti-asGM1 serum, or control serum (groups and numbers as in Fig. 4). Data are pooled from two individual experiments with similar results. Numbers in flow cytometry plots represent percentage of cells in the gate. Plots were pregated on CD45$^+$ live lymphocytes. Further gating is indicated in brackets. Filled circles represent individual animals, and bars represent mean ± SEM. **$p < 0.01$, ****$p < 0.0001$.

lymphocyte subsets in the kidney that might contribute to the observed phenotype (Fig. 5). Notably, administration of anti-NK1.1 Ab depleted also NK1.1$^+$CD3$^+$ NKT cells in the kidney, while CD4$^+$ and CD8$^+$ T cells, as well as γδ T cells, were unaffected (Fig. 5A). To confirm that the observed disappearance of NK1.1$^+$ NKT cells was true cell depletion and not caused by covering of NK1.1 epitopes by unlabeled NK1.1 Ab, preventing detection by fluorochrome-labeled Abs of the same clone ex vivo, we performed another set of experiments in which we used α-galactosylceramide–loaded CD1d tetramers to detect NKT cells (Supplemental Fig. 3). These analyses showed that a substantial portion of kidney-residing NKT cells express NK1.1, and that, by using the same depletion strategy as in the previous cGN experiments (see Supplemental Fig. 2), this NK1.1$^+$ NKT cell population is effectively depleted by anti-NK1.1 Ab treatment, reducing total NKT cell numbers in the nephritic kidney by ~40% (Supplemental Fig. 3A, 3B). A previous study suggested that off-target depletion of NKT cells in the spleen by NK1.1 Ab application can be circumvented by using a lower dose that was shown to be sufficient to deplete cNK cells (31). However, administration of such an 8-fold reduced dose of anti-NK1.1 (25 μg instead of 200 μg) still resulted in a similar reduction of NKT cell numbers in the kidney compared with a higher dose of anti-NK1.1 (Supplemental Fig. 3C). Among lymphocytes, the asGM1 Ag is known to be expressed on NKT cells, CD8$^+$ T cells, CD4$^+$ T cells, and γδ T cells, and previous studies reported variable reduction of these cell types in the spleen after anti-asGM1 application in mice (30, 32). Unexpectedly, we observed a substantial reduction in kidney CD8$^+$ T cell numbers in anti-asGM1–treated animals, while NKT cells, γδ T cells, and CD4$^+$ T cells in the kidney were unchanged after anti-asGM1 application (Fig. 5B). These

data demonstrate substantial off-target effects of both widely used depletion strategies, questioning their utility in studying NK cell function in kidney disease models.

NCR$^+$ ILC subset depletion in NKT and CD8$^+$ T cell–deficient mice does not aggravate cGN

The off-target effects of both Abs on kidney lymphocyte subsets that have been implicated in pathogenesis of experimental cGN (33–35) led us to hypothesize that NK cell depletion may not be the major driver of the phenotype observed after Ab treatment, and that NKT cells and/or asGM1-positive CD8$^+$ T cells might contribute to protection from immune-mediated glomerular disease. We therefore aimed to exclude participation of NKT and CD8$^+$ T cells by performing similar depletion experiments in NKT cell–deficient TCR-Jα18$^{-/-}$ mice and CD8$^+$ T cell–deficient $Cd8a^{-/-}$ mice (Fig. 6). Indeed, neither total NCR$^+$ ILC depletion by anti-NK1.1 application (Fig. 6A, 6B) nor cNK cell depletion by anti-asGM1 treatment (Fig. 6C, 6D) in the respective mice resulted in aggravated crescent formation, indicating that cNK cells and ILC1s might be dispensable in experimental cGN.

Genetic deletion of Eomes$^+$ NK cells does not alter the course of experimental cGN

To test this, we aimed to generate a more specific model for cNK cell deficiency. Therefore, we generated $Ncr1^{Cre/wt} \times Eomes^{fl/fl}$ mice in which the transcription factor Eomes that is central in development of cNK cells is deleted in all NKp46$^+$ cells (11). Analyses of kidney leukocytes isolated from these mice at day 9 after induction of cGN confirmed a substantial reduction of Eomes protein expression in the remaining NKp46$^+$ cells, while Eomes expression in CD8$^+$
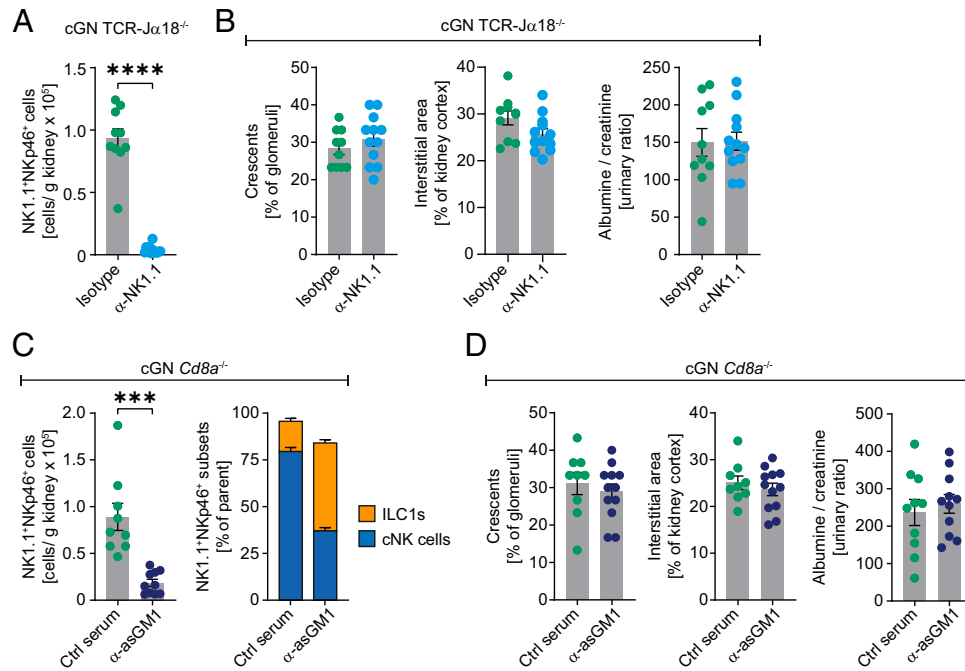
FIGURE 6. NCR^{+} ILC subset depletion in NKT- and CD8^{+} T cell–deficient mice does not aggravate cGN. (**A**) Quantification of NCR^{+} ILCs on day 9 after induction of cGN in the kidney of TCR-αJ18^{−/−} mice treated with either anti-NK1.1 antibody or IgG2a isotype control ($n = 9$ for anti-NK1.1–treated TCR-αJ18^{−/−} mice; $n = 12$ for isotype-treated TCR-αJ18^{−/−} mice). (**B**) Histopathological quantification of tissue damage (glomerular crescents, interstitial area) and albuminuria on day 9 after induction of cGN in the two groups of TCR-αJ18^{−/−} mice. (**C**) Quantification of NCR[+] ILC subsets on day 9 after induction of cGN in the kidney of *Cd8a*^{−/−} mice treated with either anti-asGM1 serum or control serum ($n = 9$ for anti-asGM1–treated *Cd8a*^{−/−} mice; $n = 12$ for control serum-treated *Cd8a*^{−/−} mice). (**D**) Histopathological quantification of tissue damage (glomerular crescents, interstitial area) and albuminuria on day 9 after induction of cGN in the two groups of *Cd8a*^{−/−} mice. Filled circles represent individual animals. Bars represent mean ± SEM. Data are pooled from two individual experiments with similar results. ***$p < 0.001$, ****$p < 0.0001$.

T cells was unchanged or even slightly increased, demonstrating the specificity of the genetic deletion (Fig. 7A, 7B). Importantly, CD49b^{+} cNK cell numbers in the kidney of *Ncr1*[Cre/wt] × *Eomes*^{fl/fl} mice with cGN were reduced by ∼80% as compared with *Ncr1*[Cre/wt] control mice, while CD49a^{+} ILCs, in contrast, were significantly increased in percentage and numbers (Fig. 7C–E). Notably, numbers of CD8^{+} T cells and NKT cells in the kidneys were unchanged by genetic deletion of Eomes in NKp46^{+} cells (Fig. 7F).

However, the specific reduction of cNK cells in this genetic model did not result in an altered outcome of experimental cGN (Fig. 7G), arguing against a substantial role of cNK cells in this model of immune-mediated glomerular disease.

Discussion

Over the years, numerous studies have highlighted the diverse phenotypes, developmental pathways, and functional roles of T-bet–expressing ILC populations (group 1 ILCs) in various anatomical locations (7, 10, 13). Research in the field has been impeded by nonuniform definition and nomenclature of group 1 ILC subsets, and the relationship between circulating cNK cells, trNK cells, and "helper-like" ILC1s remains a matter of debate (14). Recent reports used single-cell transcriptomics to define key markers for ILC1s and cNK cells across murine tissues and proposed that ILC1s should be defined by the expression of *Zfp683* (encoding for Hobit), *Rora*, *Bcl11b*, and *Ahr* and the lack of *Eomes*, while cNK cells are marked by the expression of *Eomes*, *Gzma*, and *Gzmb* (12, 28). In this study, to our knowledge, we provide the first transcriptional profiling of NCR^{+} T-bet^{+} ILC populations in the murine kidney, clearly identifying two subsets: CD49b^{+} cNK cells (*Eomes*^{+}*Gzma*^{+}*Gzmb*^{+}) and CD49a^{+} "helper-like" ILC1s (*Eomes*^{−}*Zfp683*^{+}*Rora*^{+}*Bcl11b*^{+}*Ahr*^{+}). Therefore, we

suggest that the term ILC1s, rather than trNK cells, should be used for the latter subset, because the transcriptional profile of these kidney ILC1s showed striking similarities with that of ILC1s residing in the liver and small intestine (11, 28, 36). These findings are supported by a previous report that identified these populations by flow cytometry and demonstrated that the kidney CD49a^{+} ILC1 subset is tissue resident, which is a basic property of "helper-like" ILCs, while kidney CD49b^{+} cNK cells recirculate via the bloodstream (20). Moreover, a very recent study identified an important role of the transcription factor Hobit in effector differentiation of ILC1 subpopulations in several organs, including the kidney (28), suggesting shared developmental pathways and, potentially, similar functional properties of ILC1s across tissues.

Our GO analyses of subset-specific transcriptomes indicated that cNK cells in the kidney might predominantly exert cytotoxic functions, while ILC1s expressed multiple genes involved in intratissue localization and regulation of other immune cells. In the human kidney, NK cells represent up to 25% of all lymphocytes and, similar to other organs, CD56^{dim}CD16^{+} and CD56^{bright}CD16^{−} NK cell subsets have been described (37). Kidney CD56^{bright}CD16^{−} NK cells are characterized by expression of the tissue residency marker CD69 and are perforin low, indicating that they might resemble features of murine "helper-like" ILC1s (37, 38). Interestingly, this CD56^{bright} subset produces IFN-γ in the kidney tissue and, regardless of the underlying pathology, correlates with the degree of fibrosis in renal biopsy specimens (38). However, the role of T-bet[+] ILCs in specific kidney disease entities, such as GN, in humans is still unknown and requires further study.

With respect to preclinical models, a growing body of evidence points toward an important function of group 1 ILCs in renal allograft rejection and acute kidney injury (16), but interventional
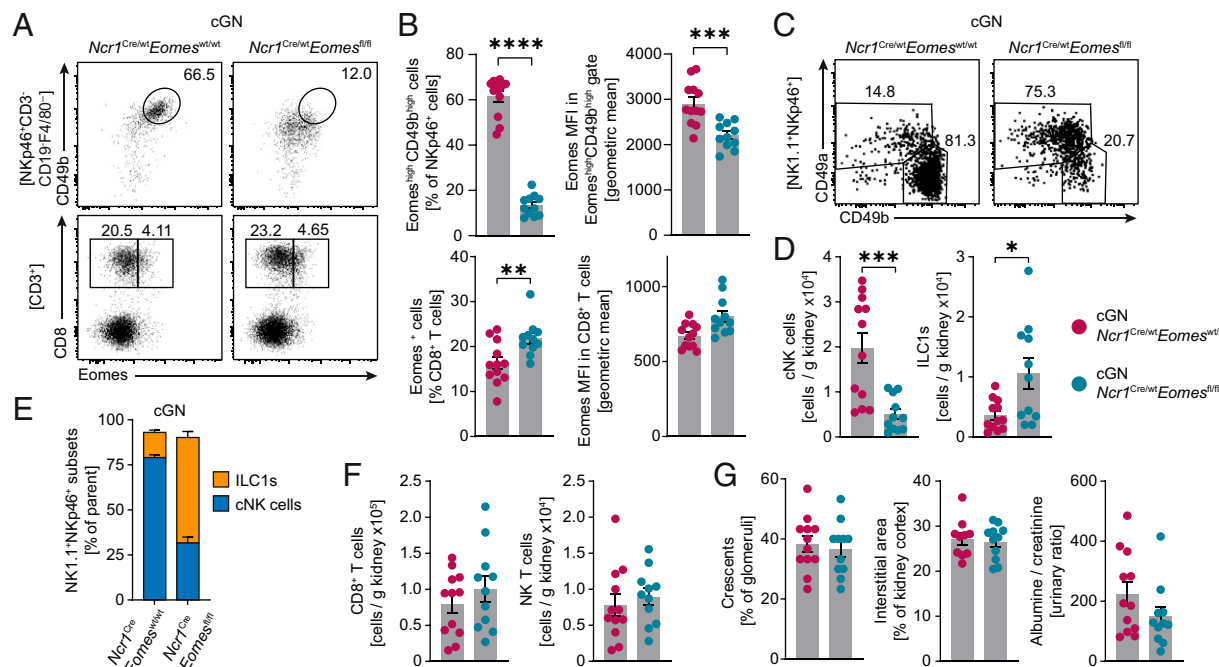
FIGURE 7. Genetic deletion of Eomes^{+} NK cells does not alter the course of experimental cGN. (**A**) Representative flow cytometry plots of kidney leukocytes isolated from $Ncr1^{Cre/wt} \times Eomes^{fl/fl}$ and $Ncr1^{Cre/wt} \times Eomes^{wt/wt}$ mice on day 9 of cGN. Plots are pregated on CD45^{+} live lymphocytes, and further gating is specified in brackets. Numbers represent percentage of cells in the gates. (**B**) Quantification of the frequency of Eomes^{+} cells in Nkp46^{+} ILCs and CD8^{+} T cells, as well as Eomes mean fluorescence intensity (MFI) in the respective cell subsets in the kidney on day 9 of cGN ($n = 12$ for $Ncr1^{Cre/wt} \times Eomes^{wt/wt}$ mice; $n = 11$ for $Ncr1^{Cre/wt} \times Eomes^{fl/fl}$ mice). (**C–E**) Representative flow cytometry plots pregated on NCR[+] ILCs (C) and quantification of NCR[+] ILC subsets (D and E) in the kidney of $Ncr1^{Cre/wt} \times Eomes^{fl/fl}$ and $Ncr1^{Cre/wt} \times Eomes^{wt/wt}$ mice on day 9 of cGN. (**F**) Quantification of NKT cells and CD8^{+} T cells in the kidney of the two groups on day 9 of cGN. (**G**) Histopathological quantification of tissue damage (glomerular crescents, interstitial area) and albuminuria on day 9 after induction of cGN in the two groups of mice (group numbers in D–G as in B). Filled circles represent individual animals, and bars represent mean ± SEM. Data are pooled from two individual experiments with similar results. *$p < 0.05$, **$p < 0.01$, ***$p < 0.001$, ****$p < 0.0001$.

studies in experimental models of GN are still scarce. Glomerular infiltration, activation, and IFN-γ production of NKp46^{+} cells were observed in the MRL-*lpr* mouse model of systemic lupus erythematosus, suggesting a proinflammatory role of NCR[+] ILCs in autoimmune renal inflammation (39). In a mouse model of progressive glomerular sclerosis (Adriamycin-induced nephropathy), kidney infiltration of CD49b^{+} NK cells was also evident, but neither depletion of cNK cells by application of anti-asGM1 serum nor impaired function of NK cells in NOD-SCID mice altered disease outcome (40). A more recent study identified a population of ILC1-like CD8^{+} lineage-negative cells expressing PPARα in the glomeruli of rats with experimental GN and patients with anti-glomerular basement membrane GN (41). However, the identity and specific functional importance of these cells that lacked expression of the pan-ILC marker CD161 awaits further study.

So far, subset-specific analyses of group 1 ILC function are hampered by the complexity of selective depletion strategies for cNK cells and ILC1s. A recent study addressed the subset-specific roles of cNK and ILC1s (i.e., trNK cells) in an ischemia-reperfusion injury model of AKI in mice by harnessing the relative lack of asGM1 expression on kidney ILC1s (20). Although depletion of total NCR[+] ILCs by applying anti-NK1.1 Ab substantially improved AKI outcome in this model, preferential depletion of cNK cells by anti-asGM1 serum injection had no effect on outcome, leading to the conclusion that (in the absence of cNK cells) ILC1s promote renal tissue injury in AKI (20). In this study, we adopted this strategy to address the subset-specific role of cNK cells and ILC1s in a widely used experimental model of cGN in mice. Both depletion strategies resulted in aggravation of glomerular crescent formation in wt mice; however, careful analyses of other lymphocyte

subsets revealed substantial off-target effects on kidney NKT cells (in the case of anti-NK1.1) and CD8^{+} T cells (in the case of anti-asGM1). Hence conclusions of experiments using these depletion strategies to study the role of group 1 ILC subsets in kidney models (20, 42) should be interpreted with caution. Notably, in the AKI model (20), the protective effect of NK1.1 Ab application was preserved even in $Cd1d^{-/-}$ mice that lack NKT cells. In the cGN model, in contrast, total NCR^{+} ILC depletion and preferential cNK cell depletion in the absence of NKT cells or CD8^{+} T cells, respectively, had no effect on outcome and thereby confirmed that the observed phenotype depended on these cell types. This suggests that cNK cells and ILC1s do not influence the pathogenesis in experimental cGN. The discrepancies between the data presented in this article and previously published work are most probably related to substantial differences in the models examined. The study by Victorino et al. (20) analyzed an ischemia-reperfusion−induced acute kidney injury model at a 24-h time point that results in ischemic necrosis of tubular epithelial cells. In this primarily non−immune-mediated model, the impact of NK cells is well established (16), indicating that the innate lymphoid response to sterile tissue injury might be an important player in this context. In this study, we focus on immune-mediated glomerular damage developing over several days as a result of a dysregulation in the adaptive immune response (43). Given the predominance of Th1 cells among T-bet−expressing lymphocytes in the cGN model, it is conceivable that the T-bet−expressing ILC populations might play a less prominent role in GN.

An alternative explanation for the dependence of the observed effects on NKT cells and CD8^{+} T cells, respectively, would be that downregulation of glomerular damage by group 1 ILCs is mediated by interaction with these cell types, a mechanism that has been

described for cNK cell–CD8$^+$ T cell interactions in viral infections (31). However, specific genetic deletion of cNK cells in *Ncr1*$^{Cre/wt}$ *Eomes*$^{fl/fl}$ mice did not influence the outcome of cGN, so this hypothesis could be discarded for cNK cells. Although a role for ILC1s in downregulation of glomerular damage cannot formally be excluded by the data presented in this article, it is important to emphasize that depletion of total NCR$^+$ ILCs did not alter cGN outcome in the absence of NKT cells, arguing against a substantial effect of ILC1s in immune-mediated glomerular disease.

In summary, we provide a detailed characterization of cNK cells and ILC1s in the murine kidney and show that they are largely dispensable for initiation and progression of experimental cGN. We further add to the existing evidence (30, 32) that standard Ab depletion methods for group 1 ILCs in mice have significant off-target effects, illustrating the urgent need for the development of more specific models to study ILC1 function.

Acknowledgments

Disclosures

The authors have no financial conflicts of interest.

References

1. Kiessling, R., E. Klein, and H. Wigzell. 1975. "Natural" killer cells in the mouse. I. Cytotoxic cells with specificity for mouse Moloney leukemia cells. Specificity and distribution according to genotype. *Eur. J. Immunol.* 5: 112–117.
2. Kiessling, R., E. Klein, H. Pross, and H. Wigzell. 1975. "Natural" killer cells in the mouse. II. Cytotoxic cells with specificity for mouse Moloney leukemia cells. Characteristics of the killer cell. *Eur. J. Immunol.* 5: 117–121.
3. Vivier, E., D. Artis, M. Colonna, A. Diefenbach, J. P. Di Santo, G. Eberl, S. Koyasu, R. M. Locksley, A. N. J. McKenzie, R. E. Mebius, et al. 2018. Innate lymphoid cells: 10 years on. *Cell* 174: 1054–1066.
4. Chiossone, L., P. Y. Dumas, M. Vienne, and E. Vivier. 2018. Natural killer cells and other innate lymphoid cells in cancer. [Published erratum appears in 2018 *Nat. Rev. Immunol.* 18: 726.] *Nat. Rev. Immunol.* 18: 671–688.
5. Björkström, N. K., B. Strunz, and H. G. Ljunggren. 2021. Natural killer cells in antiviral immunity. *Nat. Rev. Immunol.* DOI: 10.1038/s41577-021-00558-3.
6. Zwirner, N. W., C. I. Domaica, and M. B. Fuertes. 2021. Regulatory functions of NK cells during infections and cancer. *J. Leukoc. Biol.* 109: 185–194.
7. Björkström, N. K., H. G. Ljunggren, and J. Michaëlsson. 2016. Emerging insights into natural killer cells in human peripheral tissues. *Nat. Rev. Immunol.* 16: 310–320.
8. Michel, T., A. Poli, A. Cuapio, B. Briquemont, G. Iserentant, M. Ollert, and J. Zimmer. 2016. Human CD56bright NK cells: an update. *J. Immunol.* 196: 2923–2931.
9. Walzer, T., M. Bléry, J. Chaix, N. Fuseri, L. Chasson, S. H. Robbins, S. Jaeger, P. André, L. Gauthier, L. Daniel, et al. 2007. Identification, activation, and selective in vivo ablation of mouse NK cells via NKp46. *Proc. Natl. Acad. Sci. USA* 104: 3384–3389.
10. Peng, H., and Z. Tian. 2017. Diversity of tissue-resident NK cells. *Semin. Immunol.* 31: 3–10.
11. Weizman, O. E., N. M. Adams, I. S. Schuster, C. Krishna, Y. Pritykin, C. Lau, M. A. Degli-Esposti, C. S. Leslie, J. C. Sun, and T. E. O'Sullivan. 2017. ILC1 confer early host protection at initial sites of viral infection. *Cell* 171: 795–808.e12.
12. McFarland, A. P., A. Yalin, S. Y. Wang, V. S. Cortez, T. Landsberger, R. Sudan, V. Peng, H. L. Miller, B. Ricci, E. David, et al. 2021. Multi-tissue single-cell analysis deconstructs the complex programs of mouse natural killer and type 1 innate lymphoid cells in tissues and circulation. *Immunity* 54: 1320–1337.e4.
13. Spits, H., J. H. Bernink, and L. Lanier. 2016. NK cells and type 1 innate lymphoid cells: partners in host defense. *Nat. Immunol.* 17: 758–764.
14. O'Sullivan, T. E. 2019. Dazed and confused: NK cells. *Front. Immunol.* 10: 2235.
15. Floege, J., and K. Amann. 2016. Primary glomerulonephritides. *Lancet* 387: 2036–2048.
16. Turner, J. E., C. Rickassel, H. Healy, and A. J. Kassianos. 2019. Natural killer cells in kidney health and disease. *Front. Immunol.* 10: 587.
17. Ikezumi, Y., H. Kawachi, S. Toyabe, M. Uchiyama, and F. Shimizu. 2000. An anti-CD5 monoclonal antibody ameliorates proteinuria and glomerular lesions in rat mesangioproliferative glomerulonephritis. *Kidney Int.* 58: 100–114.
18. Furuichi, K., T. Wada, Y. Iwata, N. Sakai, K. Yoshimoto, M. Shimizu, K. Kobayashi, K. Takasawa, H. Kida, S. Takeda, et al. 2001. Upregulation of fractalkine in human crescentic glomerulonephritis. *Nephron* 87: 314–320.
19. Huang, X. R., P. G. Tipping, J. Apostolopoulos, C. Oettinger, M. D'Souza, G. Milton, and S. R. Holdsworth. 1997. Mechanisms of T cell-induced glomerular injury in anti-glomerular basement membrane (GBM) glomerulonephritis in rats. *Clin. Exp. Immunol.* 109: 134–142.
20. Victorino, F., D. K. Sojka, K. S. Brodsky, E. N. McNamee, J. C. Masterson, D. Homann, W. M. Yokoyama, H. K. Eltzschig, and E. T. Clambey. 2015. Tissue-resident NK cells mediate ischemic kidney injury and are not depleted by anti-Asialo-GM1 antibody. *J. Immunol.* 195: 4973–4985.
21. Narni-Mancinelli, E., J. Chaix, A. Fenis, Y. M. Kerdiles, N. Yessaad, A. Reynders, C. Gregoire, H. Luche, S. Ugolini, E. Tomasello, et al. 2011. Fate mapping analysis of lymphoid cells expressing the NKp46 cell surface receptor. *Proc. Natl. Acad. Sci. USA* 108: 18324–18329.
22. Panzer, U., O. M. Steinmetz, H. J. Paust, C. Meyer-Schwesinger, A. Peters, J. E. Turner, G. Zahner, F. Heymann, C. Kurts, H. Hopfer, et al. 2007. Chemokine receptor CXCR3 mediates T cell recruitment and tissue injury in nephrotoxic nephritis in mice. *J. Am. Soc. Nephrol.* 18: 2071–2084.
23. Bolger, A. M., M. Lohse, and B. Usadel. 2014. Trimmomatic: a flexible trimmer for Illumina sequence data. *Bioinformatics* 30: 2114–2120.
24. Dobin, A., C. A. Davis, F. Schlesinger, J. Drenkow, C. Zaleski, S. Jha, P. Batut, M. Chaisson, and T. R. Gingeras. 2013. STAR: ultrafast universal RNA-seq aligner. *Bioinformatics* 29: 15–21.
25. Lawrence, M., W. Huber, H. Pagès, P. Aboyoun, M. Carlson, R. Gentleman, M. T. Morgan, and V. J. Carey. 2013. Software for computing and annotating genomic ranges. *PLOS Comput. Biol.* 9: e1003118.
26. Love, M. I., W. Huber, and S. Anders. 2014. Moderated estimation of fold change and dispersion for RNA-seq data with DESeq2. *Genome Biol.* 15: 550.
27. Dahlgren, M. W., S. W. Jones, K. M. Cautivo, A. Dubinin, J. F. Ortiz-Carpena, S. Farhat, K. S. Yu, K. Lee, C. Wang, A. V. Molofsky, et al. 2019. Adventitial stromal cells define group 2 innate lymphoid cell tissue niches. *Immunity* 50: 707–722.e6.
28. Friedrich, C., R. L. R. E. Taggenbrock, R. Doucet-Ladevèze, P. Golda, R. Moenius, P. Arampatzi, N. A. M. Kragten, M. Kreymborg, M. Gomez de Agüero, W. Kastenmüller, et al. 2021. Effector differentiation downstream of lineage commitment in ILC1s is driven by Hobit across tissues. *Nat. Immunol.* 22: 1256–1267.
29. Kurts, C., U. Panzer, H. J. Anders, and A. J. Rees. 2013. The immune system and kidney disease: basic concepts and clinical implications. *Nat. Rev. Immunol.* 13: 738–753.
30. Nishikado, H., K. Mukai, Y. Kawano, Y. Minegishi, and H. Karasuyama. 2011. NK cell-depleting anti-asialo GM1 antibody exhibits a lethal off-target effect on basophils in vivo. *J. Immunol.* 186: 5766–5771.
31. Waggoner, S. N., R. T. Taniguchi, P. A. Mathew, V. Kumar, and R. M. Welsh. 2010. Absence of mouse 2B4 promotes NK cell-mediated killing of activated CD8+ T cells, leading to prolonged viral persistence and altered pathogenesis. *J. Clin. Invest.* 120: 1925–1938.
32. Slifka, M. K., R. R. Pagarigan, and J. L. Whitton. 2000. NK markers are expressed on a high percentage of virus-specific CD8+ and CD4+ T cells. *J. Immunol.* 164: 2009–2015.
33. Yang, S. H., S. J. Kim, N. Kim, J. E. Oh, J. G. Lee, N. H. Chung, S. Kim, and Y. S. Kim. 2008. NKT cells inhibit the development of experimental crescentic glomerulonephritis. *J. Am. Soc. Nephrol.* 19: 1663–1671.
34. Mesnard, L., A. C. Keller, M. L. Michel, S. Vandermeersch, C. Rafat, E. Letavernier, Y. Tillet, E. Rondeau, and M. C. Leite-de-Moraes. 2009. Invariant natural killer T cells and TGF-beta attenuate anti-GBM glomerulonephritis. *J. Am. Soc. Nephrol.* 20: 1282–1292.
35. Reynolds, J., V. A. Norgan, U. Bhambra, J. Smith, H. T. Cook, and C. D. Pusey. 2002. Anti-CD8 monoclonal antibody therapy is effective in the prevention and treatment of experimental autoimmune glomerulonephritis. *J. Am. Soc. Nephrol.* 13: 359–369.
36. Peng, H., X. Jiang, Y. Chen, D. K. Sojka, H. Wei, X. Gao, R. Sun, W. M. Yokoyama, and Z. Tian. 2013. Liver-resident NK cells confer adaptive immunity in skin-contact inflammation. *J. Clin. Invest.* 123: 1444–1456.
37. Carrega, P., I. Bonaccorsi, E. Di Carlo, B. Morandi, P. Paul, V. Rizzello, G. Cipollone, G. Navarra, M. C. Mingari, L. Moretta, and G. Ferlazzo. 2014. CD56(bright)perforin(low) noncytotoxic human NK cells are abundant in both healthy and neoplastic solid tissues and recirculate to secondary lymphoid organs via afferent lymph. *J. Immunol.* 192: 3805–3815.
38. Law, B. M. P., R. Wilkinson, X. Wang, K. Kildey, M. Lindner, M. J. Rist, K. Beagley, H. Healy, and A. J. Kassianos. 2017. Interferon-γ production by tubulointerstitial human CD56^{bright} natural killer cells contributes to renal fibrosis and chronic kidney disease progression. *Kidney Int.* 92: 79–88.
39. Spada, R., J. M. Rojas, S. Pérez-Yagüe, V. Mulens, P. Cannata-Ortiz, R. Bragado, and D. F. Barber. 2015. NKG2D ligand overexpression in lupus nephritis correlates with increased NK cell activity and differentiation in kidneys but not in the periphery. *J. Leukoc. Biol.* 97: 583–598.
40. Zheng, G., L. Zheng, Y. Wang, H. Wu, L. Kairaitis, C. Zhang, Y. C. Tay, Y. Wang, S. I. Alexander, and D. C. Harris. 2006. NK cells do not mediate renal injury in murine adriamycin nephropathy. *Kidney Int.* 69: 1159–1165.
41. Okabayashi, Y., S. Nagasaka, G. Kanzaki, N. Tsuboi, T. Yokoo, and A. Shimizu. 2019. Group 1 innate lymphoid cells are involved in the progression of experimental anti-glomerular basement membrane glomerulonephritis and are regulated by peroxisome proliferator-activated receptor α. *Kidney Int.* 96: 942–956.
42. Wee, Y. M., H. Go, M. Y. Choi, H. R. Jung, Y. M. Cho, Y. H. Kim, D. J. Han, and S. Shin. 2019. Tissue-resident natural killer cells exacerbate tubulointerstitial fibrosis by activating transglutaminase 2 and syndecan-4 in a model of aristolochic acid-induced nephropathy. *BMB Rep.* 52: 554–559.
43. Tipping, P. G., and S. R. Holdsworth. 2006. T cells in crescentic glomerulonephritis. *J. Am. Soc. Nephrol.* 17: 1253–1263.